Vibration Isolation of a Horizontal Rigid Plate Supported by Pre-bent Struts

by

Ann E. Jeffers

Thesis submitted to the Faculty of the
Virginia Polytechnic Institute and State University
in partial fulfillment of the requirements for the degree of

Master of Science
in
Civil Engineering

APPROVED BY:

_____

Dr. Raymond H. Plaut, Chairman

_____ _____

Dr. Kamal B. Rojiani Dr. Elisa D. Sotelino

December 2005
Blacksburg, VA

Keywords: Vibration isolation, buckled structures, dynamic response

Vibration Isolation of a Horizontal Rigid Plate Supported by Pre-bent Struts

by

Ann E. Jeffers

Dr. Raymond H. Plaut, Chairman

Charles E. Via, Jr. Department of Civil and Environmental Engineering

(ABSTRACT)

The purpose of this research is to analyze a new type of vibration isolator consisting of two pre-bent struts which are clamped at both ends and intermediately bonded with a viscoelastic filler. The proposed isolation device has the ability to support a relatively large static load with little deflection and offers a low axial resistance under dynamic excitation, making it ideal for isolating vertical vibrations. In this research, four of these vibration isolators are used to support a rigid, square plate. The symmetric case is analyzed first. Then the plate has a center of mass which is located at some distance from the geometric center of the plate. When the system is subjected to vertical harmonic base excitations, this eccentric weight introduces rotational as well as vertical motions of the plate. This research will investigate the effects of various eccentricities on the efficiency of the vibration isolators in the configuration described.

The displacement transmissibility will be the measure of the isolators' effectiveness at mitigating vibrations transmitted from the base to the rigid plate. For each case, the nonlinear equilibrium equations and the governing equations of motion for small vibrations about equilibrium are numerically solved, and the transmissibility is calculated and plotted over a wide range of frequencies. These plots are used to recognize ranges of frequencies for which isolation is achieved and frequencies at which resonance occurs in the system. At the resonant frequencies, the physical behavior of the system is analyzed to determine the types of vibration modes which occur in the system. A free vibration analysis is also performed to obtain a better understanding of resonances in the system.

Acknowledgments

I'd like to thank everyone at Virginia Tech who has contributed to my education and to this research. I would especially like to thank the members of my advisory committee, Dr. Raymond Plaut, Dr. Elisa Sotelino, and Dr. Kamal Rojiani, for their terrific efforts and valuable advice. I'd like to express my sincerest gratitude to Dr. Plaut for giving me the opportunity to work on this project and for sparking my interest in analytical research. I would also like to acknowledge the National Science Foundation for sponsoring this research and my education via Grant No. CMS-0301084.

Table of Contents

List of Figures

List of Tables

Chapter 1: Introduction

For decades, engineers and scientists have endeavored to develop effective methods for mitigating unwanted vibrations. Suppressing vibrations is often a critical issue, as vibrations have been known to cause structural damage and annoyance in a whole host of systems. Such examples range from a “bumpy” ride in an automobile to fatigue failures in aircraft components. In order to minimize the effects of these unwanted vibrations, a multitude of isolation devices have been designed for use in applications ranging from machinery and automobiles to buildings and aerospace structures (Sciulli, 1997). Because the factors that affect the performance of an isolator are numerous, the type of vibration isolator to be used depends largely on the application of the device.

This research will focus on analyzing a new type of vibration isolator which consists of two pre-bent struts clamped at both ends and bonded intermediately by a viscoelastic material. Previous research suggests that this device may have the potential to effectively isolate harmonic vibrations, and it has properties that give it an advantage over traditional types of vibration isolators for certain applications, e.g., systems which require the isolator to support a large mass. Before going into the details of this analysis, it is necessary to discuss several fundamental concepts relevant to the study of vibration isolation systems. This chapter will provide an overview of vibration isolation concepts, followed by a brief discussion of some of the common types of vibration isolators. The last two sections in this chapter include a review of the literature relevant to this research and the objectives and scope of this thesis.

1.1 Concepts of Vibration Isolation

Vibration isolation is achieved by placing an isolation device in the path of transmission between a vibrating source and a receiver. Typical sources of vibration include an earthquake or a machine, while common receivers may include a person or a piece of vibration-sensitive equipment. Depending on where the isolator is placed within a system, vibrations may be isolated at the source of vibration or at the receiving end of the vibration (Nelson, 1994). Common examples of vibration isolators include shock

absorbers found in vehicle suspension systems and rubber mounts used for isolating vibrating machinery.

Oftentimes, a vibration isolation system is modeled as a single-degree-of-freedom (SDF) system, as shown in Figure 1.1. In such a system, the foundation and mass are assumed to be rigid and the motion is restricted to one direction (e.g., the vertical direction). The most basic model for a vibration isolator consists of a massless spring with stiffness k and a viscous damper with damping coefficient c. In the case shown in Figure 1.1, the excitation takes the form of an imposed displacement $u(t)$ at the base. This excitation causes the mass to displace from its initial position to some location $x(t)$. The base displacement $u(t)$ and the response $x(t)$ have amplitudes denoted u_o and x_o, respectively.

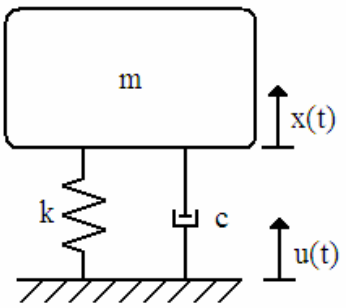

Figure 1.1: Single-Degree-of-Freedom System

In order to measure the effectiveness of the isolator, it is common to calculate the transmissibility for the system. If the excitation is an imposed displacement, the transmissibility is defined as the ratio of the magnitude of the response to the magnitude of the excitation. For example, the transmissibility TR for the system shown in Figure 1.1 can be computed as $TR = \frac{x_o}{u_o}$. For an isolator to be effective, the transmissibility should be significantly less than unity, meaning that the magnitude of the response is less than the magnitude of the excitation. It should be noted that, if the excitation takes the form of an applied force, the transmissibility can similarly be computed in terms of the force transmitted from a vibrating source to the foundation or attached body.

For simple-harmonic excitations, the transmissibility for a system is typically plotted over a range of excitation frequencies to determine the frequencies at which the isolator can be considered effective. In Figure 1.2, the transmissibility is plotted versus the ratio of the excitation frequency ω to the natural frequency ω_n for various damping ratios ζ in the SDF system shown in Figure 1.1. One characteristic of the SDF system is that the maximum response (also called *resonance*) occurs when the excitation frequency is approximately equal to the natural frequency of the system (i.e., $\omega/\omega_n \approx 1$). For the undamped system, the magnitude of the response at this peak is infinite. As the damping ratio increases, the magnitude of the maximum response decreases. In such a system, it is useful to have sufficient damping so that, in the event that the system is excited at or near its natural frequency, the maximum response will not be so great as to cause damage to the system.

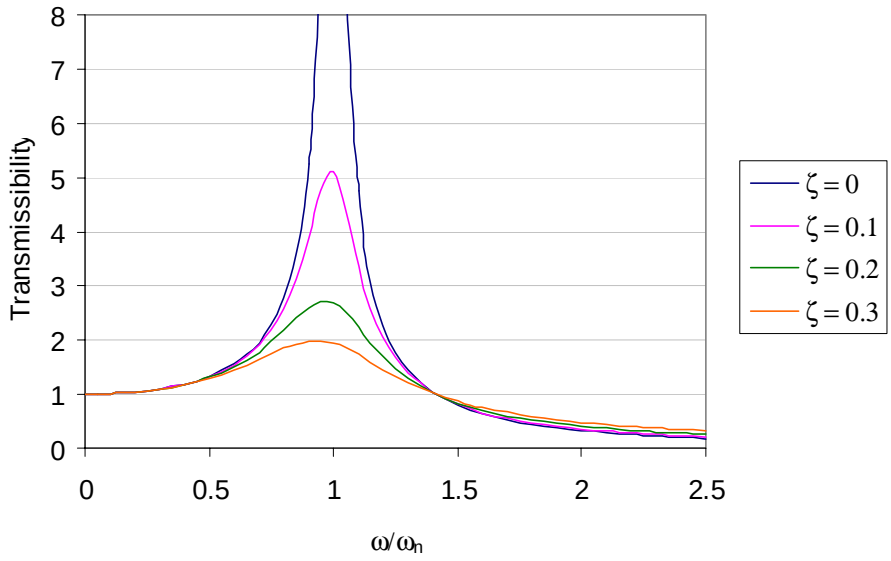

Figure 1.2: Displacement Transmissibility for a Single-Degree-of-Freedom System

Another characteristic of the SDF system is that the isolator is effective (i.e., the transmissibility is below unity) for frequencies ω greater than $\sqrt{2}\omega_n$. In order to isolate low-frequency vibrations, it is therefore necessary for the system to have a low natural frequency. In a SDF system, the natural frequency is defined as the square root of the ratio of the stiffness of the spring to the mass (i.e., $\omega_n = \sqrt{k/m}$). Assuming that the mass

in a system will remain constant, the only way to minimize the natural frequency is to reduce the stiffness of the spring as much as possible. The major disadvantage to reducing the spring's stiffness is that, in a vertical system like the one shown in Figure 1.1, the static deflection of the mass becomes excessively large. Thus, it may be desirable to employ a spring with nonlinear characteristics that would be stiff enough to support a large mass while being flexible enough under dynamic excitation to effectively isolate vibrations.

Although the SDF representation of an isolation system is useful for many applications, it may sometimes be advantageous or necessary to model a system with multiple degrees of freedom. For example, suppose a piece of vibration-sensitive equipment is mounted on a rectangular plate which is supported at each corner by a vibration isolator. If there is some eccentricity in the weight of the system, then the system may rotate as well as translate when subjected to a base excitation. Such a system is considered to have multiple degrees of freedom because the motion is no longer restricted to one direction. In a multi-degree-of-freedom (MDF) system, there exist a multiple number of natural vibration modes, each corresponding to a distinct natural frequency of the system. A transmissibility plot for a MDF system will have multiple peaks, and it is therefore necessary to consider the contribution of several vibration modes in determining the effectiveness of the isolator (Crede and Ruzicka, 1976).

1.2 Types of Vibration Isolators

Vibration isolators are available in all shapes and sizes and are made with a variety of materials. Common types of isolators include elastomeric isolators, plastic isolators, metal springs, and pneumatic (or air) springs (Racca and Harris, 2002). The behavior of each type of isolator is dependent not only on the materials used in constructing the isolator, but also on the configuration of the device and the conditions to which it will be subjected within a system. When selecting an isolator, it is important to know the type of disturbance (e.g., periodic vibration, random vibration, or shock excitation) and the allowable response of the system (e.g., a maximum allowable acceleration, velocity, or displacement). The system may have space constraints as to where the isolator(s) may be

placed, or may have a limit on the amount of static deflection that is allowed. There may also be environmental factors (e.g., the ambient temperature) that must be taken into consideration.

Vibration isolators may be passive, active, or a combination of both passive and active elements. A passive vibration isolator, like the one investigated in this research, uses the inherent properties of the isolation device (i.e., stiffness and damping) to mitigate vibrations and therefore requires no external power source to store or dissipate energy. Active isolators, on the other hand, require a substantial level of energy input to operate and typically involve some type of actuating device that responds to sensed variables within the system (Karnopp, 1995). While adding active controls to an isolator can greatly enhance the isolator's performance, active isolators tend to be much more complex, as there are a number of considerations that must be factored into the design of such devices. In addition, the design of an active isolator requires the consideration of the event of a power loss which may render the isolator useless. In a system that may experience a loss of power, it might be practical to use an isolator which has both passive and active elements to ensure that no damage occurs to the system.

1.3 Literature Review

This research is based on previous studies that have investigated the use of elastically buckled columns, also called "Euler springs," for the purpose of isolating vibrations. Columns which are loaded just above their critical buckling load maintain a relatively high stiffness under static loading. This property gives them an advantage over traditional types of vibration isolators such as springs or rubber mounts, which tend to exhibit large deflections when statically loaded. When the buckled columns are subjected to dynamic excitations, they become highly unstable, resulting in a low axial resistance. This low resistance makes these buckled columns ideal for isolating vibrations (Virgin and Plaut, 2002).

Experimental and analytical research has been conducted by Winterflood and colleagues (Winterflood et al., 2002a-c; Dumas et al., 2004; Chin et al., 2005) to investigate the use

of Euler springs as low-frequency vibration isolators. In these studies, it was found that buckled columns store a minimal amount of static energy and, compared to conventional springs, require a relatively low mass to support a large static load. It was also found that these Euler springs can be quite effective at isolating vibrations over a wide range of frequencies.

Bonello et al. (2005) devised an adaptive tuned vibration absorber which utilized a pair of pre-bent columns. The initial curvature of the columns could be adjusted so that the stiffness contributed by the columns caused the tuned frequency of the absorber to match the forcing frequency of a variable-frequency excitation. Analysis and experimental testing showed that the device was effective at reducing vibrations for a significant range of excitation frequencies.

Previous research on this National Science Foundation research project has been conducted by Professor L.N. Virgin and undergraduate student R.B. Davis at Duke University and by Professor R.H. Plaut with graduate students Laurie Alloway, Jenny Sidbury, and Helen Favor at Virginia Tech to investigate the possibility of using buckled columns as vibration isolators. Virgin and Davis (2003) conducted experimental tests of a SDF system utilizing buckled struts as vibration isolators. Laurie Alloway analyzed the nonlinear response of a buckled rigid-link mechanism for the purpose of isolating vibrations (Plaut et al., 2003). Jenny Sidbury (2003) analyzed a number of buckled struts with varying end conditions (i.e., pinned or fixed) subjected to harmonic excitations. She also considered systems with multi-frequency excitations, and columns with an initial pre-bent configuration. Helen Favor (2004) considered using buckled struts in a multi-degree-of-freedom system consisting of a horizontal rigid bar supported by vertical isolators at its ends. The bar was asymmetric in a manner that caused the bar to translate as well as rotate when the system was subjected to a vertical harmonic base excitation.

The isolation device investigated in the present thesis is made of two pre-bent struts which were clamped together at both ends and bonded intermediately by a viscoelastic filler. The advantage of using such a device is that the axial force applied does not have

to be above a specific buckling load, as was the case for the buckled struts. In addition, the intermediate filler assists in absorbing the dynamic energy and contributes a significant amount of damping to the isolator. This device was analyzed by Helen Favor (2004) in a SDF system subjected to harmonic forced vibration. The parameters that were varied included the stiffness of the filler, the amplitude of the initial shape of the struts, and the magnitude of the axial load. A similar device was also investigated at Virginia Tech by Professor F.A. Charney and graduate student Yasser Ibrahim (Ibrahim, 2005) for mitigating the damage to building structures during an earthquake.

1.4 Research Objectives and Scope

The purpose of this research is to study the effectiveness of an innovative type of vibration isolator which consists of two pre-bent struts clamped at both ends and bonded intermediately by a viscoelastic material. Similar to the single-strut isolator described in Section 1.3, this isolator is relatively stiff when statically loaded but exhibits a low axial resistance under dynamic loading. As demonstrated in Favor (2004), this device can be effective for isolating vibration in a planar system. In order to obtain a better understanding of this device's potential for isolating vibration, this research will extend preceding analyses by introducing three-dimensional motion of the supported mass into the problem.

The structure that is analyzed in this research is a rectangular rigid plate supported at the four corners by these vibration isolators, as shown in Figure 1.3. The isolators are attached to the plate with a spherical joint which transfers no moment from the plate to the struts. The plate is not uniform such that the center of mass of the weight W occurs at some distance from the geometric center of the plate. The location of the center of mass is indicated by the dimensions A_1, A_2, B_1, and B_2 in Figure 1.3. During the motion, the plate is free to move vertically and rotate about the $\overline{X}$ and $\overline{Y}$ axes. It is assumed that the system is braced laterally so as to prohibit sway and prevent collapse.

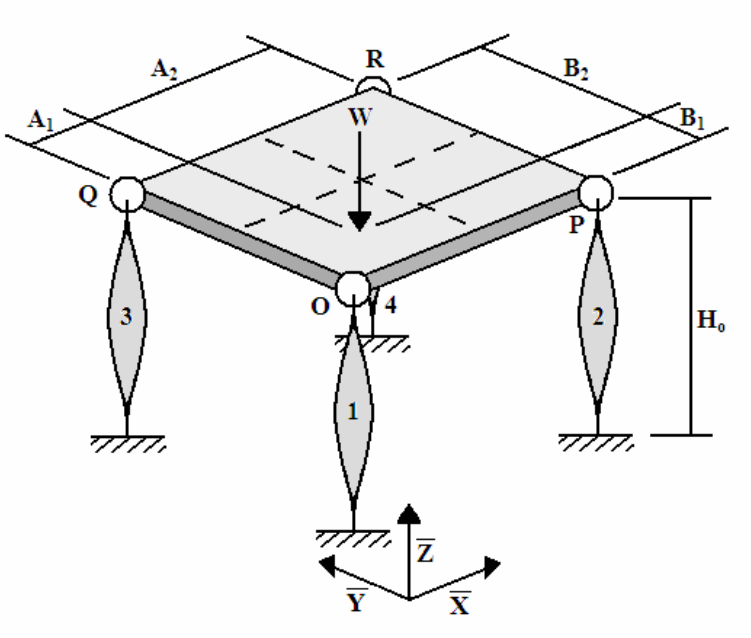

Figure 1.3: Rigid Plate Supported by Pre-Bent Struts with Intermediate Bonded Filler

It should be noted that a similar model was used by Tang et al. (2003) to analyze the three-dimensional motions of a platform system with hydraulic supports subjected to an impulse load. The platform was modeled as a rigid plate with a unit or block set on top of the platform. Similarly, the eccentric weight here is modeled as a block set on top of the rigid plate. Refer to Appendix B for more details.

A model of the vibration isolator is shown horizontally in Figure 1.4. The isolator is constructed such that the two pre-bent struts are clamped together at both ends and a viscoelastic filler is bonded to the inner sides of the struts. The filler is a material that has elastic properties similar to those of natural rubber, meaning that it can undergo large deformations without reaching its elastic limit. The filler contributes both damping and stiffness to the isolator and is represented in Figure 1.4 by a series of springs and dashpots acting along the length of the isolator. It is assumed that the filler does not contribute any stiffness or damping in the axial direction of the isolator. In this analysis, the struts are modeled as elasticas so as to allow for large deflections within the isolator. This model of the vibration isolator is the same model that Helen Favor used in her analysis.

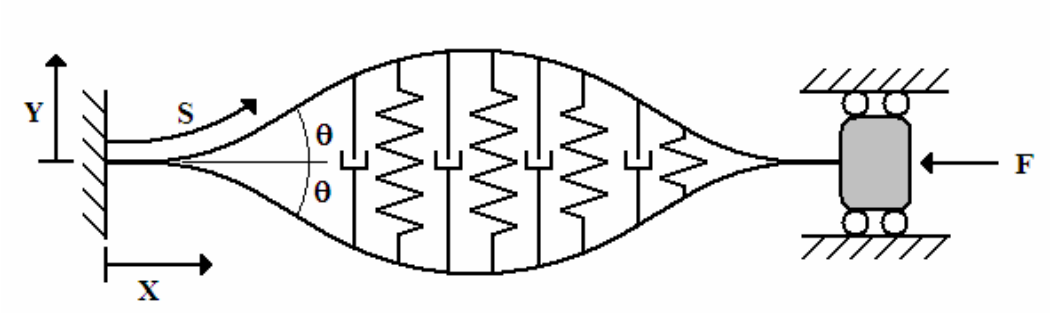

Figure 1.4: Model of Vibration Isolator under Axial Load *F*

The structure is first analyzed under static loading. To simulate desirable conditions, the stiffnesses of the bonded struts are adjusted so that the bottom of the plate is perfectly horizontal when the system is in equilibrium. After the system is in equilibrium, small vertical vibrations are applied to the base of the structure. The displacement imposed at the base of each isolator is a simple harmonic function which has the form $U(T) = U_o \sin(\Omega T)$, where $U(T)$ is the vertical base displacement at any time T, U_o is the amplitude of the base displacement, and Ω is the circular frequency. Under steady-state conditions, the behavior of the system is analyzed for various locations of the center of mass of the plate.

The equations of equilibrium and the equations of motion required for this analysis are derived for the system shown in Figure 1.3. The equations of motion are linearized for small motions, and the variables in all of the equations are nondimensionalized so that the results are valid irrespective of specific materials, lengths, and so on, and only depend on a few nondimensional parameters. A program written in Mathematica (2004) is used to numerically solve the equations of equilibrium and the equations of motion. The program uses a shooting method to iteratively solve for the unknown variables using the boundary conditions for the struts in the isolators and initial guesses for the unknown variables.

The displacement transmissibility is calculated and plotted over a wide range of frequencies for various locations of the center of mass. This data will be used to determine ranges of frequencies for which the isolators are effective, and conclusions will

be made as to the effect that the eccentric center of mass has on the system. The plate has three degrees of freedom and each isolator has an infinite number of degrees of freedom. Therefore, the transmissibility plots will have a number of peaks in the frequency range of interest, which correspond to various vibration modes. Additional information about the system is obtained by analyzing the physical behavior of the system at these resonant frequencies. It will be shown that some of these peaks correspond to large rotations and/or displacements of the plate, while the remaining peaks correspond to vibration modes within the isolators. In order to obtain additional information about resonance in the system, a free vibration analysis of the system is also included in this research.

Chapter 2: Analysis of Equilibrium State

The derivation of the equations required for the equilibrium analysis is broken into two parts. First, an analysis of the rigid plate must be performed to determine the relationship between the eccentric weight of the nonuniform plate and the forces transmitted to each of the four supporting isolators. Secondly, the behavior of each pair of struts must be evaluated in terms of the deflected shape and the forces and moments in the struts. After these equations of equilibrium are determined, the equations will be solved in a Mathematica program which uses a shooting method, as will be discussed later.

2.1 Rigid Plate Analysis

Referring back to Figure 1.3, the plate has the ability to move vertically and rotate about the $\overline{X}$ and $\overline{Y}$ axes. The horizontal movements at the corners of the plate due to such rotations will be ignored in the equilibrium analysis because only small rotations of the plate will be considered. As a result, the plate will be analyzed as a three-degree-of-freedom system.

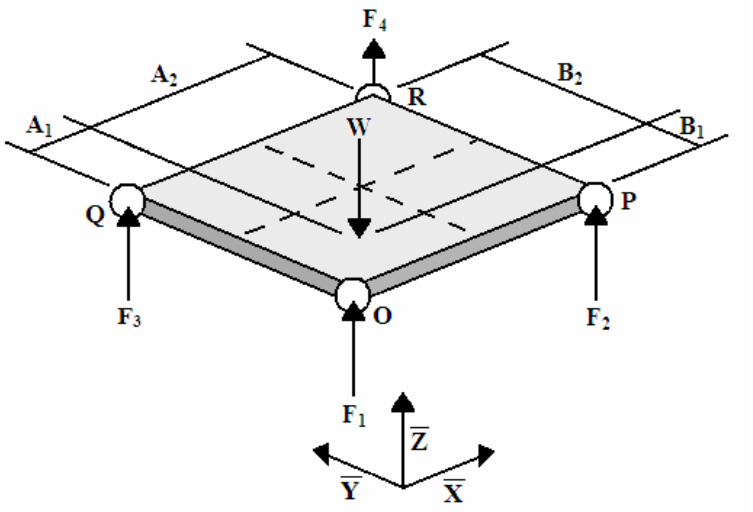

Figure 2.1: Free-Body Diagram of the Plate in Equilibrium

Upon considering the free body diagram of the plate shown in Figure 2.1, one apparent observation is that there are four unknown forces, F_1, F_2, F_3, and F_4, acting at the corners of the plate, but only three equations result from equilibrium. These equations are:

$$\Sigma F_z = 0; \qquad F_1 + F_2 + F_3 + F_4 = W \tag{2.1}$$

$$\Sigma M_x = 0; \qquad (F_1 + F_2)B_1 - (F_3 + F_4)B_2 = 0 \tag{2.2}$$

$$\Sigma M_y = 0; \qquad (F_1 + F_3)A_1 - (F_2 + F_4)A_2 = 0 \tag{2.3}$$

Thus, one more equation is needed to determine the unknown forces transmitted from the plate to the supporting struts. The fourth equation can be determined by recognizing the relationship that exists between the vertical displacements, Z_O, Z_P, Z_Q, and Z_R, at the corners of the plate (which are labeled *O*, *P*, *Q*, and *R* in Figure 2.1) when it rotates at some angle about the $\overline{X}$ and $\overline{Y}$ axes. The following geometric relationship,

$$Z_O - Z_P - Z_Q + Z_R = 0, \tag{2.4}$$

is based on the assumption that the plate does not twist or bend. These vertical displacements will be obtained from the analysis of the individual isolators. Equations (2.1) – (2.4) can be solved simultaneously to obtain the four unknown forces, F_1, F_2, F_3, and F_4, and will be used in the analysis of the individual isolators.

2.2 Analysis of the Vibration Isolator

Now that the axial force applied to the top of each isolator can be determined, it is necessary to examine the force-displacement relationship for each isolator. As stated earlier, the isolator, shown horizontally in Figure 2.2, consists of two struts which are clamped together at both ends and bonded intermediately by a viscoelastic material. The filler contributes both damping and stiffness to the isolator and is represented in Figure 2.2 by a series of springs and dashpots acting along the length of the isolator. For simplicity, the isolator is restrained against horizontal (*Y*-direction) displacement and rotation at both ends. This is done because the horizontal displacement of the plate is negligible and this assumption will greatly simplify the problem by allowing the use of symmetry. As a result, only one strut in each isolator will be analyzed from here on.

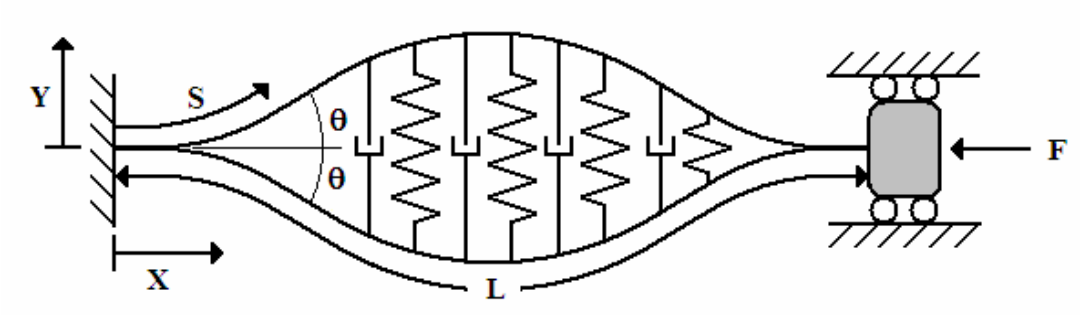

Figure 2.2: Model of Vibration Isolator under Static Axial Load *F*

Before any load is applied to the isolator, each strut has an initial shape with an amplitude a_o. All four isolators will have the same initial shape and so this part of the analysis holds for each strut in all four isolators. The initial angle $\theta_o(S)$ is assumed as

$$\theta_o(S) = a_o \cdot \sin\left(\frac{2\pi S}{L}\right) \tag{2.5}$$

where L is the length of the strut. The initial angle is chosen such that it satisfies the condition that the slope is zero {i.e., $\theta_o(S) = 0$ } when $S = 0$, $\frac{L}{2}$, and L.

The initial deflection $Y_o(S)$ is equal to the integral of the sine of the initial angle over the length of the strut. For small angles, this is approximately equal to the integral of the initial angle $\theta_o(S)$ over the length of the strut. This gives

$$Y_o(S) \approx \frac{a_o L}{2\pi} \cdot \left(1 - \cos\left(\frac{2\pi S}{L}\right)\right) \tag{2.6}$$

Note that the initial deflection has a maximum value of $\frac{a_o L}{\pi}$ when $S = \frac{L}{2}$, and the initial deflection is zero when $S = 0$ and L.

The stiffness and damping contributed by the filler depend on the thickness of the filler and, since the thickness varies along the length of the isolator, the stiffness and damping will be functions of the initial shape $Y_o(S)$ of the strut. It is assumed that the filler is unstretched when the struts are not loaded. The filler's stiffness per unit length will be

defined as $\frac{K_f}{Y_o}$, where K_f is a stiffness parameter. The damping per unit length is defined as $C_f Y_o$, where C_f is a damping parameter.

The variables used for the remaining portion of this analysis are defined below. The subscript *e* is used to indicate that these variables are part of the equilibrium analysis. Note that the subscript *i* is used to distinguish between isolators, which are numerically labeled in Figure 1.4. While the values of each variable will differ between isolators, the derivation of the following relationships is the same for all four isolators.

$i =$ an integer that ranges from one to four

$\theta_{i,e} =$ angle of the deflected strut in the i^{th} isolator measured from the *X*-axis

$P_{i,e} =$ component of force acting in the *X*-direction of the strut in the i^{th} isolator

$Q_{i,e} =$ component of force acting in the *Y*-direction of the strut in the i^{th} isolator

$M_{i,e} =$ bending moment in the strut in the i^{th} isolator

$E =$ modulus of elasticity of the strut (assumed to be the same for all struts)

$I =$ moment of inertia of the cross-section of the strut about the axis of bending (assumed to be the same for all struts)

$\beta_i =$ stiffness modification factor for the strut in the i^{th} isolator

$dS_i =$ small element of length along the arc of the strut in the i^{th} isolator

$dX_{i,e} =$ projection of dS_i in the *X*-direction

$dY_{i,e} =$ projection of dS_i in the *Y*-direction

A free-body diagram of a small element of the strut is shown in Figure 2.3. When a load F_i is applied to the isolator, the strut deflects from the initial configuration to a new position $Y_{i,e}(S)$. The filler resists this motion, resulting in a distributed force of $\frac{K_f}{Y_o} \cdot 2\left(Y_{i,e} - Y_o\right)$ acting in the negative *Y*-direction along the length of the strut.

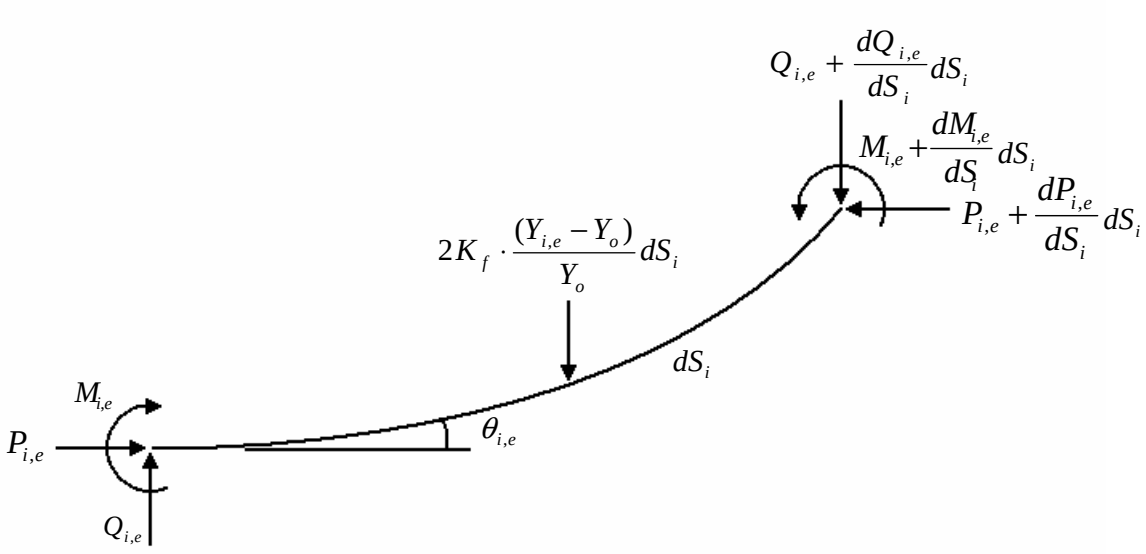

Figure 2.3: Free-Body Diagram of an Element of the Strut in Equilibrium

From geometry, equilibrium, and the elastic constitutive law for the strut, the following relationships can be obtained:

$$\frac{dX_{i,e}}{dS_i} = \cos\theta_{i,e} \tag{2.7}$$

$$\frac{dY_{i,e}}{dS_i} = \sin\theta_{i,e} \tag{2.8}$$

$$\frac{dQ_{i,e}}{dS_i} = \frac{-2K_f}{Y_o} \cdot \left(Y_{i,e} - Y_o\right) \tag{2.9}$$

$$\frac{dM_{i,e}}{dS_i} = -P_{i,e}\sin\theta_{i,e} + Q_{i,e}\cos\theta_{i,e} \tag{2.10}$$

$$M_{i,e} = \beta_i EI \cdot \left(\frac{d\theta_{i,e}}{dS_i} - \frac{d\theta_o}{dS_i}\right) \tag{2.11}$$

where $\left(\frac{d\theta_{i,e}}{dS_i} - \frac{d\theta_o}{dS_i}\right)$ is the change in curvature. Note that the bending stiffness *EI* for each strut is multiplied by a modification factor β_i. The stiffness modification factors will be chosen so that the downward deflection at the top of each strut due to the static load F_i is the same for all four isolators. In other words, each isolator will have the same initial height H_o when the system is in equilibrium.

Taking the derivative of Equation (2.5) gives

$$\frac{d\theta_o}{dS_i} = \frac{2\pi}{L} a_o \cos\left(\frac{2\pi S_i}{L}\right) \tag{2.12}$$

Substituting Equation (2.12) into Equation (2.11) and rearranging terms gives

$$\frac{d\theta_{i,e}}{dS_i} = \frac{M_{i,e}}{\beta_i EI} + \frac{2\pi}{L} a_o \cos\left(\frac{2\pi S_i}{L}\right) \tag{2.13}$$

Additionally,

$$\frac{dY_o}{dS_i} = \sin(\theta_o) = \sin\left[a_o \sin\left(\frac{2\pi S_i}{L}\right)\right] \tag{2.14}$$

Because of symmetry, the axial force $P_{i,e}$ in the strut is equal to half of the total load F_i applied to the isolator. That is,

$$P_{i,e} = \frac{F_i}{2} \tag{2.15}$$

2.3 Nondimensionalization

All computations in this analysis will be performed in nondimensional terms so that the results will be valid irrespective of specific materials, lengths, and so on. The nondimensional variables are defined as follows:

$$a_1 = \frac{A_1}{A_1 + A_2} \qquad a_2 = \frac{A_2}{A_1 + A_2} \tag{2.16, 2.17}$$

$$b_1 = \frac{B_1}{A_1 + A_2} = \alpha \frac{B_1}{B_1 + B_2} \qquad b_2 = \frac{B_2}{A_1 + A_2} = \alpha \frac{B_2}{B_1 + B_2} \tag{2.18, 2.19}$$

where the aspect ratio α of the plate is defined as

$$\alpha = \frac{B_1 + B_2}{A_1 + A_2} \tag{2.20}$$

It follows that $a_1 + a_2 = 1$ and $b_1 + b_2 = \alpha$. The remaining nondimensional variables are defined below:

$$x_{i,e} = \frac{X_{i,e}}{A_1 + A_2} \qquad y_{i,e} = \frac{Y_{i,e}}{A_1 + A_2} \tag{2.21, 2.22}$$

$$s_i = \frac{S_i}{A_1 + A_2} \qquad y_o = \frac{Y_o}{A_1 + A_2} \tag{2.23, 2.24}$$

$$l = \frac{L}{A_1 + A_2} \qquad h_o = \frac{H_o}{A_1 + A_2} \tag{2.25, 2.26}$$

$$k_f = \frac{2K_f \left(A_1 + A_2\right)^3}{EI} \qquad w = \frac{W\left(A_1 + A_2\right)^2}{EI} \tag{2.27, 2.28}$$

$$p_{i,e} = \frac{P_{i,e}\left(A_1 + A_2\right)^2}{EI} \qquad q_{i,e} = \frac{Q_{i,e}\left(A_1 + A_2\right)^2}{EI} \tag{2.29, 2.30}$$

$$m_{i,e} = \frac{M_{i,e}\left(A_1 + A_2\right)}{EI} \tag{2.31}$$

The resulting nondimensional equations defining the behavior of the i^{th} strut under static loading are:

$$\frac{dx_{i,e}}{ds_i} = \cos\theta_{i,e} \tag{2.32}$$

$$\frac{dy_{i,e}}{ds_i} = \sin\theta_{i,e} \tag{2.33}$$

$$\frac{d\theta_{i,e}}{ds_i} = \frac{m_{i,e}}{\beta_i} + 2\pi a_o \cos\left(2\pi s_i\right) \tag{2.34}$$

$$\frac{dm_{i,e}}{ds_i} = -p_{i,e}\sin\theta_{i,e} + q_{i,e}\cos\theta_{i,e} \tag{2.35}$$

$$\frac{dq_{i,e}}{ds_i} = \frac{-k_f}{y_o} \cdot \left(y_{i,e} - y_o\right) \tag{2.36}$$

$$\frac{dy_o}{ds_i} = \sin\left[a_o \sin\left(2\pi s_i\right)\right] \tag{2.37}$$

The boundary conditions required to solve Equations (2.32) – (2.37) are as follows. At $s_i = 0$, the strut is restrained against *X*- and *Y*-direction displacements { $x_{i,e}(0) = 0$,

$y_{i,e}(0) = 0$, $y_o(0) = 0$ } and against rotation { $\theta_{i,e}(0) = 0$ }. At $s_i = 1$, the strut is assumed to be restrained against *Y*-direction displacement { $y_{i,e}(1) = 0$, $y_o(1) = 0$ } and against rotation { $\theta_{i,e}(1) = 0$ }.

Recall that Equations (2.1) – (2.3) are still in terms of the total forces applied to the isolator rather than the axial forces in each strut. If we substitute the relationship in Equation (2.15), and put Equations (2.1) – (2.3) in non-dimensional form, the following equations ensue:

$$p_{1,e} + p_{2,e} + p_{3,e} + p_{4,e} = \frac{w}{2} \tag{2.38}$$

$$(p_{1,e} + p_{2,e})b_1 - (p_{3,e} + p_{4,e})b_2 = 0 \tag{2.39}$$

$$(p_{1,e} + p_{3,e})a_1 - (p_{2,e} + p_{4,e})a_2 = 0 \tag{2.40}$$

Furthermore, Equation (2.4) is in terms of the displacements at the corners of the plate. From continuity, the vertical displacement at a given corner is equal to the *X*-direction displacement at the end of the strut of the isolator attached at that corner. Specifically, $Z_O = X_{1,e}(L)$, $Z_P = X_{2,e}(L)$, $Z_Q = X_{3,e}(L)$, and $Z_R = X_{4,e}(L)$. Substituting these relationships into Equation (2.4) and putting everything in nondimensional terms gives

$$x_{1,e}(1) - x_{2,e}(1) - x_{3,e}(1) + x_{4,e}(1) = 0 \tag{2.41}$$

Using the program written in Mathematica, Equations (2.32) – (2.37) are solved numerically such that the solution satisfies the constraints specified in Equations (2.38) – (2.41) and the boundary conditions. Values for the weight *w*, the initial amplitude a_o, the filler stiffness k_f, the dimensions a_1 and b_1, the aspect ratio α, and initial guesses for the stiffness modification factors β_i are entered into the program in addition to initial guesses for the axial force $p_{i,e}$ in each strut, the shear forces $q_{i,e}(0)$, and the bending moments $m_{i,e}(0)$ at the base of each strut. A printout of the program can be found in Appendix A.

An additional requirement that must be included in this analysis is that the plate must be horizontal when the structure is statically loaded. As previously mentioned, this will be done by adjusting the stiffness of each strut using the stiffness modification factors. Since Equation (2.41) already includes a constraint on the *X*-direction displacements in the struts, this will be handled by incorporating a loop in the Mathematica program which adjusts the stiffness modification factors β_i after each run until the plate is essentially horizontal.

2.4 Results from Equilibrium Analysis

For the equilibrium analysis, the Mathematica program is run for various locations of the center of mass of the plate. The initial amplitude a_o and the stiffness parameter k_f are each assigned a value of 0.1. The weight *w* is chosen as 320 so that the axial force in each strut under the fully symmetric case (i.e., when $a_1 = 0.5$ and $b_1 = 0.5$) is 40. The significance of this number is that it is just above the nondimensional buckling load for a column which is clamped at both ends (i.e., $p_{cr} = 4\pi^2 \approx 39.478$). While this type of isolator does not need to be loaded above the critical buckling load to be an effective vibration isolator, this load will be used as a basis for this analysis. As the results of the equilibrium analysis will show, the load applied to an individual isolator may be either higher or lower than the critical load, depending on the eccentricity of the center of mass of the plate.

Table 2.1 shows values for the stiffness modification factors β_i for each isolator, the axial forces transmitted to each strut $p_{i,e}$, and the equilibrium height of the plate h_o for various locations of the applied load *w*. The first row in the table represents the case where the center of mass is at the geometric center of the plate. As would be expected, the stiffness modification factors all have a value of one and the axial force in each strut is the same for all struts. Note that the plate height of 0.781 is the lowest for this case.

In the first five rows of Table 2.1, b_1 is equal to 0.5, meaning that there is a line of symmetry through the center of the plate parallel to the $\overline{X}$ -axis (see Figure 2.1). As the load moves toward the edge *OQ* of the plate, isolators 1 and 3 become stiffer (i.e., β_1 and

β_3 are greater than one) while isolators 2 and 4 become less stiff (i.e., β_2 and β_4 are less than one). Unsurprisingly, isolators 1 and 3 have identical values for stiffness and force, as do isolators 2 and 4. In the next four rows of Table 2.1, a_1 is equal b_1, meaning again that there is a line of symmetry, this time passing from the corner *O* of the plate to corner *R*. As the load moves toward the corner *O*, isolator 1 becomes stiffer (i.e., β_1 is greater than one) while isolator 4 becomes less stiff (i.e., β_4 is less than one). For this case, isolators 2 and 3 remain equal in stiffness regardless of where the center of mass is positioned along the diagonal line of symmetry. The last six rows in Table 2.1 represent cases where the center of mass is arbitrarily positioned such that there is no symmetry. Note that for all cases the height of the plate increases as the center of mass moves from the center of the plate.

Table 2.1: Results from Equilibrium Analysis

Location of the Center of Mass		Stiffness Modification Factors				Axial Force				Plate Height
a_1	b_1	β_1	β_2	β_3	β_4	$p_{1,e}$	$p_{2,e}$	$p_{3,e}$	$p_{4,e}$	h_o
0.50	0.50	1.000	1.000	1.000	1.000	40.00	40.00	40.00	40.00	0.781
0.45	0.50	1.126	0.920	1.126	0.920	44.00	36.00	44.00	36.00	0.807
0.40	0.50	1.260	0.838	1.260	0.838	48.00	32.00	48.00	32.00	0.834
0.35	0.50	1.412	0.757	1.412	0.757	52.00	28.00	52.00	28.00	0.866
0.30	0.50	1.591	0.678	1.591	0.678	56.00	24.00	56.00	24.00	0.901
0.45	0.45	1.291	1.000	1.000	0.873	49.57	38.43	38.43	33.57	0.826
0.40	0.40	1.710	1.000	1.000	0.802	60.51	35.49	35.49	28.51	0.897
0.35	0.35	2.025	1.000	1.000	0.623	69.54	34.46	34.46	21.54	0.915
0.30	0.30	2.749	1.000	1.000	0.600	82.05	29.95	29.95	18.05	0.964
0.40	0.45	1.488	0.912	1.132	0.830	54.51	33.49	41.49	30.51	0.871
0.35	0.45	1.728	0.848	1.319	0.786	58.95	29.05	45.05	26.95	0.919
0.30	0.45	1.915	0.753	1.485	0.696	63.06	24.94	48.94	23.06	0.936
0.35	0.40	1.853	0.941	1.175	0.683	63.59	32.42	40.42	23.59	0.916
0.30	0.40	2.131	0.853	1.352	0.632	68.46	27.54	43.54	20.46	0.945
0.30	0.35	2.338	0.935	1.188	0.568	74.19	29.81	37.81	18.19	0.949

Chapter 3: Derivation of the Equations of Motion

Similar to the equilibrium analysis, the derivation of the equations of motion for the dynamic analysis is also divided into two parts. First, the equations of motion for the rigid plate are determined from the kinetic and potential energies in the system using Lagrange's equations. Then, the struts in each isolator are analyzed using D'Alembert's principle. All dynamic equations are linearized for small motions and put in nondimensional form. A program written in Mathematica is used to numerically solve these equations to determine the motion transmissibility for the system. The results from the dynamic analysis can be found in Chapter 4.

3.1 Rigid Plate Analysis

The $\overline{X}$, $\overline{Y}$, $\overline{Z}$ coordinate system is fixed in space as shown in Figure 3.1 and has unit vectors $\hat{i}$, $\hat{j}$, and $\hat{k}$. The angles θ, ψ, and ϕ are used to define coordinate rotations about the $\overline{X}$, -$\overline{Y}$, and $\overline{Z}$ axes, respectively, and are initially zero. The points *O*, *P*, *Q*, and *R* are located at the bottom of each corner of the plate, and the plate has an initial height H_o when the system is in equilibrium. The center of mass (labeled *c.m.* in Figure 3.1) is indicated by the dimensions A_1, A_2, B_1, and B_2, and it is positioned at a distance *C* above the bottom of the plate.

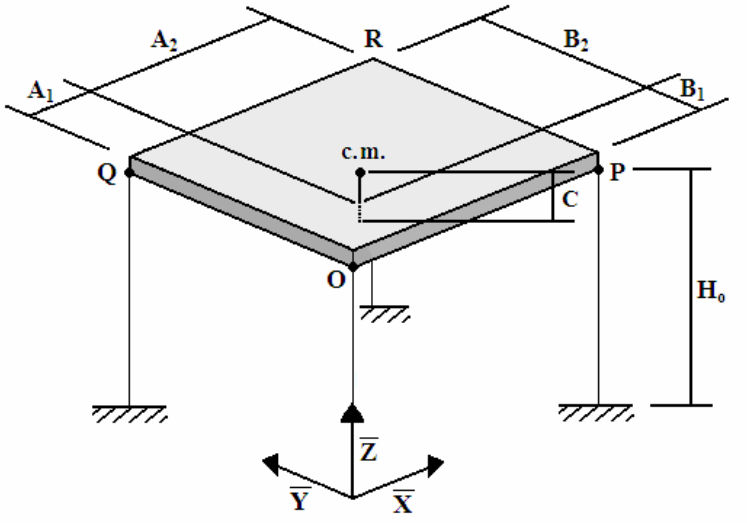

Figure 3.1: Initial Configuration of the Plate

Referring to Figure 3.1, the position vectors from the origin of the fixed coordinate system to the points *O, P, Q, R,* and to the center of mass when the system is at rest are as follows:

$$\bar{r}_O = H_o\hat{k} \tag{3.1}$$

$$\bar{r}_P = (A_1 + A_2)\hat{i} + H_o\hat{k} \tag{3.2}$$

$$\bar{r}_Q = (B_1 + B_2)\hat{j} + H_o\hat{k} \tag{3.3}$$

$$\bar{r}_R = (A_1 + A_2)\hat{i} + (B_1 + B_2)\hat{j} + H_o\hat{k} \tag{3.4}$$

$$\bar{r}_{c.m.} = A_1\hat{i} + B_1\hat{j} + (H_o + C)\hat{k} \tag{3.5}$$

The $\bar{X}_1$, $\bar{Y}_1$, $\bar{Z}_1$ coordinate system with unit vectors $\hat{i}_1$, $\hat{j}_1$, $\hat{k}_1$ has its origin at the center of mass and is parallel to the fixed $\bar{X}$, $\bar{Y}$, $\bar{Z}$ coordinate system. In other words,

$$\begin{Bmatrix} \hat{i}_1 \\ \hat{j}_1 \\ \hat{k}_1 \end{Bmatrix} = \begin{bmatrix} 1 & 0 & 0 \\ 0 & 1 & 0 \\ 0 & 0 & 1 \end{bmatrix} \begin{Bmatrix} \hat{i} \\ \hat{j} \\ \hat{k} \end{Bmatrix} \tag{3.6}$$

The $\bar{X}_2$, $\bar{Y}_2$, $\bar{Z}_2$ coordinate system with unit vectors $\hat{i}_2$, $\hat{j}_2$, $\hat{k}_2$ is obtained by rotating the $\bar{X}_1$, $\bar{Y}_1$, $\bar{Z}_1$ coordinate system by an angle θ about the $\bar{X}$-axis, as shown in Figure 3.2(a). The relationships between the $\hat{i}_1$, $\hat{j}_1$, $\hat{k}_1$ unit vectors and the $\hat{i}_2$, $\hat{j}_2$, $\hat{k}_2$ unit vectors can be determined as

$$\begin{Bmatrix} \hat{i}_2 \\ \hat{j}_2 \\ \hat{k}_2 \end{Bmatrix} = \begin{bmatrix} 1 & 0 & 0 \\ 0 & \cos\theta & \sin\theta \\ 0 & -\sin\theta & \cos\theta \end{bmatrix} \begin{Bmatrix} \hat{i}_1 \\ \hat{j}_1 \\ \hat{k}_1 \end{Bmatrix} \tag{3.7}$$

The $\bar{X}_3$, $\bar{Y}_3$, $\bar{Z}_3$ coordinate system with unit vectors $\hat{i}_3$, $\hat{j}_3$, $\hat{k}_3$ is obtained by rotating the $\bar{X}_2$, $\bar{Y}_2$, $\bar{Z}_2$ coordinate system by an angle ψ about the -$\bar{Y}$-axis, as shown in Figure 3.2(b). The relationships between the $\hat{i}_2$, $\hat{j}_2$, $\hat{k}_2$ unit vectors and the $\hat{i}_3$, $\hat{j}_3$, $\hat{k}_3$ unit vectors can be determined as

$$\begin{Bmatrix} \hat{i}_3 \\ \hat{j}_3 \\ \hat{k}_3 \end{Bmatrix} = \begin{bmatrix} \cos\psi & 0 & \sin\psi \\ 0 & 1 & 0 \\ -\sin\psi & 0 & \cos\psi \end{bmatrix} \begin{Bmatrix} \hat{i}_2 \\ \hat{j}_2 \\ \hat{k}_2 \end{Bmatrix} \tag{3.8}$$

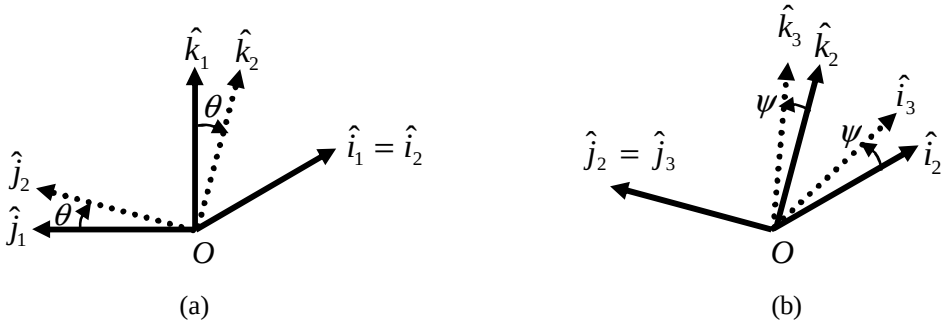

(a) (b)

Figure 3.2: Coordinate Systems for (a) Positive Rotation θ about the $\overline{X}$ -Axis and for (b) Positive Rotation ψ about the -$\overline{Y}$ -Axis

As a result, the $\overline{X}_3$, $\overline{Y}_3$, $\overline{Z}_3$ coordinate system can be related to the fixed $\overline{X}$, $\overline{Y}$, $\overline{Z}$ coordinate system by substituting Equation (3.6) into Equation (3.7), and then substituting Equation (3.7) into (3.8). This gives

$$\begin{Bmatrix} \hat{i}_3 \\ \hat{j}_3 \\ \hat{k}_3 \end{Bmatrix} = \begin{bmatrix} \cos\psi & -\sin\psi\sin\theta & \sin\psi\cos\theta \\ 0 & \cos\theta & \sin\theta \\ -\sin\psi & -\cos\psi\sin\theta & \cos\psi\cos\theta \end{bmatrix} \begin{Bmatrix} \hat{i} \\ \hat{j} \\ \hat{k} \end{Bmatrix} \tag{3.9}$$

Under dynamic excitation, the center of mass of the plate moves from its resting position to some position $X(T)$, $Y(T)$, $Z(T)$ and the plate rotates at angles θ and ψ about the $\overline{X}$ and -$\overline{Y}$ axes, respectively. Note that the rotation ϕ about the $\overline{Z}$ axis is restrained in this analysis. The position vector from the origin of the fixed coordinate system to the center of mass under dynamic excitation becomes:

$$\bar{r}_{c.m.} = [A_1 + X(T)]\hat{i} + [B_1 + Y(T)]\hat{j} + [H_o + C + Z(T)]\hat{k} \tag{3.10}$$

Using the principle of superposition, the position vectors for points *O*, *P*, *Q*, and *R* can be defined as the sum of the position vector $\bar{r}_{c.m.}$ to the center of mass and a vector from the center of mass to each corner. Specifically,

$$\bar{r}_O = \bar{r}_{c.m.} - A_1\hat{i}_3 - B_1\hat{j}_3 - C\hat{k}_3 \tag{3.11}$$

$$\bar{r}_P = \bar{r}_{c.m.} + A_2\hat{i}_3 - B_1\hat{j}_3 - C\hat{k}_3 \tag{3.12}$$

$$\bar{r}_Q = \bar{r}_{c.m.} - A_1\hat{i}_3 + B_2\hat{j}_3 - C\hat{k}_3 \tag{3.13}$$

$$\bar{r}_R = \bar{r}_{c.m.} + A_2\hat{i}_3 + B_2\hat{j}_3 - C\hat{k}_3 \tag{3.14}$$

Substituting the relationships in Equation (3.9) for the unit vectors $\hat{i}_3,\ \hat{j}_3,\ \hat{k}_3$, and substituting the equation for the position vector $\bar{r}_{c.m.}$ of the center of mass in Equation (3.10) into Equations (3.11) – (3.14) gives a set of position vectors for the corners *O*, *P*, *Q*, and *R* of the plate in terms of the unit vectors $\hat{i}$, $\hat{j}$, and $\hat{k}$ in the fixed coordinate system. These position vectors take the form

$$\bar{r}_O = X_O\hat{i} + Y_O\hat{j} + Z_O\hat{k} \tag{3.15}$$

$$\bar{r}_P = X_P\hat{i} + Y_P\hat{j} + Z_P\hat{k} \tag{3.16}$$

$$\bar{r}_Q = X_Q\hat{i} + Y_Q\hat{j} + Z_Q\hat{k} \tag{3.17}$$

$$\bar{r}_R = X_R\hat{i} + Y_R\hat{j} + Z_R\hat{k} \tag{3.18}$$

where

$$X_O = X(T) + A_1 - A_1\cos\psi + C\sin\psi \tag{3.19}$$

$$X_P = X(T) + A_1 + A_2\cos\psi + C\sin\psi \tag{3.20}$$

$$X_Q = X(T) + A_1 - A_1\cos\psi + C\sin\psi \tag{3.21}$$

$$X_R = X(T) + A_1 + A_2\cos\psi + C\sin\psi \tag{3.22}$$

$$Y_O = Y(T) + B_1 + A_1\sin\psi\sin\theta - B_1\cos\theta + C\cos\psi\sin\theta \tag{3.23}$$

$$Y_P = Y(T) + B_1 - A_2\sin\psi\sin\theta - B_1\cos\theta + C\cos\psi\sin\theta \tag{3.24}$$

$$Y_Q = Y(T) + B_1 + A_1\sin\psi\sin\theta + B_2\cos\theta + C\cos\psi\sin\theta \tag{3.25}$$

$$Y_R = Y(T) + B_1 - A_2\sin\psi\sin\theta + B_2\cos\theta + C\cos\psi\sin\theta \tag{3.26}$$

$$Z_O = Z(T) + H_o + C - A_1\sin\psi\cos\theta - B_1\sin\theta - C\cos\psi\cos\theta \tag{3.27}$$

$$Z_P = Z(T) + H_o + C + A_2\sin\psi\cos\theta - B_1\sin\theta - C\cos\psi\cos\theta \tag{3.28}$$

$$Z_Q = Z(T) + H_o + C - A_1\sin\psi\cos\theta + B_2\sin\theta - C\cos\psi\cos\theta \tag{3.29}$$

$$Z_R = Z(T) + H_o + C + A_2\sin\psi\cos\theta + B_2\sin\theta - C\cos\psi\cos\theta \tag{3.30}$$

From Equations (3.19) – (3.30), the following relationships can be established for the angles of rotation, θ and ψ (assuming that, for small angles, $\sin\psi\cos\theta \approx \sin\psi$ (Meirovitch, 1970)):

$$\sin\theta = \frac{Z_R - Z_P}{B_1 + B_2} = \frac{Z_Q - Z_O}{B_1 + B_2} \tag{3.31}$$

$$\sin\psi = \frac{Z_R - Z_Q}{A_1 + A_2} = \frac{Z_P - Z_O}{A_1 + A_2} \tag{3.32}$$

$$\cos\theta = \frac{Y_R - Y_P}{B_1 + B_2} = \frac{Y_Q - Y_O}{B_1 + B_2} \tag{3.33}$$

$$\cos\psi = \frac{X_R - X_Q}{A_1 + A_2} = \frac{X_P - X_O}{A_1 + A_2} \tag{3.34}$$

The equations of motion for the plate will be determined using Lagrange's equations. Thus, it is necessary to determine the kinetic and potential energies of all components of the system. Because it is desirable to preserve symmetry in the model for the vibration isolator, horizontal springs are added to the corners of the plate to simulate the horizontal resistance contributed by the isolators when the plate rotates. Because this horizontal motion is very small, this assumption should have a minimal effect on the results of this analysis. The springs are numbered 1 – 8 and attach to the plate as shown in Figure 3.3.

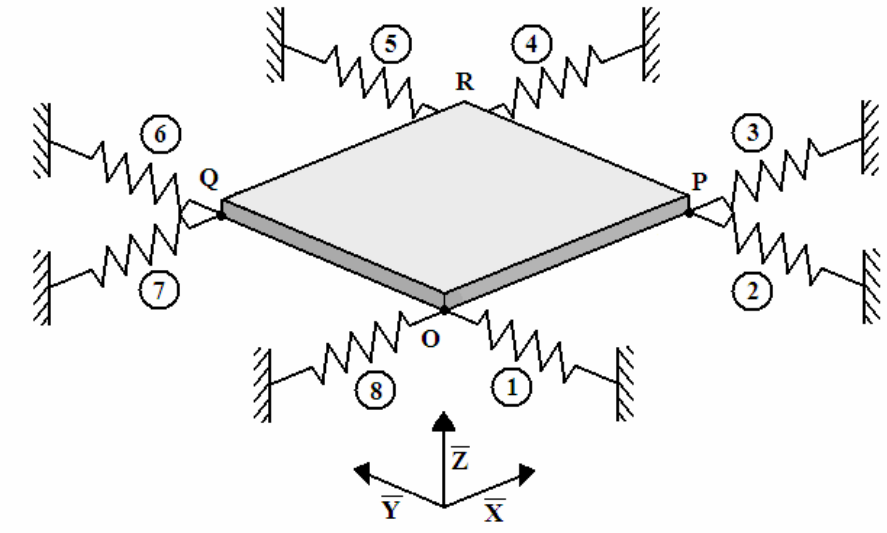

Figure 3.3: Horizontal Springs Attached to Plate

The plate has both rotational and translational kinetic energy. The translational kinetic energy for the plate with mass *M* is

$$T_{p,tr} = \frac{1}{2} M \, \dot{\bar{r}}_{c.m.} \cdot \dot{\bar{r}}_{c.m.} \tag{3.35}$$

where

$$\dot{\bar{r}}_{c.m.} = \dot{X}\hat{i} + \dot{Y}\hat{j} + \dot{Z}\hat{k} \tag{3.36}$$

Substituting Equation (3.36) into Equation (3.35) gives

$$T_{p,tr} = \frac{1}{2} M \left(\dot{X}^2 + \dot{Y}^2 + \dot{Z}^2 \right) \tag{3.37}$$

The rotational kinetic energy for the plate is defined as

$$T_{p,rot} = \frac{1}{2} \bar{\omega}_p{}^T \bar{I}_p \, \bar{\omega}_p \tag{3.38}$$

where $\bar{\omega}_p$ is the angular velocity vector and $\bar{I}_p$ is the inertia dyadic (Plaut, 1996).

The angular velocity vector $\bar{\omega}_p$ is defined as

$$\bar{\omega}_p = \dot{\theta}\hat{i}_1 - \dot{\psi}\hat{j}_2 = \dot{\theta}\hat{i} - \dot{\psi}\cos\theta\,\hat{j} - \dot{\psi}\sin\theta\hat{k} \tag{3.39}$$

The inertia dyadic is given as

$$\bar{I}_p = I_x \hat{i}_3 \cdot \hat{i}_3 + I_y \hat{j}_3 \cdot \hat{j}_3 \tag{3.40}$$

where I_x and I_y are the principal mass moments of inertia about the $\bar{X}$ and $\bar{Y}$ axes through the center of mass. The derivation of the mass moments of inertia can be found in Appendix B, and the equations for I_x and I_y are given in Equations (B.2) and (B.3).

Rewriting Equation (3.40) in terms of the unit vectors $\hat{i}$, $\hat{j}$, and $\hat{k}$, and substituting this and Equation (3.39) into Equation (3.38) gives the rotational kinetic energy of the plate as

$$T_{p,rot} = \frac{1}{2} I_x \left(\dot{\theta}\cos\psi \right)^2 + \frac{1}{2} I_y \left(\dot{\psi} \right)^2 \tag{3.41}$$

The potential energy in the springs labeled 1 – 8 in Figure 3.3 can be calculated as

$$V_{s,1} = \frac{1}{2} K_1 {Y_O}^2 \tag{3.42}$$

$$V_{s,2} = \frac{1}{2} K_2 {Y_P}^2 \tag{3.43}$$

$$V_{s,3} = \frac{1}{2} K_3 \left(X_P - A_1 - A_2 \right)^2 \tag{3.44}$$

$$V_{s,4} = \frac{1}{2} K_4 \left(X_R - A_1 - A_2 \right)^2 \tag{3.45}$$

$$V_{s,5} = \frac{1}{2} K_5 \left(Y_R - B_1 - B_2 \right)^2 \tag{3.46}$$

$$V_{s,6} = \frac{1}{2} K_6 \left(Y_Q - B_1 - B_2 \right)^2 \tag{3.47}$$

$$V_{s,7} = \frac{1}{2} K_7 {X_Q}^2 \tag{3.48}$$

$$V_{s,8} = \frac{1}{2} K_8 {X_O}^2 \tag{3.49}$$

Substituting the relationships in Equations (3.19) – (3.26) and using small-angle approximations (i.e., $\sin\psi \sin\theta \approx 0$ and $\cos\psi \sin\theta \approx \sin\theta$) gives the following equations for the potential energy:

$$V_{s,1} = \frac{1}{2} K_1 \left(Y + B_1 - B_1 \cos\theta + C \sin\theta \right)^2 \tag{3.50}$$

$$V_{s,2} = \frac{1}{2} K_2 \left(Y + B_1 - B_1 \cos\theta + C \sin\theta \right)^2 \tag{3.51}$$

$$V_{s,3} = \frac{1}{2} K_3 \left(X + A_2 \cos\psi - A_2 + C \sin\psi \right)^2 \tag{3.52}$$

$$V_{s,4} = \frac{1}{2} K_4 \left(X + A_2 \cos\psi - A_2 + C \sin\psi \right)^2 \tag{3.53}$$

$$V_{s,5} = \frac{1}{2} K_5 \left(Y + B_2 \cos\theta - B_2 + C \sin\theta \right)^2 \tag{3.54}$$

$$V_{s,6} = \frac{1}{2} K_6 \left(Y + B_2 \cos\theta - B_2 + C \sin\theta \right)^2 \tag{3.55}$$

$$V_{s,7} = \frac{1}{2} K_7 \left(X + A_1 - A_1 \cos\psi + C \sin\psi \right)^2 \tag{3.56}$$

$$V_{s,8} = \frac{1}{2} K_8 \left(X + A_1 - A_1 \cos\psi + C \sin\psi \right)^2 \tag{3.57}$$

Lagrange's equations for this system in terms of the Lagrangian L are

$$\frac{d}{dT}\left(\frac{\partial L}{\partial \dot{X}}\right) - \frac{\partial L}{\partial X} = Q_X \tag{3.58}$$

$$\frac{d}{dT}\left(\frac{\partial L}{\partial \dot{Y}}\right) - \frac{\partial L}{\partial Y} = Q_Y \tag{3.59}$$

$$\frac{d}{dT}\left(\frac{\partial L}{\partial \dot{Z}}\right) - \frac{\partial L}{\partial Z} = Q_Z \tag{3.60}$$

$$\frac{d}{dT}\left(\frac{\partial L}{\partial \dot{\theta}}\right) - \frac{\partial L}{\partial \theta} = Q_\theta \tag{3.61}$$

$$\frac{d}{dT}\left(\frac{\partial L}{\partial \dot{\psi}}\right) - \frac{\partial L}{\partial \psi} = Q_\psi \tag{3.62}$$

where $L = T - V$ and Q_X, Q_Y, Q_Z, Q_θ, and Q_ψ are the generalized forces. Substituting Equation (3.37), Equation (3.41), and Equations (3.50) – (3.57) into Equations (3.58) – (3.62) and specifying the generalized forces gives

$$M\ddot{X} + \left(K_3 + K_4\right)\left(X + A_2 \cos\psi - A_2 + C \sin\psi\right) + \left(K_7 + K_8\right)\left(X + A_1 - A_1 \cos\psi + C \sin\psi\right) = 0 \tag{3.63}$$

$$M\ddot{Y} + \left(K_1 + K_2\right)\left(Y + B_1 - B_1 \cos\theta + C \sin\theta\right) + \left(K_5 + K_6\right)\left(Y + B_2 \cos\theta - B_2 + C \sin\theta\right) = 0 \tag{3.64}$$

$$M\ddot{Z} = F_1 + F_2 + F_3 + F_4 - W \tag{3.65}$$

$$I_x \ddot{\theta} \cos\psi + \left(K_1 + K_2\right)\left(Y + B_1 - B_1 \cos\theta + C \sin\theta\right)\left(C \cos\theta + B_1 \sin\theta\right) + \left(K_5 + K_6\right)\left(Y + B_2 \cos\theta - B_2 + C \sin\theta\right)\left(C \cos\theta - B_2 \sin\theta\right) = -\left(F_1 + F_2\right)B_1 + \left(F_3 + F_4\right)B_2 \tag{3.66}$$

$$I_y \ddot{\psi} + \left(K_3 + K_4\right)\left(X + A_2 \cos\psi - A_2 + C \sin\psi\right)\left(C \cos\psi - A_2 \sin\psi\right) + \left(K_7 + K_8\right)\left(X + A_1 - A_1 \cos\psi + C \sin\psi\right)\left(C \cos\psi + A_1 \sin\psi\right) = -\left(F_1 + F_3\right)A_1 + \left(F_2 + F_4\right)A_2 \tag{3.67}$$

Note that these equations are in terms of the displacements *X*, *Y*, *Z*, θ, and ψ at the center of mass. It is desirable to write these equations in terms of the movement at the corners of the plate so that they will be compatible with the equations from the analysis of the vibration isolators.

The position vector $\bar{r}_{c.m.}$ to the center of mass can be written in terms of the position vector $\bar{r}_O$ to the point *O* on the plate. Specifically,

$$\bar{r}_{c.m.} = \bar{r}_O + A_1\hat{i}_3 + B_1\hat{j}_3 + C\hat{k}_3 \tag{3.68}$$

Recall that $\bar{r}_{c.m.}$ is also defined in terms of the *X*, *Y*, and *Z* displacements in Equation (3.10). If Equation (3.68) is put in terms of the unit vectors $\hat{i}$, $\hat{j}$, $\hat{k}$ and is equated to Equation (3.10), the following relationships for the displacements *X*, *Y*, and *Z* can be formed:

$$X = X_O - A_1 + A_1\cos\psi - C\sin\psi \tag{3.69}$$

$$Y = Y_O - B_1 - A_1\sin\psi\sin\theta + B_1\cos\theta - C\cos\psi\sin\theta \tag{3.70}$$

$$Z = Z_O - H_O - C + A_1\sin\psi\cos\theta + B_1\sin\theta + C\cos\psi\cos\theta \tag{3.71}$$

Using Equations (3.31) – (3.34) and small-angle approximations (i.e., $\sin\psi\sin\theta \approx 0$, $\sin\psi\cos\theta \approx \sin\psi$, and $\cos\psi\sin\theta \approx \sin\theta$), Equations (3.69) – (3.71) become

$$X = X_O - A_1 + \frac{A_1}{A_1 + A_2}(X_P - X_O) - \frac{C}{A_1 + A_2}(Z_P - Z_O) \tag{3.72}$$

$$Y = Y_O - B_1 + \frac{B_1}{B_1 + B_2}(Y_Q - Y_O) - \frac{C}{B_1 + B_2}(Z_Q - Z_O) \tag{3.73}$$

$$Z = Z_O - H_O - C + \frac{A_1}{A_1 + A_2}(Z_P - Z_O) + \frac{B_1}{B_1 + B_2}(Z_Q - Z_O) + C\frac{(X_P - X_O)(Y_Q - Y_O)}{(A_1 + A_2)(B_1 + B_2)} \tag{3.74}$$

By differentiating Equations (3.72) – (3.74) twice and dropping the higher order terms, the equations for the accelerations $\ddot{X}$, $\ddot{Y}$, and $\ddot{Z}$ are

$$\ddot{X} = \frac{1}{A_1 + A_2}\left(A_1\ddot{X}_P + A_2\ddot{X}_O - C\ddot{Z}_P + C\ddot{Z}_O\right) \tag{3.75}$$

$$\ddot{Y} = \frac{1}{B_1 + B_2}\left(B_1\ddot{Y}_Q + B_2\ddot{Y}_O - C\ddot{Z}_Q + C\ddot{Z}_O\right) \tag{3.76}$$

$$\ddot{Z} = \frac{1}{A_1 + A_2}\left(A_1\ddot{Z}_P + A_2\ddot{Z}_O + C\ddot{X}_P - C\ddot{X}_O\right) + \frac{1}{B_1 + B_2}\left[B_1\left(\ddot{Z}_Q - \ddot{Z}_O\right) + C\left(\ddot{Y}_Q - \ddot{Y}_O\right)\right] \tag{3.77}$$

Recall that the angles θ and ψ can be related to the coordinates of the corners of the plate in Equations (3.31) and (3.32). Using small-angle approximations (i.e., $\sin\theta \approx \theta$ and $\sin\psi \approx \psi$), θ and ψ can be approximated as

$$\theta \approx \frac{Z_Q - Z_O}{B_1 + B_2} \tag{3.78}$$

$$\psi \approx \frac{Z_P - Z_O}{A_1 + A_2} \tag{3.79}$$

Taking the second derivative of Equations (3.78) and (3.79) gives

$$\ddot{\theta} = \frac{1}{B_1 + B_2}\left(\ddot{Z}_Q - \ddot{Z}_O\right) \tag{3.80}$$

$$\ddot{\psi} = \frac{1}{A_1 + A_2}\left(\ddot{Z}_P - \ddot{Z}_O\right) \tag{3.81}$$

Substituting Equations (3.31) – (3.34), Equations (3.72) – (3.77), and Equations (3.80) – (3.81) into Equations (3.63) – (3.67) gives the equations of motion as

$$\frac{M}{A_1 + A_2}\left(A_1\ddot{X}_P + A_2\ddot{X}_O - C\ddot{Z}_P + C\ddot{Z}_O\right) + \left(K_3 + K_4\right)\left(X_P - A_1 - A_2\right) + \left(K_7 + K_8\right)X_O = 0 \tag{3.82}$$

$$\frac{M}{B_1 + B_2}\left(B_1\ddot{Y}_Q + B_2\ddot{Y}_O - C\ddot{Z}_Q + C\ddot{Z}_O\right) + \left(K_1 + K_2\right)Y_O + \left(K_5 + K_6\right)\left(Y_Q - B_1 - B_2\right) = 0 \tag{3.83}$$

$$\frac{M}{A_1 + A_2}\left(A_1\ddot{Z}_P + A_2\ddot{Z}_O + C\ddot{X}_P - C\ddot{X}_O\right) + \frac{M}{B_1 + B_2}\left(B_1\ddot{Z}_Q - B_1\ddot{Z}_O + C\ddot{Y}_Q - C\ddot{Y}_O\right) = F_1 + F_2 + F_3 + F_4 - W \tag{3.84}$$

$$\frac{I_x}{B_1 + B_2}\left(\ddot{Z}_Q - \ddot{Z}_O\right) + \left(\frac{K_1 + K_2}{B_1 + B_2}\right)\cdot Y_O\left[C\left(Y_Q - Y_O\right) + B_1\left(Z_Q - Z_O\right)\right] + \left(\frac{K_5 + K_6}{B_1 + B_2}\right)\left(Y_Q - B_1 - B_2\right)\left[C\left(Y_Q - Y_O\right) - B_2\left(Z_Q - Z_O\right)\right] = -\left(F_1 + F_2\right)B_1 + \left(F_3 + F_4\right)B_2 \tag{3.85}$$

$$\frac{I_Y}{A_1+A_2}\left(\ddot{Z}_P-\ddot{Z}_O\right)+\left(\frac{K_3+K_4}{A_1+A_2}\right)\left(X_P-A_1-A_2\right)\left[C\left(X_P-X_O\right)-A_2\left(Z_P-Z_O\right)\right]+$$
$$\left(\frac{K_7+K_8}{A_1+A_2}\right)\cdot X_O\left[C\left(X_P-X_O\right)+A_1\left(Z_P-Z_O\right)\right]=-\left(F_1+F_3\right)A_1+\left(F_2+F_4\right)A_2 \tag{3.86}$$

From continuity, the vertical displacement at a given corner is equal to the *X*-direction displacement at the end of the strut of the isolator attached at that corner. Specifically, $Z_O = X_1(L,T)$, $Z_P = X_2(L,T)$, $Z_Q = X_3(L,T)$, and $Z_R = X_4(L,T)$. The strut displacements $X_1(L,T)$, $X_2(L,T)$, $X_3(L,T)$, and $X_4(L,T)$ can be written in terms of the equilibrium and dynamic parts of the motion. Thus, locations of the corners *O*, *P*, *Q*, and *R* of the plate at any time *T* are given by the following equations:

$$Z_O = H_o + X_{1,d}(L)\, e^{\mathbb{i}\Omega T} \tag{3.87}$$

$$Z_P = H_o + X_{2,d}(L)\, e^{\mathbb{i}\Omega T} \tag{3.88}$$

$$Z_Q = H_o + X_{3,d}(L)\, e^{\mathbb{i}\Omega T} \tag{3.89}$$

$$Z_R = H_o + X_{4,d}(L)\, e^{\mathbb{i}\Omega T} \tag{3.90}$$

where $\mathbb{i}$ is the imaginary unit (i.e., $\mathbb{i} = \sqrt{-1}$) and Ω is the forcing frequency. The subscript *d* is used to indicate variables which result from the dynamic analysis. Note that the equilibrium height H_o has been substituted for the location of the top of the strut when the system is in equilibrium.

Similarly, using the equilibrium values for the coordinates of the plate corners, the $\overline{X}$ and $\overline{Y}$ direction displacements at the corners of the plate can be written as

$$X_O = X_{O,d}\, e^{\mathbb{i}\Omega T} \tag{3.91}$$

$$X_P = A_1 + A_2 + X_{P,d}\, e^{\mathbb{i}\Omega T} \tag{3.92}$$

$$X_Q = X_{Q,d}\, e^{\mathbb{i}\Omega T} \tag{3.93}$$

$$X_R = A_1 + A_2 + X_{R,d}\, e^{\mathbb{i}\Omega T} \tag{3.94}$$

$$Y_O = Y_{O,d}\, e^{\mathbb{i}\Omega T} \tag{3.95}$$

$$Y_P = Y_{P,d}\ e^{\mathbb{i}\Omega T} \tag{3.96}$$

$$Y_Q = B_1 + B_2 + Y_{Q,d}\ e^{\mathbb{i}\Omega T} \tag{3.97}$$

$$Y_R = B_1 + B_2 + Y_{R,d}\ e^{\mathbb{i}\Omega T} \tag{3.98}$$

Using symmetry, the forces transmitted from the plate to each isolator can be put in terms of the axial force on one of the struts in the isolator. Again the forces are broken into equilibrium and dynamic parts. Thus, the forces F_1, F_2, F_3, and F_4 are defined as

$$F_1 = 2P_{1,e} + 2P_{1,d}\ e^{\mathbb{i}\Omega T} \tag{3.99}$$

$$F_2 = 2P_{2,e} + 2P_{2,d}\ e^{\mathbb{i}\Omega T} \tag{3.100}$$

$$F_3 = 2P_{3,e} + 2P_{3,d}\ e^{\mathbb{i}\Omega T} \tag{3.101}$$

$$F_4 = 2P_{4,e} + 2P_{4,d}\ e^{\mathbb{i}\Omega T} \tag{3.102}$$

Equations (3.84) – (3.99) can be substituted into Equations (3.79) – (3.83) and the equilibrium part of each equation can be dropped from both sides of the equation. With only the dynamic part left, all higher-order terms (i.e., terms multiplied by $\left[e^{\mathbb{i}\Omega T}\right]^2$) can be canceled from the equation and the remaining terms have a common factor of $e^{\mathbb{i}\Omega T}$. After dividing by $e^{\mathbb{i}\Omega T}$, the equations of motion for the plate become

$$-\frac{M\Omega^2}{A_1 + A_2}\left[A_1 X_{P,d} + A_2 X_{O,d} - CX_{2,d}(L) + CX_{1,d}(L)\right] + \left(K_3 + K_4\right)X_{P,d} + \left(K_7 + K_8\right)X_{O,d} = 0 \tag{3.103}$$

$$-\frac{M\Omega^2}{B_1 + B_2}\left[B_1 Y_{Q,d} + B_2 Y_{O,d} - CX_{3,d}(L) + CX_{1,d}(L)\right] + \left(K_1 + K_2\right)Y_{O,d} + \left(K_5 + K_6\right)Y_{Q,d} = 0 \tag{3.104}$$

$$-\frac{M\Omega^2}{A_1 + A_2}\left[A_1 X_{2,d}(L) + A_2 X_{1,d}(L) + CX_{P,d} - CX_{O,d}\right] -$$

$$\frac{M\Omega^2}{B_1 + B_2}\left[B_1 X_{3,d}(L) - B_1 X_{1,d}(L) + CY_{Q,d} - CY_{O,d}\right] = 2\left[P_{1,d}(L) + P_{2,d}(L) + P_{3,d}(L) + P_{4,d}(L)\right] \tag{3.105}$$

$$-\frac{I_x\Omega^2}{B_1+B_2}\left[X_{3,d}(L)-X_{1,d}(L)\right]=-2\left[P_{1,d}(L)+P_{2,d}(L)\right]B_1+2\left[P_{3,d}(L)+P_{4,d}(L)\right]B_2 \qquad (3.106)$$

$$-\frac{I_y\Omega^2}{A_1+A_2}\left[X_{2,d}(L)-X_{1,d}(L)\right]=-2\left[P_{1,d}(L)+P_{3,d}(L)\right]A_1+2\left[P_{2,d}(L)+P_{4,d}(L)\right]A_2 \qquad (3.107)$$

Using the relationships for $\sin\theta$ and $\cos\theta$ in Equations (3.31) and (3.33), the following geometric relationship can be obtained:

$$(Z_Q - Z_O)\cos\theta = (Y_Q - Y_O)\sin\theta \qquad (3.108)$$

After making some substitutions and manipulations, this equation results in the following constraint:

$$Y_{Q,d} = Y_{O,d} \qquad (3.109)$$

Similarly, Equations (3.32) and (3.34) can be used to establish the following relationship:

$$(Z_P - Z_O)\cos\psi = (X_P - X_O)\sin\psi \qquad (3.110)$$

After making some substitutions and manipulations, this equation results in the following constraint:

$$X_{P,d} = X_{O,d} \qquad (3.111)$$

3.2 Analysis of the Vibration Isolator

Figure 3.4 shows the isolator subjected to a harmonic base excitation $U(T)$, where $U(T)$ was defined in Section 1.4 as $U(T) = U_o \cdot \sin(\Omega T)$. This imposed base displacement is resisted at the top of the isolator by the force F_i, which is now a portion of the combined effects of the weight W of the plate and the inertial load from the mass of the plate. In the analysis of the vibration isolator, it is again assumed that the horizontal movements $X_{O,d}$, $X_{P,d}$, $X_{Q,d}$, $X_{R,d}$, $Y_{O,d}$, $Y_{P,d}$, $Y_{Q,d}$, and $Y_{R,d}$ at the corners of the plate are small enough that they can be neglected and symmetry can be used in the analysis of each isolator.

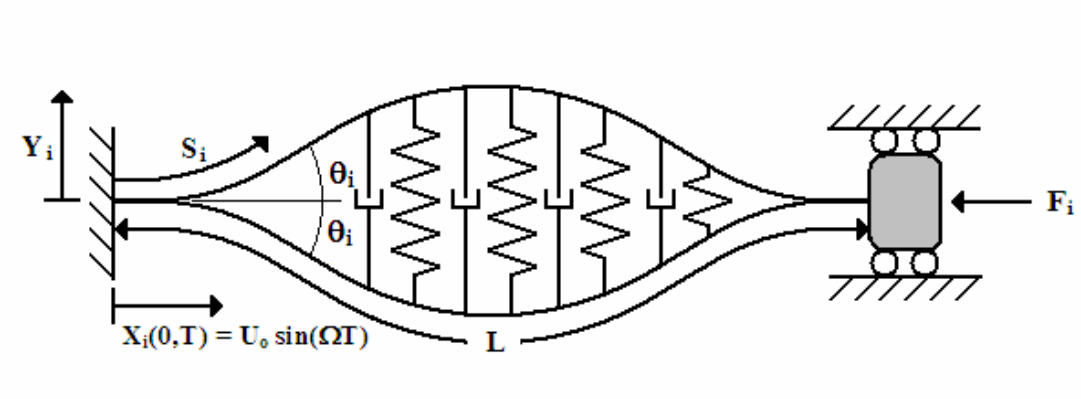

Figure 3.4: Isolator Under Forced Harmonic Excitation

In order to analyze the behavior of each isolator, a free-body diagram of an element of the strut is drawn using D'Alembert's principle. The free-body diagram includes the forces due to the stiffness and damping contributed by the filler in addition to the fictitious inertia forces due to the mass of the strut. The inertia forces act in the opposite direction of the acceleration of the strut and are equal to the product of the strut's mass per unit length and its acceleration in the *X* and *Y* directions (Chopra, 2001).

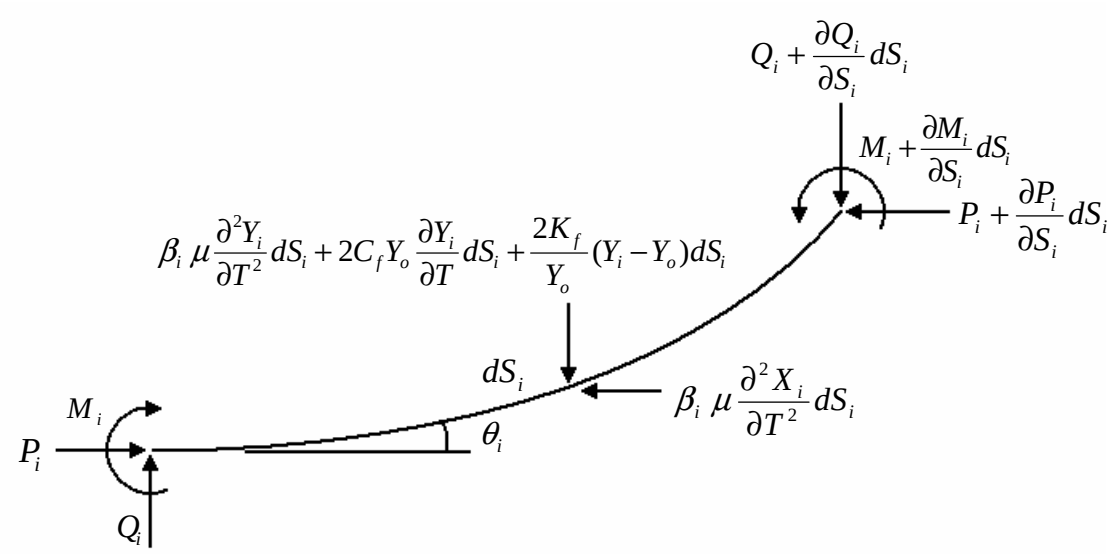

Figure 3.5: Free-Body Diagram of an Element of the Strut Under Forced Harmonic Vibration

Notice that the mass per unit length μ of the strut is multiplied by the factor β_i that was used to adjust the bending stiffness *EI* in the equilibrium analysis. Assuming that the same material is used in each strut (i.e., the modulus of elasticity *E* remains constant), the bending stiffness can be modified by changing the cross-section of the strut so that the

moment of inertia about the axis of bending becomes $\beta_i I$. If the cross-section of the strut is a rectangle with a width b and a thickness h as shown in Figure 3.6(a), the moment of inertia can be modified by a factor of β_i by simply changing the width b of the section by a factor of β_i, as shown in Figure 3.6(b). In doing so, the area of the section changes by the same factor β_i and, assuming that the material has a constant density, the mass of the strut also changes by the same factor β_i. Thus, each strut has a mass $\beta_i \mu$.

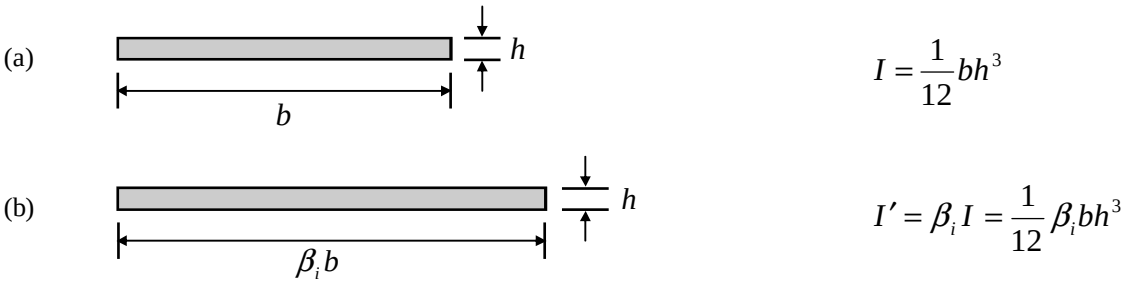

Figure 3.6: Cross-Section of Strut (a) Before and (b) After Modifying the Bending Stiffness

From the geometry, equilibrium, and the elastic constitutive laws for the strut, the following relationships can be established for the strut subjected to forced harmonic vibrations:

$$\frac{\partial X_i}{\partial S_i} = \cos\theta_i \tag{3.112}$$

$$\frac{\partial Y_i}{\partial S_i} = \sin\theta_i \tag{3.113}$$

$$\frac{\partial \theta_i}{\partial S_i} = \frac{M_i}{\beta_i EI} + \frac{2\pi}{L} a_o \cos\left(\frac{2\pi S_i}{L}\right) \tag{3.114}$$

$$\frac{\partial M_i}{\partial S_i} = -P_i \sin\theta_i + Q_i \cos\theta_i \tag{3.115}$$

$$\frac{\partial P_i}{\partial S_i} = -\beta_i \mu \frac{\partial^2 X_i}{\partial T^2} \tag{3.116}$$

$$\frac{\partial Q_i}{\partial S_i} = -\beta_i \mu \frac{\partial^2 Y_i}{\partial T^2} - 2C_f Y_o \frac{\partial Y_i}{\partial T} - \frac{2K_f}{Y_o} \cdot (Y_i - Y_o) \tag{3.117}$$

Each of these variables can be written in terms of the equilibrium and dynamic parts of the motion. Specifically,

$$X_i(S_i,T) = X_{i,e}(S_i) + X_{i,d}(S_i)\, e^{\mathbb{i}\Omega T} \tag{3.118}$$

$$Y_i(S_i,T) = Y_{i,e}(S_i) + Y_{i,d}(S_i)\, e^{\mathbb{i}\Omega T} \tag{3.119}$$

$$\theta_i(S_i,T) = \theta_{i,e}(S_i) + \theta_{i,d}(S_i)\, e^{\mathbb{i}\Omega T} \tag{3.120}$$

$$M_i(S_i,T) = M_{i,e}(S_i) + M_{i,d}(S_i)\, e^{\mathbb{i}\Omega T} \tag{3.121}$$

$$P_i(S_i,T) = P_{i,e} + P_{i,d}(S_i)\, e^{\mathbb{i}\Omega T} \tag{3.122}$$

$$Q_i(S_i,T) = Q_{i,e}(S_i) + Q_{i,d}(S_i)\, e^{\mathbb{i}\Omega T} \tag{3.123}$$

Equations (3.118) – (3.123) can be substituted into Equations (3.112) – (3.117) and, using small-angle approximations, the equilibrium portions of the equations can be dropped from both sides of the equations (see Equations (2.7) – (2.10) and (2.13)). After dropping all higher-order terms (i.e., terms multiplied by $\left[e^{\mathbb{i}\Omega T}\right]^2$), the equations for the dynamic parts of the motion become:

$$\frac{dX_{i,d}}{dS_i} = -\theta_{i,d}\sin\theta_{i,e} \tag{3.124}$$

$$\frac{dY_{i,d}}{dS_i} = \theta_{i,d}\cos\theta_{i,e} \tag{3.125}$$

$$\frac{d\theta_{i,d}}{dS_i} = \frac{M_{i,d}}{\beta_i EI} \tag{3.126}$$

$$\frac{dM_{i,d}}{dS_i} = \left(Q_{i,d} - P_{i,e}\theta_{i,d}\right)\cos\theta_{i,e} - \left(P_{i,d} + Q_{i,e}\theta_{i,d}\right)\sin\theta_{i,e} \tag{3.127}$$

$$\frac{dP_{i,d}}{dS_i} = \beta_i \mu \Omega^2 X_{i,d} \tag{3.128}$$

$$\frac{dQ_{i,d}}{dS_i} = \left(\beta_i \mu \Omega^2 - \mathbb{i}\Omega\left(2C_f Y_o\right) - \frac{2K_f}{Y_o}\right)\cdot Y_{i,d} \tag{3.129}$$

3.3 Nondimensionalization

Equations (3.103) – (3.107), (3.109), (3.111), and (3.124) – (3.129) will now be put in nondimensional form.

If p_w is defined as the ratio of the weight of the plate to the weight of one strut (i.e., $p_w = \frac{W}{\mu g L}$) and the nondimensional weight of the plate w is defined in Equation (2.28), then a stiffness parameter r can be defined as the ratio of p_w to w. Specifically,

$$r = \frac{EI}{\mu g L (A_1 + A_2)^2} \tag{3.130}$$

Using the stiffness parameter r, the total mass of the plate can be defined in terms of the total nondimensional weight w as

$$m = rw \tag{3.131}$$

Using the subscript j to indicate the number of the horizontal spring (refer to Figure 3.3 for the location of each spring), the stiffnesses of the springs 1 – 8 can be nondimensionalized as

$$k_j = \frac{K_j (A_1 + A_2)^3}{EI} \tag{3.132}$$

The remaining nondimensional variables are defined as follows:

$$\omega = \Omega \sqrt{\frac{\mu L^4}{EI}} \qquad t = T \sqrt{\frac{EI}{\mu L^4}} \tag{3.133, 3.134}$$

$$x_{O,d} = \frac{X_{O,d}}{A_1 + A_2} \qquad x_{P,d} = \frac{X_{P,d}}{A_1 + A_2} \tag{3.135, 3.136}$$

$$y_{O,d} = \frac{Y_{O,d}}{A_1 + A_2} \qquad y_{Q,d} = \frac{Y_{Q,d}}{A_1 + A_2} \tag{3.137, 3.138}$$

$$x_{i,d} = \frac{X_{i,d}}{A_1 + A_2} \qquad y_{i,d} = \frac{Y_{i,d}}{A_1 + A_2} \tag{3.139, 3.140}$$

$$u_o = \frac{U_o}{A_1 + A_2} \qquad p_{i,d} = \frac{P_{i,d}\left(A_1 + A_2\right)^2}{EI} \tag{3.141, 3.142}$$

$$q_{i,d} = \frac{Q_{i,d}\left(A_1 + A_2\right)^2}{EI} \qquad m_{i,d} = \frac{M_{i,d}\left(A_1 + A_2\right)}{EI} \tag{3.143, 3.144}$$

$$c_f = \frac{2C_f\left(A_1 + A_2\right)^3}{\sqrt{\mu EI}} \tag{3.145}$$

In addition, the vertical distance C from the bottom of the plate to the centroid is nondimensionalized in Equation (B.7) in Appendix B, and the nondimensional mass moments of inertia i_x and i_y are given in Equations (B.15) – (B.16).

Using the relationships in Equations (3.135) – (3.138), Equations (3.109) and (3.111) become:

$$y_{O,d} = y_{Q,d} \tag{3.146}$$

$$x_{O,d} = x_{P,d} \tag{3.147}$$

Using the nondimensional variables defined in Equations (2.16) – (2.31), Equations (3.131) – (3.145), Equation (B.7), and Equations (B.15) – (B.16), the equations of motion for the plate can be put in nondimensional form as

$$-rw\omega^2\left[a_1 x_{P,d} + a_2 x_{O,d} - cx_{2,d}(l) + cx_{1,d}(l)\right] + \left(k_3 + k_4\right)x_{P,d} + \left(k_7 + k_8\right)x_{O,d} = 0 \tag{3.148}$$

$$-\frac{rw\omega^2}{\alpha}\left[b_1 y_{Q,d} + b_2 y_{O,d} - cx_{3,d}(l) + cx_{1,d}(l)\right] + \left(k_1 + k_2\right)y_{O,d} + \left(k_5 + k_6\right)y_{Q,d} = 0 \tag{3.149}$$

$$-rw\omega^2\left[a_1 x_{2,d}(l) + a_2 x_{1,d}(l) + cx_{P,d} - cx_{O,d}\right] - \frac{rw\omega^2}{\alpha}\left[b_1 x_{3,d}(l) - b_1 x_{1,d}(l) + cy_{Q,d} - cy_{O,d}\right]$$
$$= 2\left[p_{1,d}(l) + p_{2,d}(l) + p_{3,d}(l) + p_{4,d}(l)\right] \tag{3.150}$$

$$-\frac{i_x\omega^2}{\alpha}\left[x_{3,d}(l) - x_{1,d}(l)\right] = -2\left[p_{1,d}(l) + p_{2,d}(l)\right]b_1 + 2\left[p_{3,d}(l) + p_{4,d}(l)\right]b_2 \tag{3.151}$$

$$-i_y\omega^2\left[x_{2,d}(l) - x_{1,d}(l)\right] = -2\left[p_{1,d}(l) + p_{3,d}(l)\right]a_1 + 2\left[p_{2,d}(l) + p_{4,d}(l)\right]a_2 \tag{3.152}$$

Similarly, the dynamic equations for the strut can be written as

$$\frac{dx_{i,d}}{ds_i} = -\theta_{i,d} \sin\theta_{i,e} \tag{3.153}$$

$$\frac{dy_{i,d}}{ds_i} = \theta_{i,d} \cos\theta_{i,e} \tag{3.154}$$

$$\frac{d\theta_{i,d}}{ds_i} = \frac{m_{i,d}}{\beta_i} \tag{3.155}$$

$$\frac{dm_{i,d}}{ds_i} = \left(q_{i,d} - p_{i,e}\theta_{i,d}\right)\cos\theta_{i,e} - \left(p_{i,d} + q_{i,e}\theta_{i,d}\right)\sin\theta_{i,e} \tag{3.156}$$

$$\frac{dp_{i,d}}{ds_i} = \beta_i \omega^2 x_{i,d} \tag{3.157}$$

$$\frac{dq_{i,d}}{ds_i} = \left(\beta_i \omega^2 - \mathbb{i}\,\omega c_f y_o - \frac{k_f}{y_o}\right) \cdot y_{i,d} \tag{3.158}$$

The boundary conditions required to solve Equations (3.153) – (3.158) are as follows. At $s_i = 0$, the strut is restrained against *Y*-direction displacements $\{ y_{i,d}(0) = 0 \}$ and against rotation $\{ \theta_{i,d}(0) = 0 \}$. At $s_i = 0$, the *X*-direction displacement is set equal to the amplitude of the base displacement $\{ x_{i,d}(0) = u_o \}$. At $s_i = 1$, the strut is assumed to be restrained against *Y*-direction displacement $\{ y_{i,d}(1) = 0 \}$ and against rotation $\{ \theta_{i,d}(1) = 0 \}$.

A program written in Mathematica is used to numerically solve Equations (3.153) – (3.158) using the conditions specified in Equations (3.146) – (3.152) and the boundary conditions for the struts. Similar to the equilibrium program in Appendix A, the dynamic program uses a shooting method to iteratively solve the equations for the struts using the results from the equilibrium analysis along with the conditions specified for the dynamic analysis. Values for the filler stiffness c_f, the horizontal spring stiffnesses $k_1 – k_8$, and the plate and block dimensions h_1, h_2, and d defined in Appendix B are entered into the program in addition to initial guesses for the horizontal movements $x_{O,d}$, $x_{P,d}$, $y_{O,d}$, and

$y_{Q,d}$ at the corners of the plate, the axial force $p_{i,d}$ in each strut, and the shear forces $q_{i,d}(0)$ and the bending moments $m_{i,d}(0)$ at the base of each strut. A printout of the dynamic program can be found in Appendix C.

The transmissibility for the system will be calculated as the average transmissibility of the four corners of the plate. The transmissibility at each corner will depend on the vertical motion of the isolator attached to the corner and the amplitude of the base displacement. The vertical motion will consist of both real and imaginary parts, and so the square root of the sum of the squares of the real and imaginary parts will be used to determine the vertical motion at a corner. The transmissibility at the top of the i^{th} isolator is defined as

$$TR_i = \frac{\sqrt{\left\{\mathrm{Re}\left[x_{i,d}(1)\right]\right\}^2 + \left\{\mathrm{Im}\left[x_{i,d}(1)\right]\right\}^2}}{\left|u_o\right|} \tag{3.159}$$

Using an average value of the transmissibility at the corners of the plate, the transmissibility of the system is defined as

$$TR = \frac{TR_1 + TR_2 + TR_3 + TR_4}{4} \tag{3.160}$$

Chapter 4: Analysis and Results

Using the Mathematica program in Appendix C, the equations of motion derived in Chapter 3 for the system are numerically solved for various cases with increasing complexity. First, the system is analyzed for the fully symmetric case, i.e., the center of mass is positioned at the geometric center of the plate, as shown in Figure 4.1(a). Secondly, the center of mass is positioned at several points along a line that runs through the center of the plate perpendicular to the edge *OQ* of the plate, as shown in Figure 4.1(b). Thirdly, the center of mass is positioned at several points along a line of symmetry that passes diagonally from corner *O* to corner *R*, as shown in Figure 4.1(c). Lastly, the center of mass is arbitrarily positioned such that no symmetry exists in the system, as shown in Figure 4.1(d).

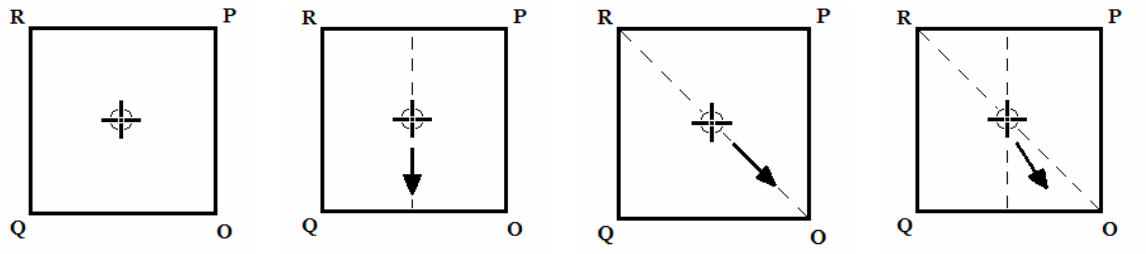

(a) (b) (c) (d)

Figure 4.1: Location of the Center of Mass for (a) Case 1, (b) Case 2, (c) Case 3, and (d) Case 4

For each of these cases, the transmissibility is computed and plotted for a wide range of nondimensional excitation frequencies. The transmissibility plots are used to recognize frequencies at which resonance occurs in the system and frequency ranges in which the transmissibility is small. At the resonant frequencies, the physical behavior of the system is analyzed to understand what types of vibration modes occur in the system. In order to obtain a better understanding of resonance in the system, a free vibration analysis is also performed. The results from the free vibration analysis can be found in the last section in this chapter.

4.1 Forced Vibration Analysis

Using the Mathematica program in Appendix C, the equations of motion are solved for the four cases shown in Figure 4.1. For all cases, the nondimensional weight w is set at 320, as was done in the equilibrium analysis. Similarly, the initial amplitude a_o of the struts and the stiffness parameter k_f are each assigned a value of 0.1. The filler is given a damping coefficient c_f of 1, and the stiffnesses k_j of the eight horizontal springs attached to the plate are each set at 0.1. The aspect ratio α of the plate is set equal to 1 for all cases, meaning that the plate remains square in this analysis. This will allow for a special case of symmetry (e.g., Case 3 discussed on pages 53 to 61) to be analyzed which only exists for a square. The plate and block dimensions h_1, h_2, and d required to calculate the vertical distance c to the center of mass and the mass moments of inertia, i_x and i_y (see Appendix B), are set equal to 0.05, 0.3, and 0.3, respectively. The stiffness modification factor β_i and the equilibrium portion of the axial force $p_{i,e}$, the shear force $q_{i,e}$, and the bending moment $m_{i,e}$ for each strut are obtained from the equilibrium analysis. From the solution of the equations of motion, the transmissibility TR is calculated for various excitation frequencies ω using Equations (3.159) and (3.160).

Case 1

First, the system is analyzed for the case where the center of mass is located at the geometric center of the plate, as shown in Figure 4.1(a). To do this, the nondimensional variables a_1 and b_1 are both set at 0.5 in the program. Because of the symmetry, the plate does not rotate for this case, and so the plate moves with only one degree of freedom. This is the base case and will be used to compare the results of the remaining cases.

In Figure 4.2, the transmissibility is plotted for nondimensional excitation frequencies ranging from 0.1 to 100. The transmissibility plot has three distinct peaks which occur at frequencies $\omega_1 = 0.922$, $\omega_2 = 44.48$, and $\omega_3 = 78.53$. Between each of these peaks, the transmissibility drops well below unity for a wide range of excitation frequencies. The region between the first and second peak is of particular interest because it is likely that this isolation device would be used to isolate vibrations in this range of frequencies.

At the first resonant frequency ω_1, the transmissibility reaches a maximum value of approximately 2250. This means that the ground motion is amplified more than 2000 times, which seems highly unrealistic. Recall that the magnitude of the transmissibility at a peak is dependent on the damping in the system. In this analysis, it was assumed that the filler is the only source of damping in the system. This assumption is unreasonable because there are a number of other sources in the real system that would provide damping (e.g., the connections between the isolator and the plate). Thus, the magnitude of the response for the real system would be substantially less than the magnitude of the response for the theoretical system. However, the frequency at which the peaks occur in the transmissibility plots and the vibration modes which occur at these peaks are practically independent of the amount of damping, and so the theoretical system is still quite useful for analyzing the behavior of the system presented in this thesis.

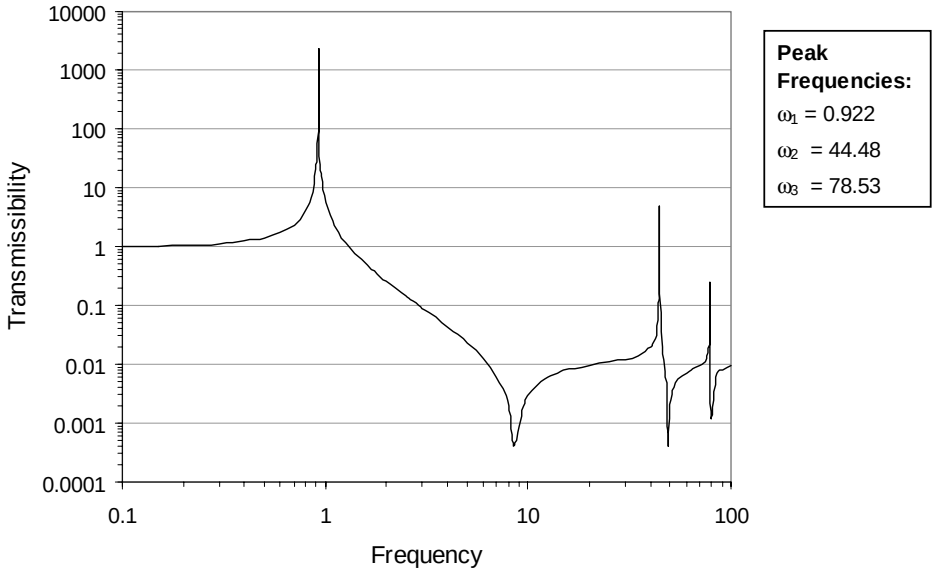

Figure 4.2: Transmissibility vs. Frequency for the Fully Symmetric Case **(**$a_1 = 0.5$, $b_1 = 0.5$)

The vibration modes for one of the struts in each isolator at the resonant frequencies ω_1, ω_2, and ω_3 are shown in Figure 4.3. In each of these figures, the horizontal deflection $y_{i,d}$ caused by a base displacement with a nondimensional amplitude u_o of 0.001 is plotted along the length of the strut. Because of symmetry, all four isolators have the same shape. At the first resonant frequency, the vertical displacement $x_{i,d}$ at the top of each strut has a magnitude of 2.21, meaning that the first vibration mode corresponds to a large vertical

displacement of the plate. At the second and third resonant frequencies, the vertical movement of the plate is relatively small ($x_{i,d}$ equals 0.004 at the second resonant frequency, and $x_{i,d}$ equals 0.0002 at the third resonant frequency), but the struts exhibit distinct vibration modes, similar to those observed in previous analyses performed by Sidbury (2003) and Favor (2004) for the single-strut isolator. In each of these vibration modes, the horizontal deflection of the strut from equilibrium is extremely large.

Frequency	0.922	44.48	78.53
y_d **for Struts 1-4**	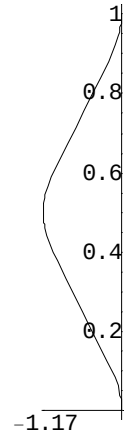	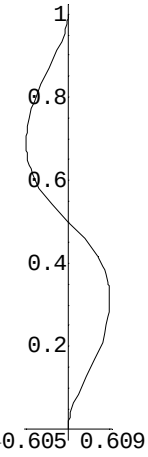	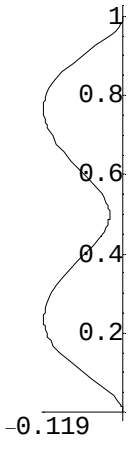

Figure 4.3: Resonant Vibration Modes for the Symmetric Case ($a_1 = 0.5$, $b_1 = 0.5$)

Case 2

The second case to be analyzed is the case where the center of mass is positioned at several points along a line that runs through the center of the plate perpendicular to the edge *OQ* of the plate, as shown in Figure 4.1(b). For this case, the plate moves with two degrees of freedom, i.e., the plate will move vertically and/or rotate at an angle ψ about the *Y*-axis when the system is subjected to a base excitation. In this analysis, the distance b_1 is fixed at 0.5 and the distance a_1 is varied from 0.45 to 0.3 in increments of 0.05. Note that as a_1 decreases, the eccentricity of the weight increases.

In Figures 4.4 – 4.7, the transmissibility is plotted for nondimensional frequencies ranging from 0.1 to 100. On each plot, the results from the analysis of the symmetric case (i.e., Case 1) are included so that it is easy to see how the transmissibility changes for various eccentricities. The most notable observation is that the eccentricity introduces an

additional peak in each transmissibility plot at a frequency slightly higher than the first resonant frequency. This peak occurs over a very small range of frequencies, and the maximum transmissibility at this peak appears to become larger as the eccentricity increases (i.e., as a_1 becomes smaller). The physical behavior of the system at this resonant frequency will be investigated in the analysis of the vibration modes to determine the source of this additional peak and the reason for the increase in the transmissibility with increasing eccentricity.

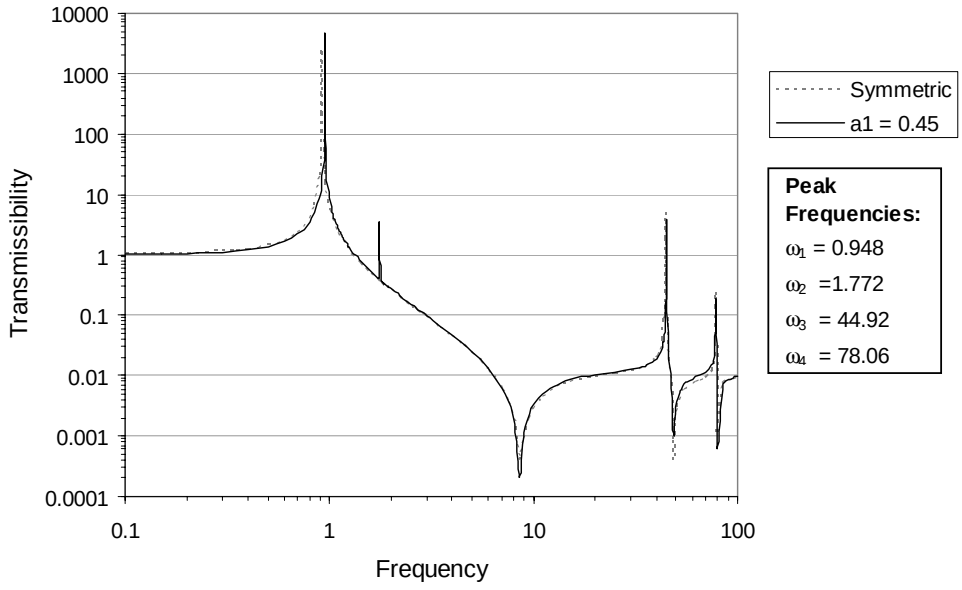

Figure 4.4: Transmissibility vs. Frequency for Center of Mass Positioned at $a_1 = 0.45$, $b_1 = 0.5$

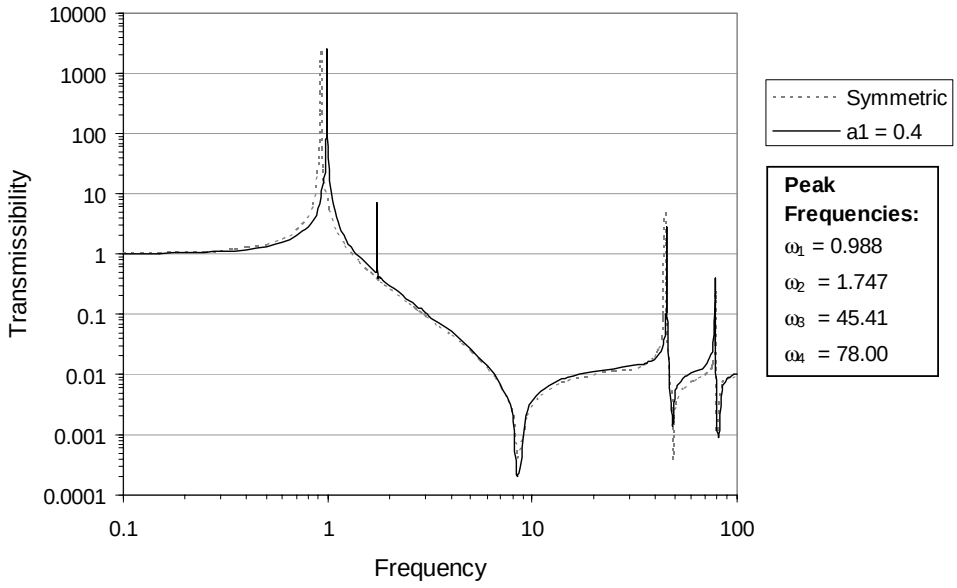

Figure 4.5: Transmissibility vs. Frequency for Center of Mass Positioned at $a_1 = 0.4$, $b_1 = 0.5$

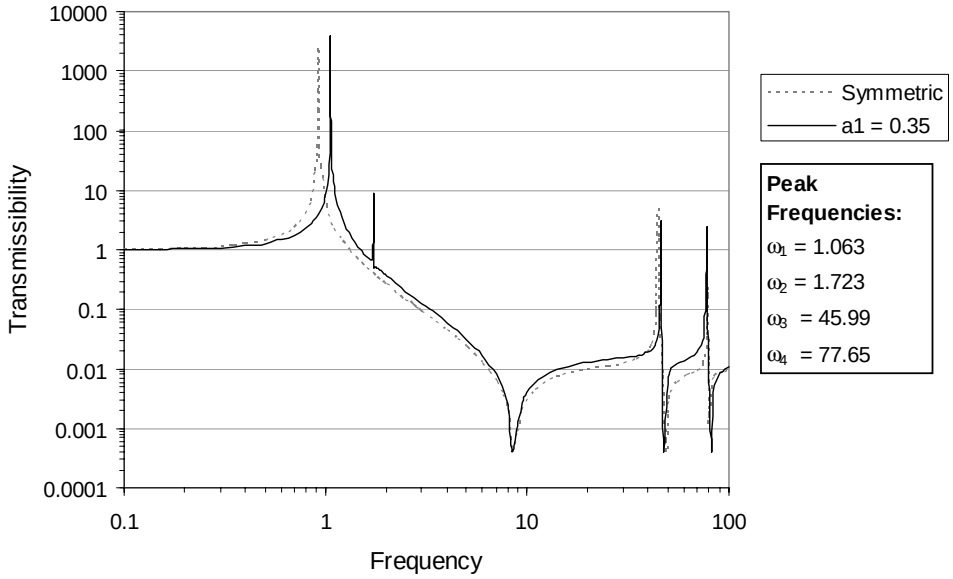

Figure 4.6: Transmissibility vs. Frequency for Center of Mass Positioned at $a_1 = 0.35$, $b_1 = 0.5$

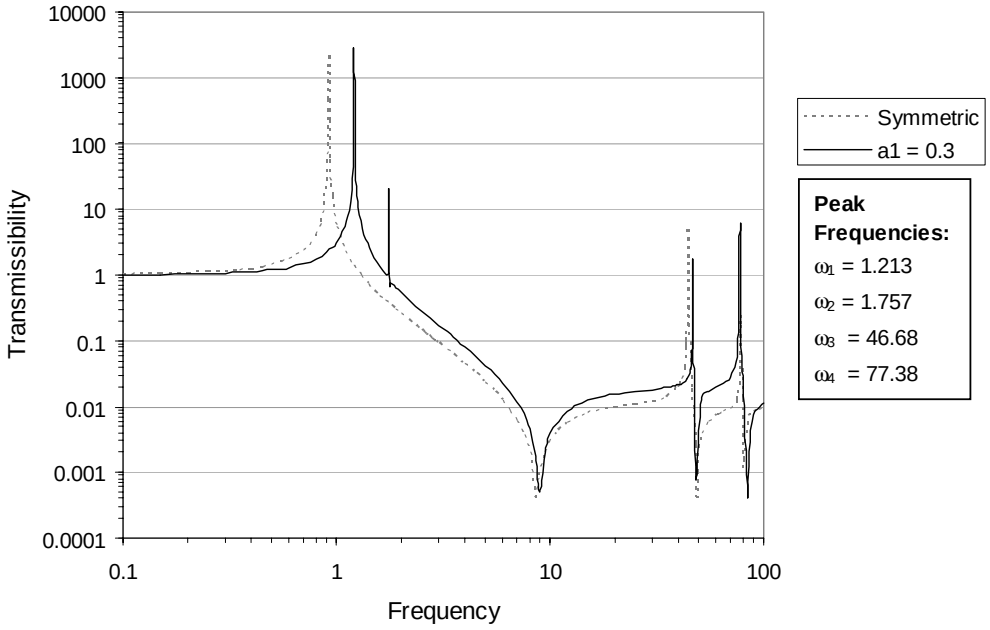

Figure 4.7: Transmissibility vs. Frequency for Center of Mass Positioned at $a_1 = 0.3$, $b_1 = 0.5$

The transmissibility plots shown in Figures 4.4 – 4.7 for Case 2 have the same general shape as the transmissibility plot for the symmetric case with the exception of the additional peak. It appears that, as the eccentricity increases (i.e., as a_1 goes from 0.45 to 0.3), the first, third, and fourth peaks tend to shift away from the peaks for the symmetric case. To better understand how the eccentricity affects the frequencies at which these peaks occur, a comparison of the resonant frequencies for the symmetric case and the four cases illustrated in Figures 4.4 – 4.7 is shown in Table 4.1.

Table 4.1: A Comparison of Resonant Frequencies for Case 1 and Case 2

Case 1	*Case 2*			
$a_1 = 0.5$	$a_1 = 0.45$	$a_1 = 0.4$	$a_1 = 0.35$	$a_1 = 0.3$
0.922	0.948	0.988	1.063	1.213
-------	1.772	1.747	1.725	1.757
44.48	44.92	45.41	45.99	46.68
78.53	78.06	78.00	77.65	77.38

Upon considering the data in Table 4.1 and Figures 4.4 – 4.7, it becomes apparent that the first and third peaks for Case 2 move towards frequencies higher than the first and second

peaks for Case 1, and the fourth peak for Case 2 moves toward a frequency lower than the third peak for Case 1. Because the equilibrium height for the plate and the stiffnesses of the struts in each isolator vary with eccentricity (refer to Table 2.1), no reasonable comparisons can be made between the resonant frequencies for the various eccentricities for Case 2.

Because the first and third peaks for Case 2 both move toward higher frequencies, it is not clear whether the size of the lowest range of frequencies for which isolation is achieved is larger or smaller than for the symmetric case. In Table 4.2, the lower and upper bounds are shown for the lowest range of frequencies for which the transmissibility is less than 0.1. In this table, it is apparent that both the lower and upper bounds on this region increase as the eccentricity increases, as evidenced in the transmissibility plots shown in Figures 4.4 – 4.7. While both bounds move toward higher frequencies, the size of the range of isolation actually increases by up to a few percent for all locations of the center of mass for Case 2. Although the eccentricity increases the size of this range, it should be noted that, because the eccentricity increases the lower bound of this region, the system becomes less effective at isolating low-frequency vibrations.

Table 4.2: Range of Frequencies for Which the Transmissibility is Less Than 0.1 for Case 2

Location of the Center of Mass		Range of Frequencies for Which the Transmissibility is Less Than 0.1		Percentage Increase in Size of Range
a_1	b_1	*Lower Bound*	*Upper Bound*	
0.50	0.50	2.90	43.99	-----
0.45	0.50	2.97	44.48	1.02
0.40	0.50	3.08	44.98	1.97
0.35	0.50	3.28	45.61	3.02
0.30	0.50	3.69	46.41	3.97

The vibration shapes for the center of mass positioned at $a_1 = 0.4$ and $a_1 = 0.3$ are shown in Figures 4.8 and 4.9, respectively. As in Figure 4.3, the horizontal deflection $y_{i,d}$ caused by a base displacement with a nondimensional amplitude u_o of 0.001 is plotted for each strut. Because of symmetry, the struts in isolators 1 and 3 have the same shape, and the

struts in isolators 2 and 4 have the same shape. Also included in Figures 4.8 and 4.9 are diagrams showing the maximum displacement of the plate when the system is excited at each resonant frequency. In these diagrams, the blue rectangle represents the plate in equilibrium, while the orange rectangle depicts the plate at its maximum displacement during steady-state motion. The black dot indicates the location of the center of mass. Because the amplitude of the base motion is small, the angle of rotation of the plate measured perpendicular to the nodal line is also included in Figures 4.8 and 4.9 so that comparisons can be made as to the amount of rotation that occurs for each vibration mode.

As was the instance in the symmetric case, the first resonant frequency ω_1 corresponds to a large vertical movement of the plate. Due to the eccentric weight, the plate also rotates somewhat at this frequency (e.g., the angle of rotation is 0.0017 radians for $a_1 = 0.4$ and 0.0346 radians for $a_1 = 0.3$); however, the vertical movement dominates the motion. At the second resonant frequency ω_2, the plate does not move significantly in the vertical direction, but exhibits a noticeable rotation in ψ. At the time shown, the light region is above the equilibrium position and the dark region is below it. As the eccentricity increases, the angle of rotation increases, accounting for the rise in transmissibility at this peak for increasing eccentricity. Because of the symmetry in Case 1, the plate did not demonstrate any rotation, which explains why this peak did not show up in the transmissibility plot for Case 1. The third and fourth vibration modes for Case 2 correspond to the second and third vibration modes in the symmetric case (refer to Figure 4.3). This makes sense because the third and fourth peaks on the transmissibility plots for Case 2 are close to the second and third peaks for the symmetric case.

	$y_{i,d}$ for Struts 1 & 3	$y_{i,d}$ for Struts 2 & 4	Plate Movement
Frequency 0.988 **Angle of Rotation (Radians)** 0.0017	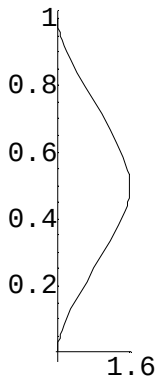	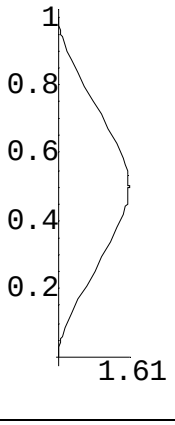	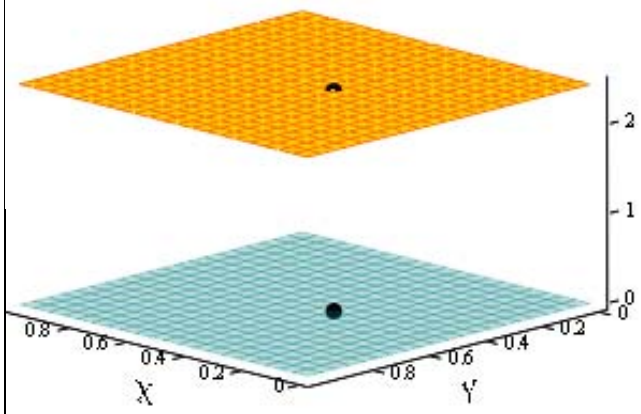
Frequency 1.747 **Angle of Rotation (Radians)** 0.0133	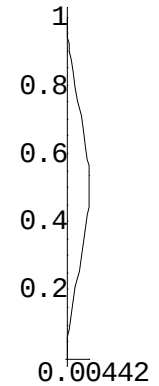	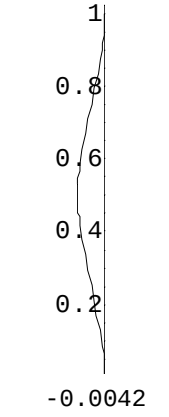	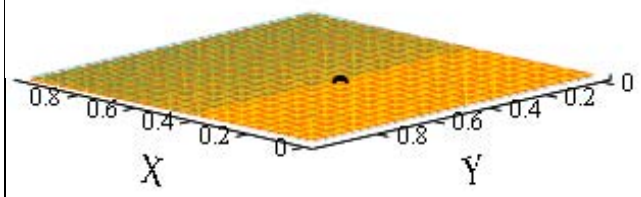
Frequency 45.39 **Angle of Rotation (Radians)** 0.0025	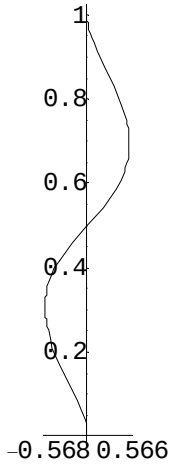	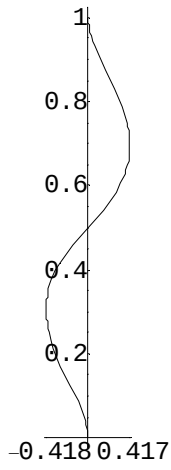	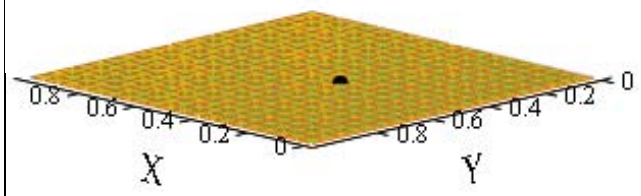

Figure 4.8: Resonant Vibration Modes for Center of Mass Positioned at $a_1 = 0.4$, $b_1 = 0.5$

	$y_{i,d}$ for Struts 1 & 3	$y_{i,d}$ for Struts 2 & 4	Plate Movement
Frequency 78.00	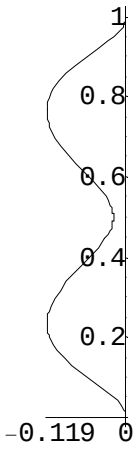	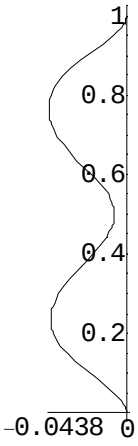	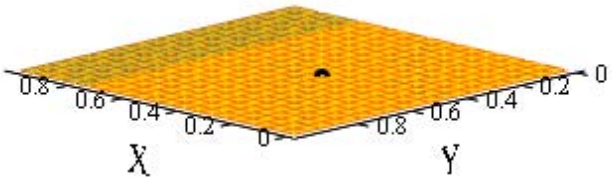
Angle of Rotation (Radians) 0.0008			

Figure 4.8 (Cont'd): Resonant Vibration Modes for Center of Mass Positioned at $a_1 = 0.4$, $b_1 = 0.5$

	$y_{i,d}$ for Struts 1 & 3	$y_{i,d}$ for Struts 2 & 4	Plate Movement
Frequency 1.213 **Angle of Rotation (Radians)** 0.0346	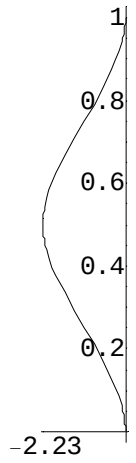	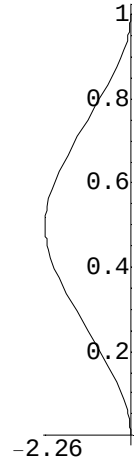	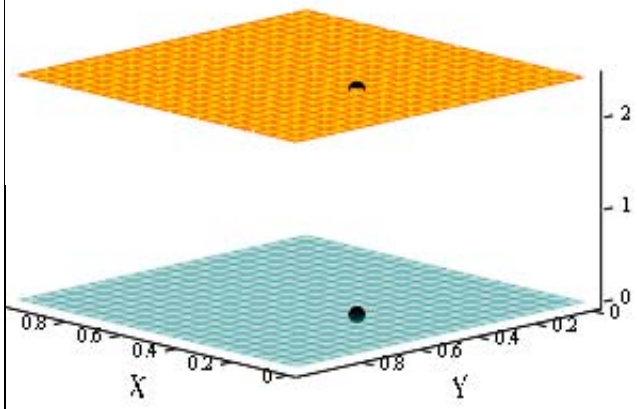
Frequency 1.757 **Angle of Rotation (Radians)** 0.0407		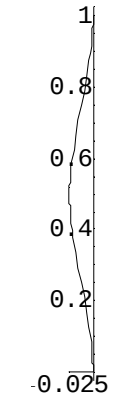	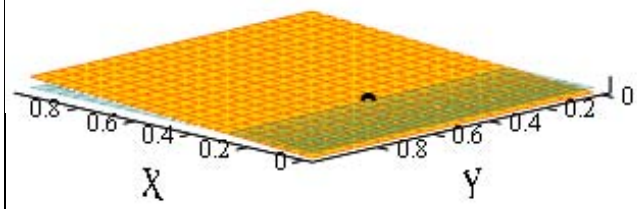
Frequency 46.68 **Angle of Rotation (Radians)** 0.0023	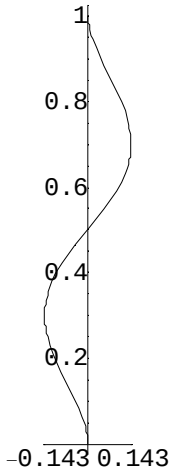	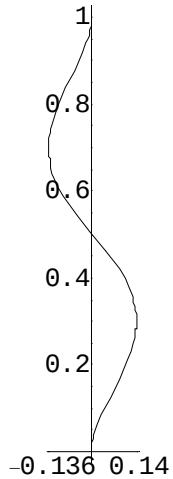	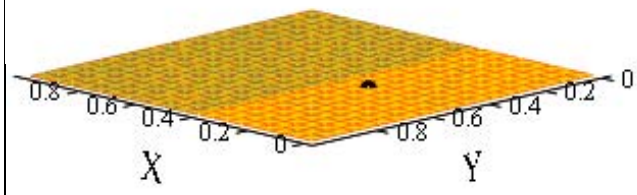

Figure 4.9: Resonant Vibration Modes for Center of Mass Positioned at $a_1 = 0.3$, $b_1 = 0.5$

	$y_{i,d}$ for Struts 1 & 3	$y_{i,d}$ for Struts 2 & 4	Plate Movement
Frequency 77.38	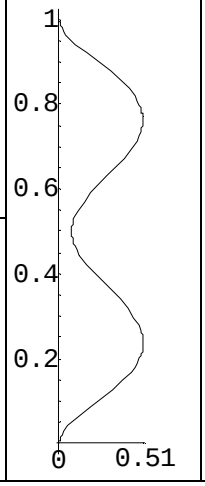	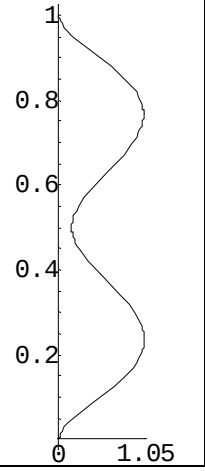	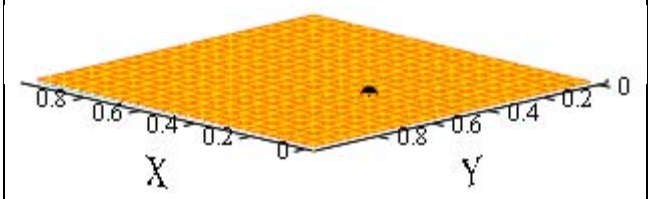
Angle of Rotation (Radians) 0.0069			

Figure 4.9 (Cont'd): Resonant Vibration Modes for Center of Mass Positioned at $a_1 = 0.3$, $b_1 = 0.5$

Case 3

The third case to be analyzed is the case where the center of mass is positioned at several points along a line that runs diagonally from corner *O* to corner *R*, as shown in Figure 4.1(c). Because of symmetry, it is expected that isolators 2 and 3 will behave identically for this case. In order to analyze this case, the variables a_1 and b_1 will be set equal to each other and will be varied from 0.45 to 0.3 in increments of 0.05. Notice that, as a_1 and b_1 decrease, the eccentricity of the weight increases.

The transmissibility for the system is plotted in Figures 4.10 – 4.13 for nondimensional excitation frequencies ranging from 0.1 to 100. The results from the analysis of the symmetric case are included on each transmissibility plot to allow for comparisons to be made between Case 1 and Case 3. As was the situation for Case 2, the eccentricity in Case 3 introduces an additional peak in the transmissibility plot at a frequency slightly higher than the first resonant frequency for the system. This peak occurs over a very narrow range of frequencies and appears to increase in size as the eccentricity increases with the exception of the case shown in Figure 4.13. In Figure 4.13, the transmissibility at the second peak is actually much smaller than in Figures 4.10 – 4.12.

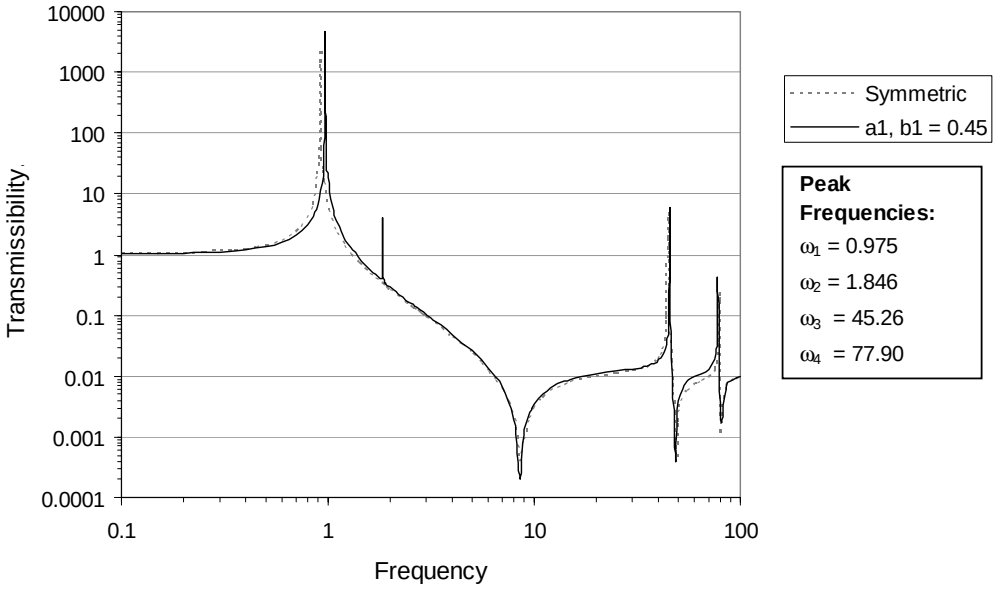

Figure 4.10: Transmissibility vs. Frequency for Center of Mass Positioned at $a_1 = 0.45$, $b_1 = 0.45$

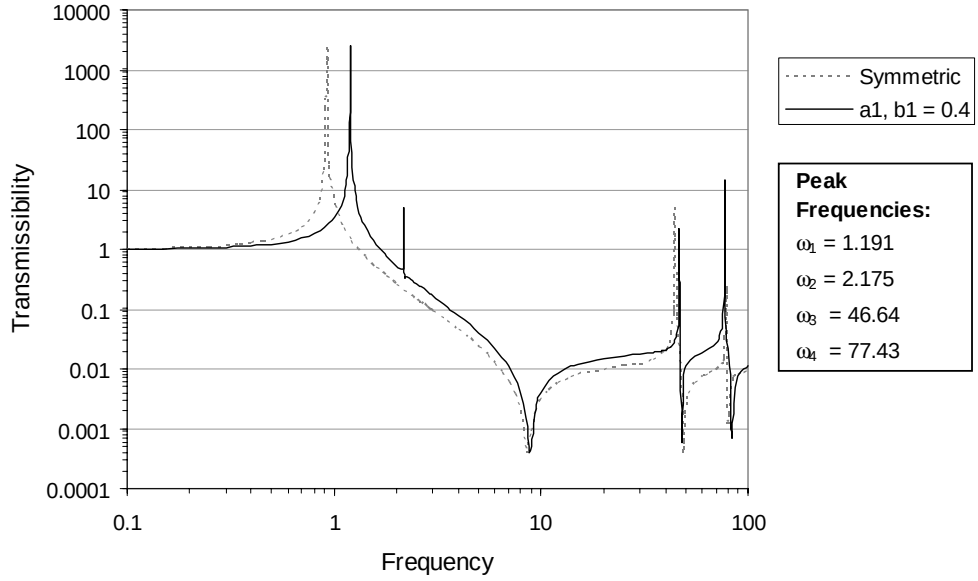

Figure 4.11: Transmissibility vs. Frequency for Center of Mass Positioned at $a_1 = 0.4$, $b_1 = 0.4$

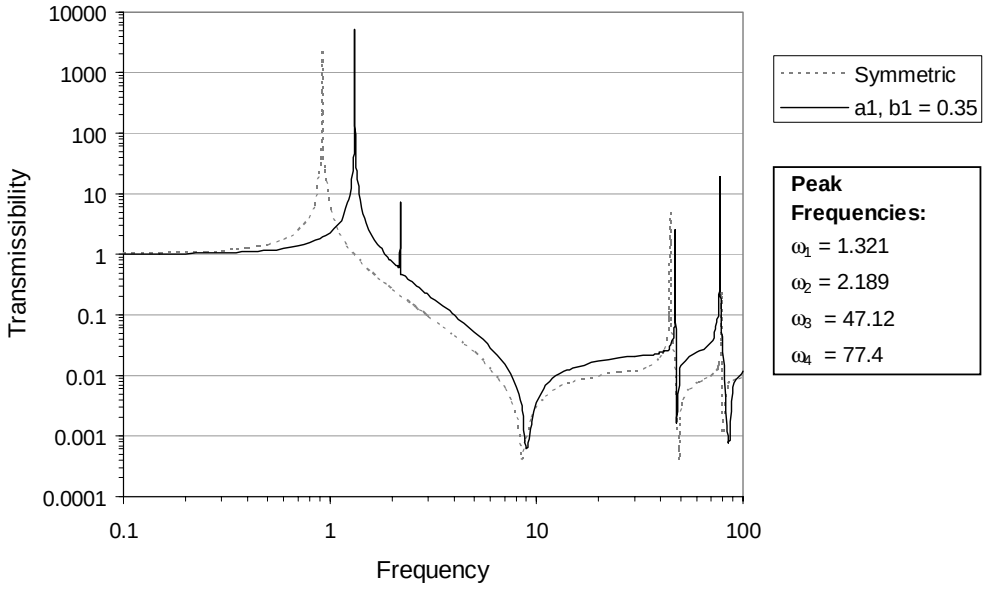

Figure 4.12: Transmissibility vs. Frequency for Center of Mass Positioned at $a_1 = 0.35$, $b_1 = 0.35$

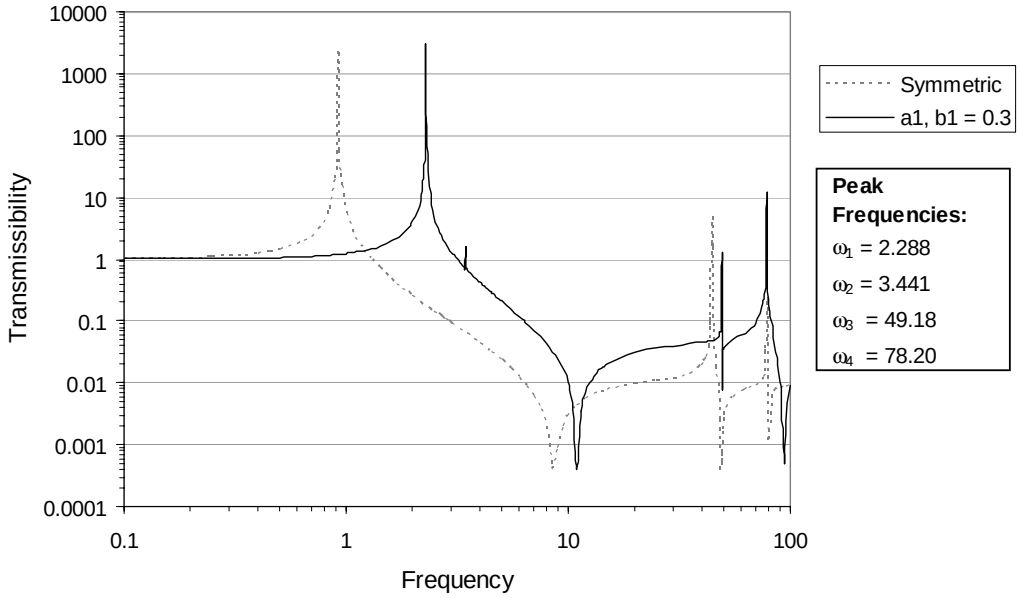

Figure 4.13: Transmissibility vs. Frequency for Center of Mass Positioned at $a_1 = 0.3$, $b_1 = 0.3$

The transmissibility plots shown in Figures 4.10 – 4.13 have the same general shape as in the symmetric case with the exception of the additional peak. As was the situation in Case 2, the first, third, and fourth peaks shift away from the peaks for the symmetric case. To better understand how the eccentricity affects the frequencies at which the peaks in

the transmissibility plots occur, a comparison of the resonant frequencies for the symmetric case and the four cases illustrated in Figures 4.10 – 4.13 is shown in Table 4.3. It appears that the eccentricity causes the first and third peaks for Case 3 to move toward higher frequencies than the first and second peaks for Case 1, and the fourth peak for Case 3 to move toward a lower frequency than the third peak in Case 1. This is consistent with the results from the analysis of Case 2. Comparisons can not be made between the various eccentricities for Case 3 because the isolators do not have equal stiffnesses.

Table 4.3: A Comparison of Resonant Frequencies for Case 1 and Case 3

Case 1	*Case 3*			
$a_1 = 0.5$ $b_1 = 0.5$	$a_1 = 0.45$ $b_1 = 0.45$	$a_1 = 0.4$ $b_1 = 0.4$	$a_1 = 0.35$ $b_1 = 0.35$	$a_1 = 0.3$ $b_1 = 0.3$
0.922	0.975	1.191	1.321	2.288
-------	1.846	2.175	2.189	3.441
44.48	45.26	46.64	47.12	49.18
78.53	77.90	77.43	77.40	78.20

To determine the effect that the eccentricity has on the effectiveness of the isolation of the system, the lower and upper bounds are shown in Table 4.4 for the lowest range of frequencies for which the transmissibility is less than 0.1. Similar to Case 2, the eccentricity in Case 3 causes the size of this range of frequencies to increase by up to a few percent. Again, it should be noted that, as the eccentricity increases, the lower bound increases, thus compromising the isolator's ability to effectively isolate low-frequency vibrations.

The vibration shapes for the center of mass positioned at $a_1 = b_1 = 0.4$ and $a_1 = b_1 = 0.35$ are shown in Figures 4.14 and 4.15, respectively. As in Figures 4.8 and 4.9, the horizontal deflection $y_{i,d}$ caused by a base displacement with a nondimensional amplitude u_o of 0.001 is plotted for each strut. Because of symmetry, the struts in isolators 2 and 3 have the same shape. Also included in Figures 4.14 and 4.15 are the diagrams showing the maximum steady-state displacements of the plate when the system is excited at each

resonant frequency. The angle of rotation of the plate measured perpendicular to the nodal line is also shown for each mode to allow comparisons between the modes.

Table 4.4: Range of Frequencies for Which the Transmissibility is Less Than 0.1 for Case 3

Location of the Center of Mass		Range of Frequencies for Which the Transmissibility is Less Than 0.1		Percentage Increase in Size of Range
a_1	b_1	*Lower Bound*	*Upper Bound*	
0.50	0.50	2.90	43.99	-----
0.45	0.45	3.04	44.83	1.70
0.40	0.40	3.63	46.32	3.89
0.35	0.35	3.98	46.81	4.23
0.30	0.30	6.35	48.95	3.67

As was the instance for Cases 1 and 2, the first resonant frequency ω_1 for Case 3 corresponds to a large vertical movement of the plate. Although the plate rotates somewhat at this frequency, the vertical movement dominates the motion. Similar to Case 2, the second resonant frequency for Case 3 corresponds to a significant rotation of the plate. For Case 3, however, the rotation is perpendicular to the line of symmetry that runs diagonally from corner *O* to corner *R* on the plate, as indicated in Figures 4.14 and 4.15. At the third and fourth resonant frequencies, the plate does not demonstrate much vertical movement or rotation, but the struts in each isolator vibrate at modes similar to the vibration modes that occurred in the symmetric case at the second and third resonant frequencies.

	$y_{i,d}$ for Strut 1	$y_{i,d}$ for Struts 2 & 3	$y_{i,d}$ for Strut 4	Plate Movement
Frequency 1.191	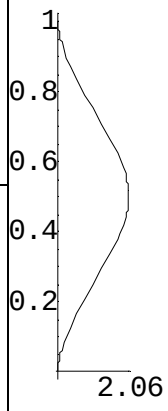	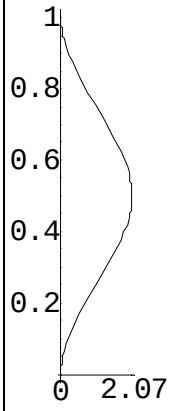	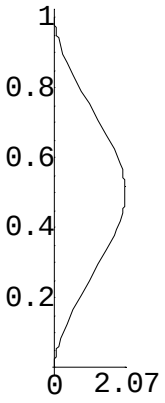	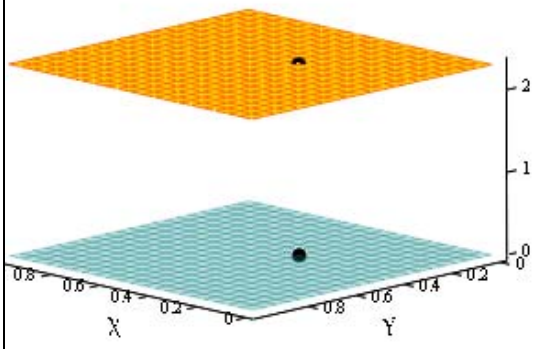
Angle of Rotation (Radians) 0.0149				
Frequency 2.175	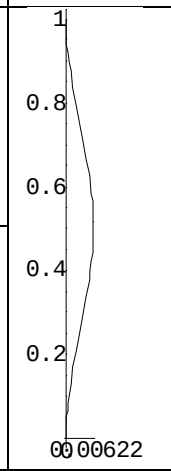	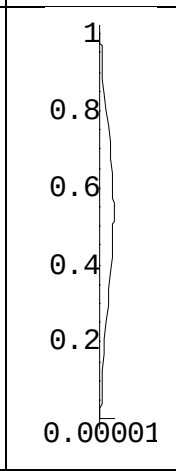	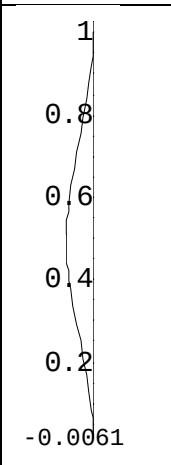	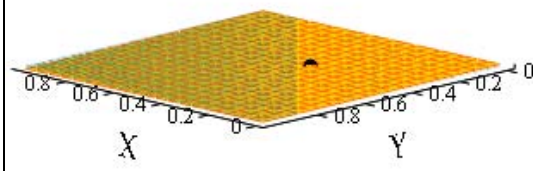
Angle of Rotation (Radians) 0.0098				
Frequency 46.64	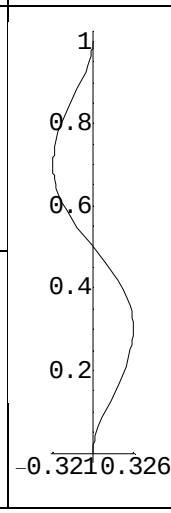	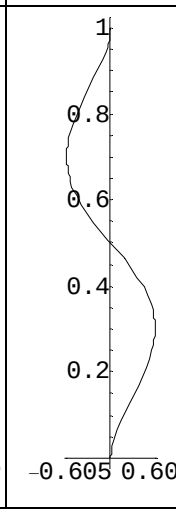	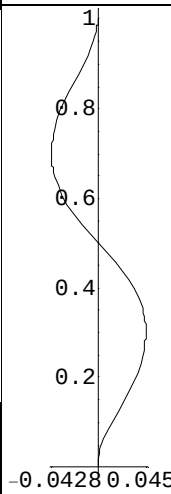	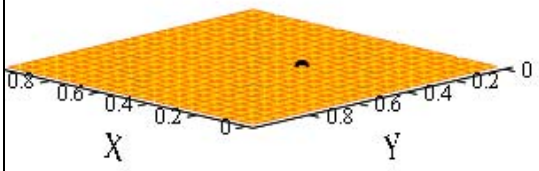
Angle of Rotation (Radians) 0.0013				

Figure 4.14: Resonant Vibration Modes for Center of Mass Positioned at $a_1 = 0.4$, $b_1 = 0.4$

	$y_{i,d}$ for Strut 1	$y_{i,d}$ for Struts 2 & 3	$y_{i,d}$ for Strut 4	Plate Movement
Frequency 77.43	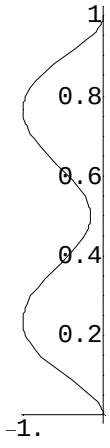	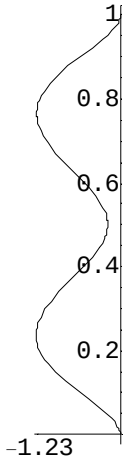	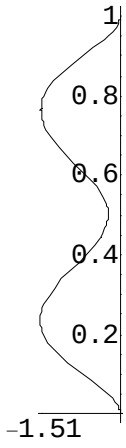	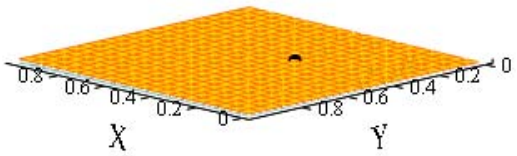
Angle of Rotation (Radians) 0.0068				

Figure 4.14 (Cont'd): Resonant Vibration Modes for Center of Mass Positioned at $a_1 = 0.4$, $b_1 = 0.4$

	$y_{i,d}$ for Strut 1	$y_{i,d}$ for Struts 2 & 3	$y_{i,d}$ for Strut 4	Plate Movement
Frequency 1.321 **Angle of Rotation (Radians)** 0.0050	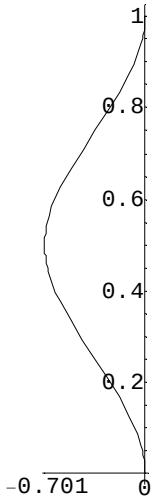	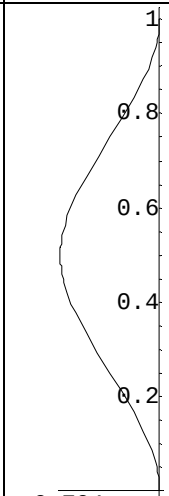	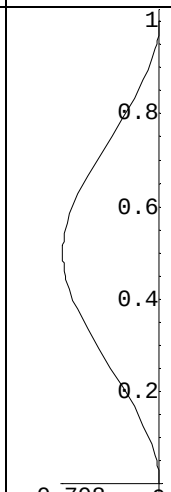	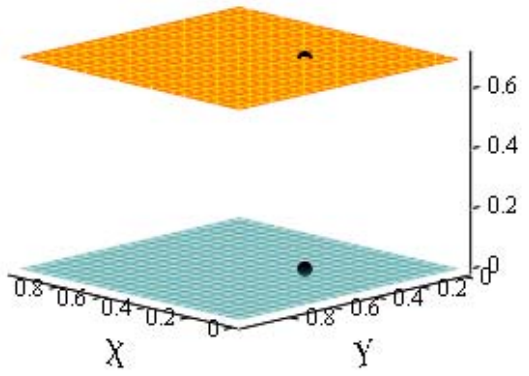
Frequency 2.188 **Angle of Rotation (Radians)** 0.0107	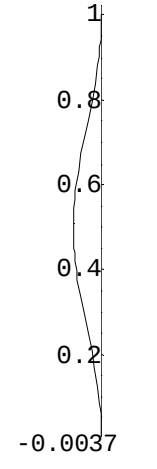	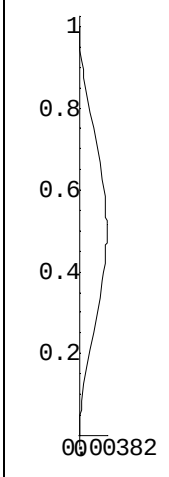	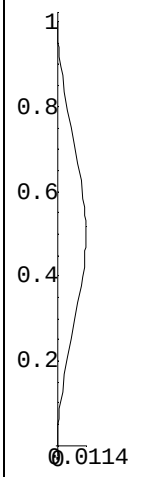	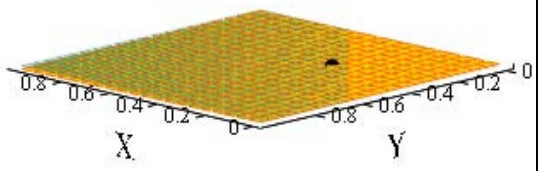
Frequency 47.12 **Angle of Rotation (Radians)** 0.0029	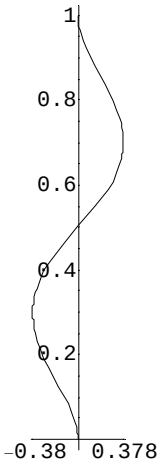	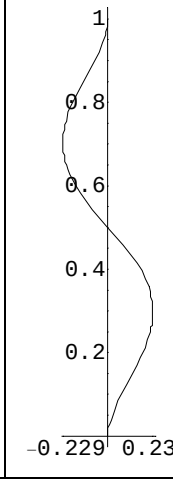	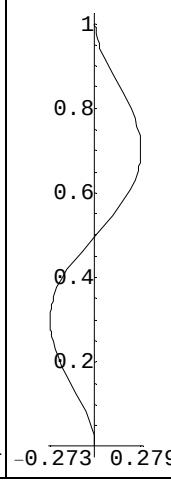	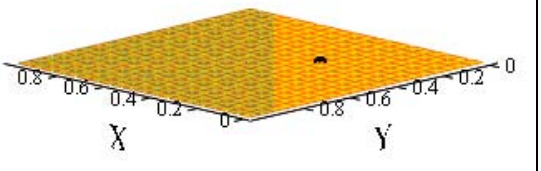

Figure 4.15: Resonant Vibration Modes for Center of Mass Positioned at $a_1 = 0.35$, $b_1 = 0.35$

	$y_{i,d}$ for Strut 1	$y_{i,d}$ for Struts 2 & 3	$y_{i,d}$ for Strut 4	Plate Movement
Frequency 77.50	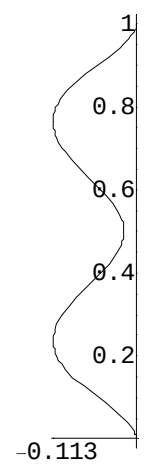	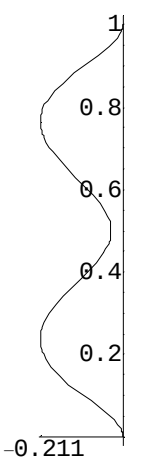	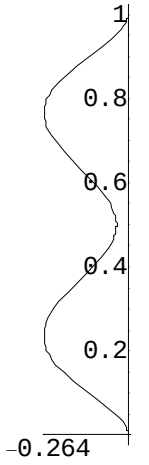	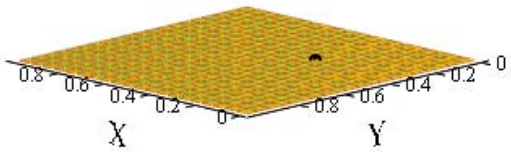
Angle of Rotation (Radians) 0.0022				

Figure 4.15 (Cont'd): Resonant Vibration Modes for Center of Mass Positioned at $a_1 = 0.35$, $b_1 = 0.35$

Case 4

The final case to be analyzed is the case where the center of mass is arbitrarily positioned such that no symmetry exists in the system, as shown in Figure 4.1(d). For this case, the center of mass is positioned at six different locations: (1) $a_1 = 0.4$, $b_1 = 0.45$; (2) $a_1 = 0.35$, $b_1 = 0.45$; (3) $a_1 = 0.3$, $b_1 = 0.45$; (4) $a_1 = 0.35$, $b_1 = 0.4$; (5) $a_1 = 0.3$, $b_1 = 0.4$; and (6) $a_1 = 0.3$, $b_1 = 0.35$. As a_1 decreases, the eccentricity in the $\overline{X}$ -direction increases, and, as b_1 decreases, the eccentricity in the $\overline{Y}$ -direction increases (refer to Figure 1.3).

The transmissibility is plotted in Figures 4.16 – 4.21 for nondimensional excitation frequencies ranging from 0.1 to 100, and the results from the symmetric case are included on each of these plots. The most significant difference between the transmissibility plots for Case 4 and for Cases 2 and 3 is that the lack of symmetry introduces *two* additional peaks near the first resonant frequency for the system instead of one. Both of these peaks occur over a narrow range of frequencies, and the maximum transmissibility for each of these peaks varies depending on the location of the center of mass. The frequencies at which these peaks occur may be affected by the location of the center of mass, but no exact conclusions can be made because of the manner that the stiffnesses of the struts in each isolator were adjusted.

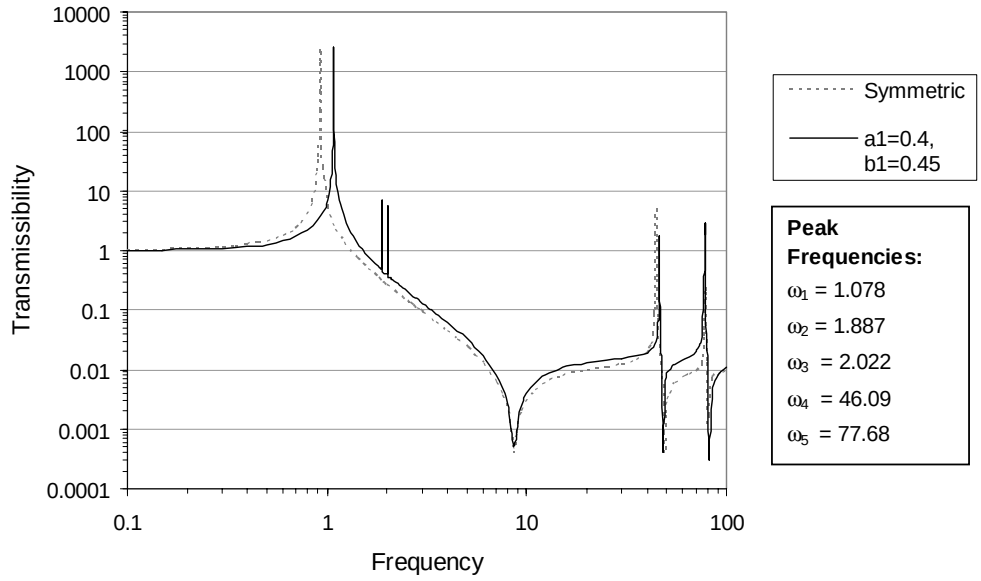

Figure 4.16: Transmissibility vs. Frequency for Center of Mass Positioned at $a_1 = 0.4$, $b_1 = 0.45$

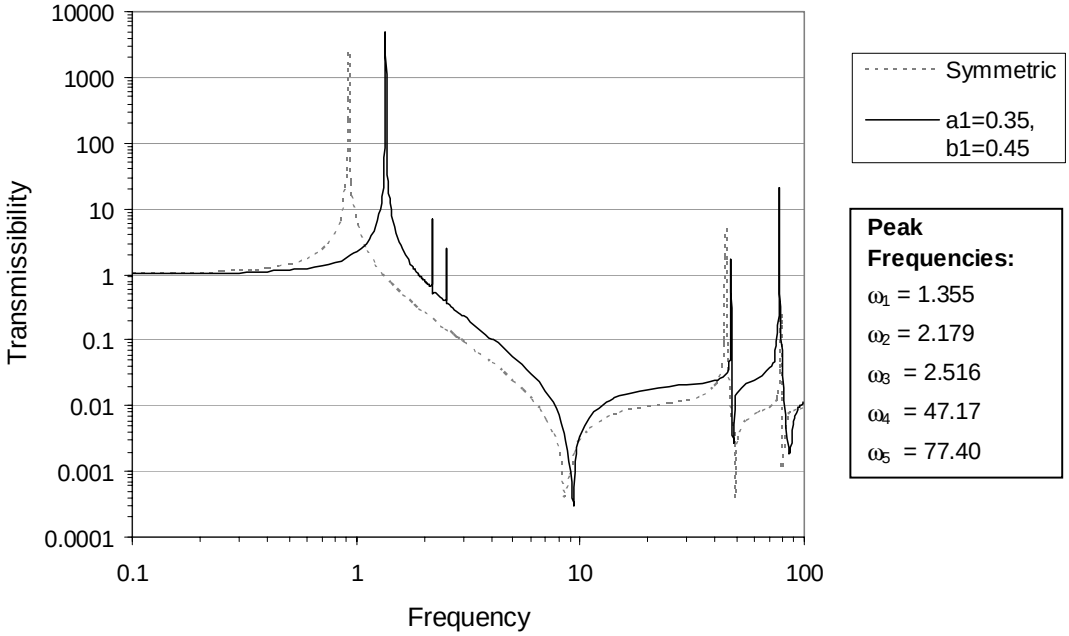

Figure 4.17: Transmissibility vs. Frequency for Center of Mass Positioned at $a_1 = 0.35$, $b_1 = 0.45$

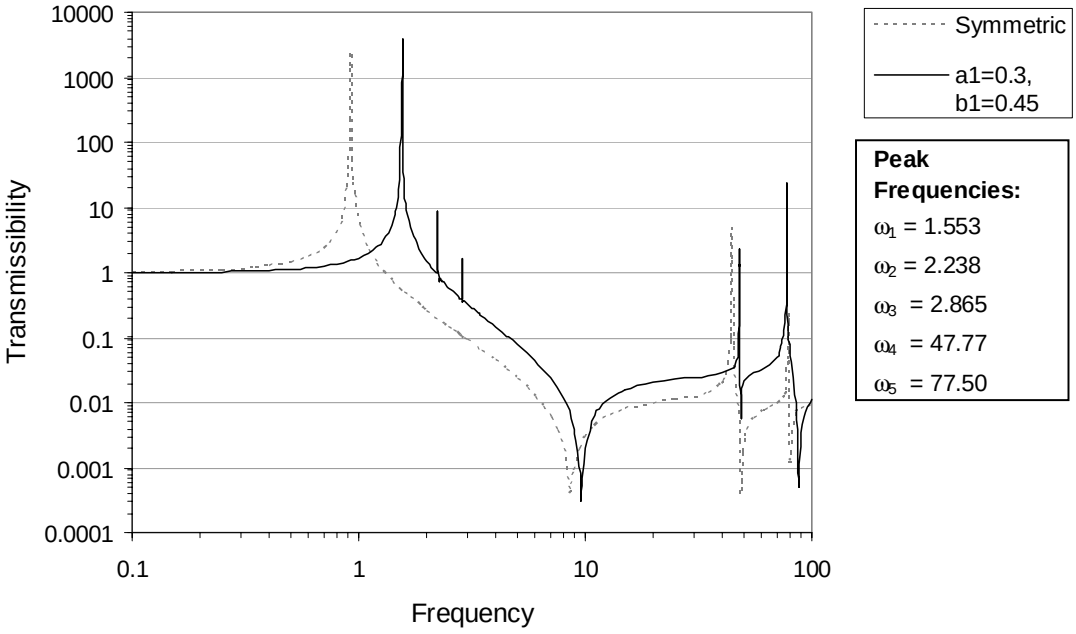

Figure 4.18: Transmissibility vs. Frequency for Center of Mass Positioned at $a_1 = 0.3$, $b_1 = 0.45$

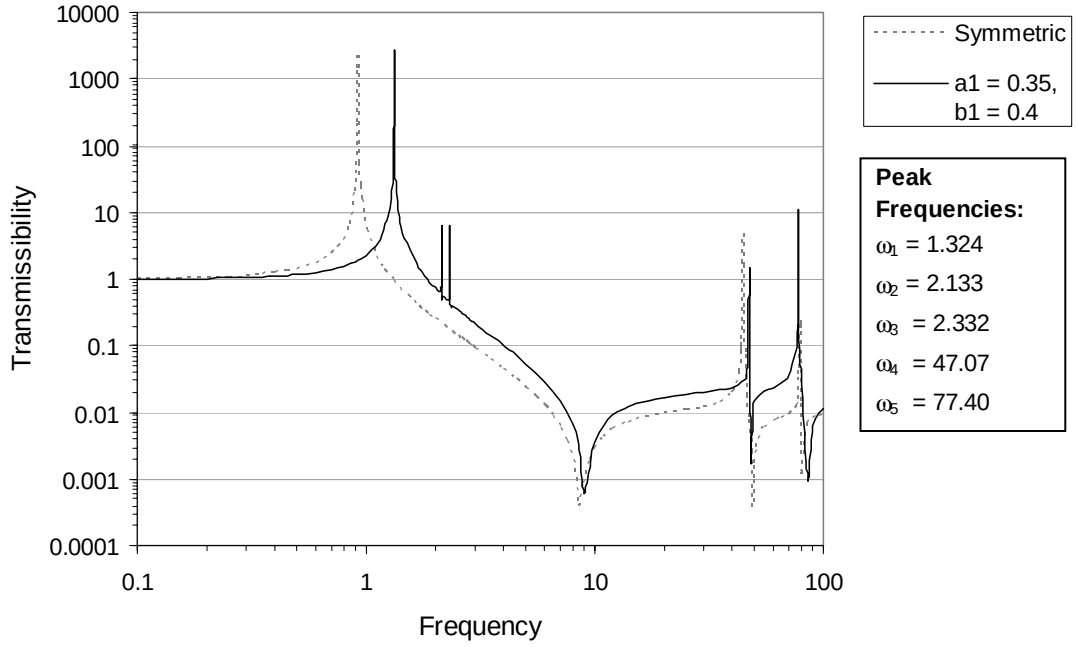

Figure 4.19: Transmissibility vs. Frequency for Center of Mass Positioned at $a_1 = 0.35$, $b_1 = 0.4$

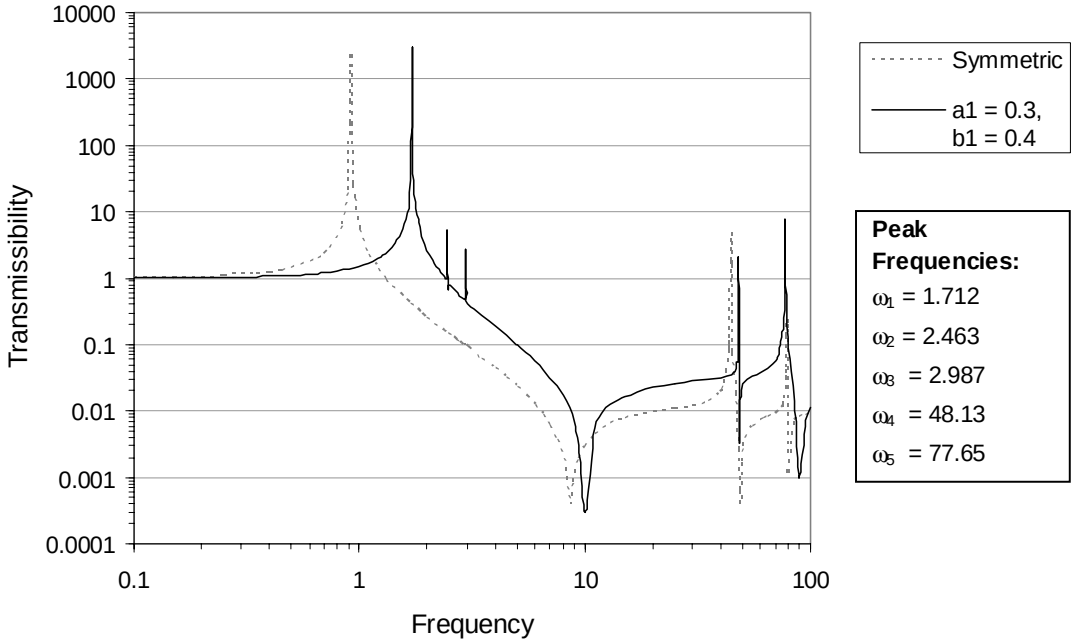

Figure 4.20: Transmissibility vs. Frequency for Center of Mass Positioned at $a_1 = 0.3$, $b_1 = 0.4$

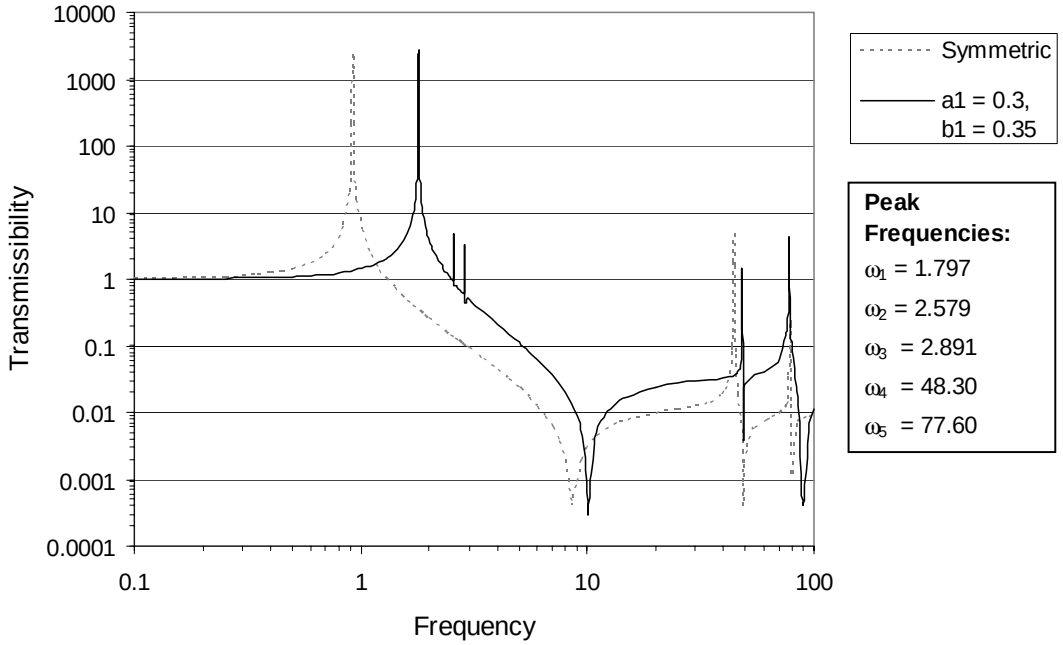

Figure 4.21: Transmissibility vs. Frequency for Center of Mass Positioned at $a_1 = 0.3$, $b_1 = 0.35$

The transmissibility plots shown in Figures 4.16 – 4.21 have a similar shape to the transmissibility plot for the symmetric case with the exception of the two additional peaks. As was the situation for Cases 2 and 3, the first, fourth, and fifth peaks in the transmissibility plot tend to shift away from the three peaks for the symmetric case. A comparison of the resonant frequencies for Case 1 and Case 4 is provided in Table 4.5, and the same trend that was observed for Cases 2 and 3 is observed for Case 4. Specifically, the first and fourth peak for Case 4 move toward frequencies higher than the first and second peaks for Case 1, and the fifth peak for Case 4 moves toward a lower frequency than the third peak for Case 1.

Table 4.5: A Comparison of Resonant Frequencies for Case 1 and Case 4

Case 1	*Case 4*					
$a_1 = 0.5$ $b_1 = 0.5$	$a_1 = 0.4$ $b_1 = 0.45$	$a_1 = 0.35$ $b_1 = 0.45$	$a_1 = 0.3$ $b_1 = 0.45$	$a_1 = 0.35$ $b_1 = 0.4$	$a_1 = 0.3$ $b_1 = 0.4$	$a_1 = 0.3$ $b_1 = 0.35$
0.922	1.078	1.355	1.553	1.324	1.712	1.797
-------	1.887	2.179	2.238	2.133	2.463	2.579
-------	2.022	2.516	2.865	2.332	2.987	2.891
44.48	46.09	47.17	47.77	47.07	48.13	48.30
78.53	77.68	77.40	77.50	77.40	77.65	77.60

To determine the effect that the eccentricity has on the effectiveness of the isolation of the system, the lower and upper bounds are shown in Table 4.6 for the lowest range of frequencies for which the transmissibility is less than 0.1. Similar to Cases 2 and 3, the eccentricity in Case 4 causes the size of this range of frequencies to increase by up to a few percent. As the eccentricity increases, the lower bound on this region again moves toward a higher frequency, and so the system is somewhat less effective at isolating low-frequency vibrations.

Table 4.6: Range of Frequencies for Which the Transmissibility is Less Than 0.1 for Case 4

Location of the Center of Mass		Range of Frequencies for Which the Transmissibility is Less Than 0.1		Percentage Increase in Size of Range
a_1	b_1	*Lower Bound*	*Upper Bound*	
0.50	0.50	2.90	43.99	-----
0.40	0.45	3.32	45.73	3.21
0.35	0.45	4.07	46.94	4.33
0.30	0.45	4.58	47.51	4.48
0.35	0.40	3.99	46.83	4.26
0.30	0.40	4.97	47.88	4.43
0.30	0.35	5.20	48.08	4.36

The vibration modes for the center of mass located at $a_1 = 0.35$, $b_1 = 0.45$ are shown in Figure 4.22. As expected, the first vibration mode corresponds to a large vertical movement of the plate. The second and third vibration modes, however, correspond to rotations of the plate in two different directions. Because there is no symmetry, it is not surprising to see that the plate has two rotational vibration modes because the plate has two rotational degrees of freedom. The nodal lines for these two modes appear to be almost perpendicular, thus illustrating that the plate is in fact rotating about two different axes. At the fourth and fifth resonant frequencies, the struts in each isolator exhibit vibration modes similar to those observed in the previous cases.

	$y_{i,d}$ for Strut 1	$y_{i,d}$ for Strut 2	$y_{i,d}$ for Strut 3	$y_{i,d}$ for Strut 4	Plate Movement
Frequency 1.355 **Angle of Rotation (Radians)** 0.0068	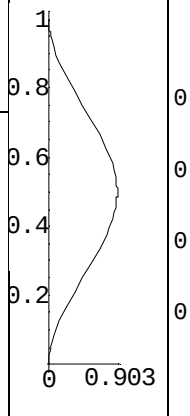	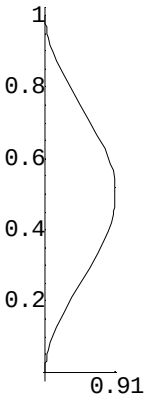	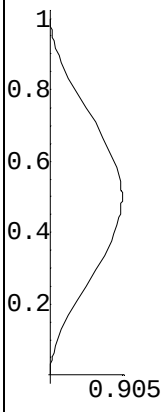	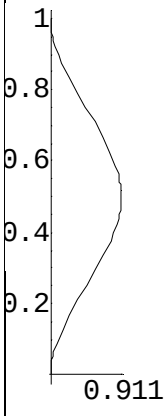	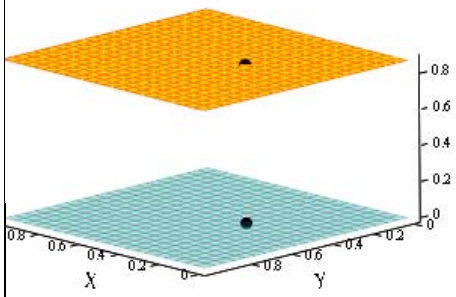
Frequency 2.179 **Angle of Rotation (Radians)** 0.0073	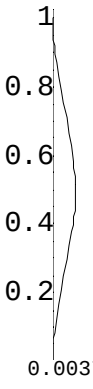	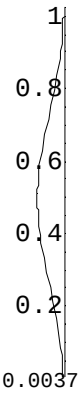			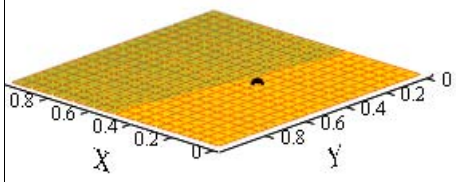
Frequency 2.516 **Angle of Rotation (Radians)** 0.0033		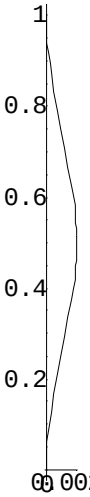	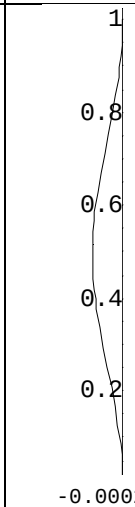	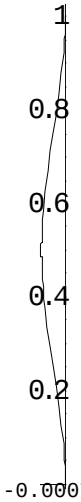	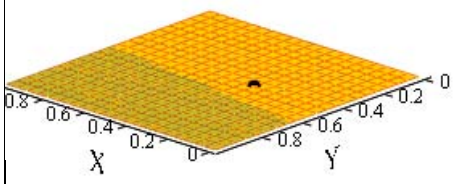

Figure 4.22: Resonant Vibration Modes for Center of Mass Positioned at $a_1 = 0.35$, $b_1 = 0.45$

	$y_{i,d}$ for Strut 1	$y_{i,d}$ for Strut 2	$y_{i,d}$ for Strut 3	$y_{i,d}$ for Strut 4	Plate Movement
Frequency 41.17 **Angle of Rotation (Radians)** 0.0016	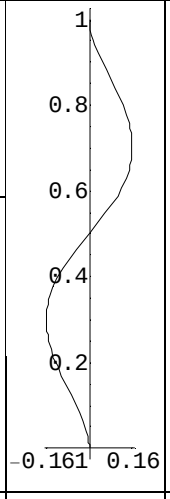	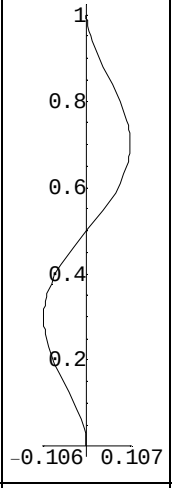	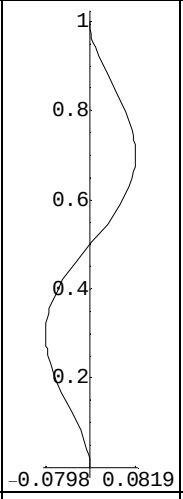	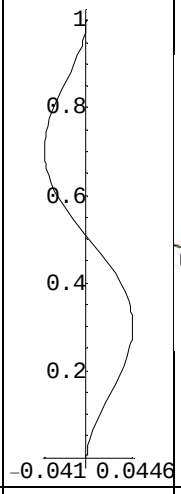	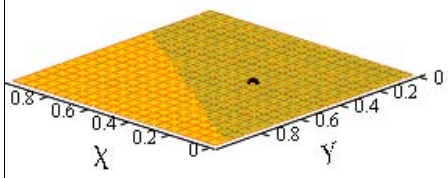
Frequency 77.40 **Angle of Rotation (Radians)** 0.0057	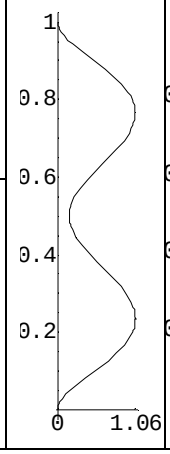	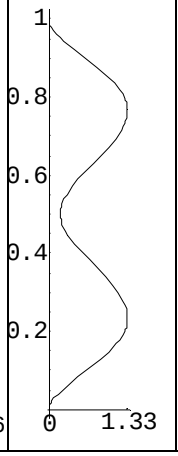	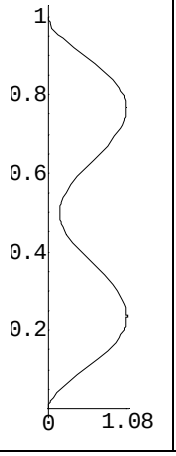	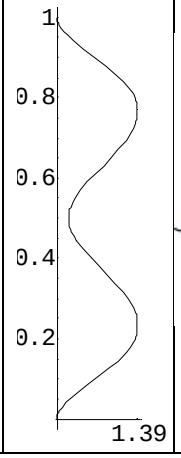	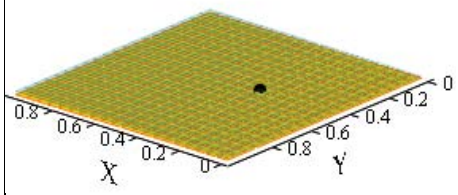

Figure 4.22 (Cont'd): Resonant Vibration Modes for Center of Mass Positioned at $a_1 = 0.35$, $b_1 = 0.45$

4.2 Free Vibration Analysis

For the free vibration analysis, the dynamic program is slightly modified so that one of the forces in the struts (e.g., $p_{1,d}$) is set equal to an arbitrary value, and the excitation frequency ω becomes an unknown variable which is computed by the program. In this analysis, the damping coefficient c_f and the magnitude of the base motion u_o are set equal to zero. Depending on the initial guesses for the frequency ω and the forces and moments in the struts, the frequency that results will be a resonant frequency corresponding to a particular vibration mode in the system. This analysis will focus solely on vibration modes of the plate, i.e., vibration modes in the isolators will be ignored. The purpose of

this analysis is (1) to check the accuracy of resonant frequencies that were obtained in the forced vibration analysis and (2) to consider all possible vibration modes in the plate, especially those which were not obtained in the forced vibration analysis.

Table 4.7 shows a comparison of the frequencies that were obtained from the free vibration analysis and from the forced vibration analysis. For all cases shown in Table 4.7, it appears that there is very good agreement between the results from the free vibration analysis and the results from the forced vibration analysis. Small differences are due to the presence of damping in the forced vibration analysis and the use of different techniques to solve for the frequencies in the two analyses. Note that there are a few frequencies obtained from the free vibration analysis that did not show up in the forced vibration analysis. Plots of the motion of the plate were generated at these frequencies to

Table 4.7: Comparison of Results from Forced Vibration Analysis and Free Vibration Analysis

Location of the Center of Mass		Resonant Frequency	
a_1	b_1	*Free Vibration Analysis*	*Forced Vibration Analysis*
0.5	0.5	0.9220	0.9220
		1.7566	-------
0.4	0.5	0.9878	0.9880
		1.7466	1.7470
		1.8787	-------
0.3	0.5	1.2139	1.2130
		1.7553	1.7570
		2.2974	-------
0.4	0.4	1.1911	1.1910
		1.4301	-------
		2.1757	2.1750
0.3	0.3	2.2219	-------
		2.2949	2.2880
		3.4348	3.4410
0.35	0.45	1.3557	1.3550
		2.1783	2.1790
		2.5197	2.5160
0.3	0.4	1.7141	1.7120
		2.4591	2.4630
		2.9949	2.9870

determine what type of motion corresponds to these additional frequencies. Figure 4.23 shows the characteristic nodal lines that were observed in the plots of the motion of the plate for Cases 1, 2, and 3.

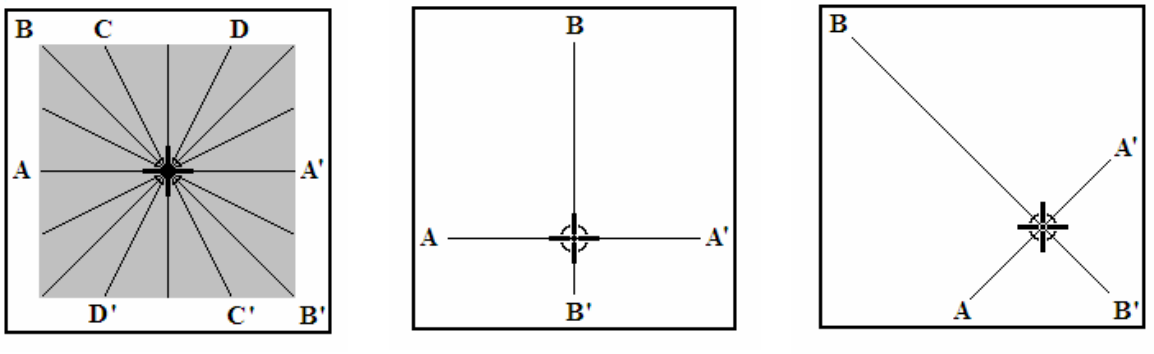

(a) (b) (c)

Figure 4.23: Diagrams Showing the Characteristic Nodal Lines Obtained from the Free Vibration Analysis for (a) Case 1, (b) Case 2, and (c) Case 3

For the case where the center of mass is positioned at the geometric center of the plate (i.e., $a_1 = 0.5$, $b_1 = 0.5$), two frequencies were obtained from the free vibration analysis, as indicated in the first case in Table 4.7. The first frequency of 0.9220 corresponds to the first resonant frequency ω_1 obtained from the forced vibration analysis for the symmetric case. The second frequency of 1.7566, however, was only obtained from the free vibration analysis. At this frequency, the plate has rotational vibration modes about *all* lines which pass through the center of the plate (i.e., the plate has an infinite number of modes). Examples of nodal lines obtained in this analysis (shown in Figure 4.23(a)) include lines $A - A'$ and $B - B'$, which are lines of symmetry, and lines $C - C'$ and $D - D'$, which are not lines of symmetry. While it may seem counterintuitive that the plate would have rotational modes about such lines, it can easily be shown for a similar system that this behavior can be expected. Refer to Appendix D for more information on this topic.

For Case 2, three frequencies were obtained from the free vibration analysis, as indicated in the second and third cases in Table 4.7. The first two frequencies (e.g., 0.9878 and 1.7466 for $a_1 = 0.4$, $b_1 = 0.5$) correspond to the first and second resonant frequencies, ω_1 and ω_2, obtained from the forced vibration analysis. The rotation at the second resonant

frequency that was observed in both the forced vibration analysis and the free vibration analysis is indicated by the line $A - A'$ in Figure 4.23(b). The third resonant frequency (e.g., 1.8787 for $a_1 = 0.4$, $b_1 = 0.5$) obtained in the free vibration analysis corresponds to a rotation about line $B - B'$ in Figure 4.23(b), which is the line of symmetry for Case 2. Because of symmetry in the system, this third mode did not occur in the forced vibration analysis.

For Case 3, three frequencies were obtained from the free vibration analysis, as indicated in the fourth and fifth cases in Table 4.7. Two of these frequencies (e.g., 1.1911 and 2.1757 for $a_1 = b_1 = 0.4$) correspond to the first and second resonant frequencies, ω_1 and ω_2, obtained from the forced vibration analysis. The rotation which corresponds to the second vibration mode obtained in the forced vibration analysis is indicated by the line $A - A'$ in Figure 4.23(c). This line runs perpendicular to the line of symmetry that runs from corner O to corner R of the plate. The third frequency (e.g., 1.4301 for $a_1 = b_1 = 0.4$) obtained in the free vibration analysis corresponds to a rotation about line $B - B'$ in Figure 4.23(c), which is the line of symmetry for Case 3. This mode did not show up in the forced vibration analysis because of symmetry.

For Case 4, three frequencies again were obtained from the free vibration analysis, as indicated in the last two cases in Table 4.7. All three of these frequencies correspond with the frequencies obtained from the forced vibration analysis, and the modes that occur at these frequencies are the same for both analyses. Because there was no symmetry in this case, all three frequencies showed up in the transmissibility plots generated in the forced vibration analysis for this case.

Chapter 5: Summary and Conclusions

The purpose of this research was to study the effectiveness of a novel type of vibration isolator intended to isolate vertical vibrations. The proposed isolation device was made of two pre-bent struts which were clamped at both ends and intermediately bonded with a viscoelastic material. In this research, four of these vibration isolators were used to support the corners of a horizontal square plate which was nonuniform such that the center of mass of the weight occurred at some distance from the geometric center of the plate (refer to Figure 1.3). The eccentricity of the weight introduced rotational as well as vertical motions of the plate when the system was subjected to vertical harmonic base excitations. The ultimate goals of this research were to investigate the effects of various eccentricities on the efficiency of the vibration isolators and to study various possible vibration modes in this system.

5.1 Summary of Results

To analyze the system, the center of mass was positioned at various locations, and the transmissibility was calculated and plotted over a wide range of excitation frequencies for each case. The locations of the center of mass were grouped in categories based on the type of symmetry that existed in the system. Using the transmissibility plots, conclusions were made as to how the various eccentricities affected the behavior of the system. These plots were also used to recognize frequencies at which resonance occurred in the system. At these resonant frequencies, the physical behavior of the system was analyzed to determine the types of vibration modes that occurred in the system.

The most noticeable observation from the forced vibration analysis was that the eccentricity introduced one or two additional peaks in the transmissibility plots near the first resonant frequency for each case. The number of peaks that were introduced depended on the degree of symmetry that existed in the system, and each of these additional peaks corresponded to a distinct rotation of the plate. Despite the introduction of additional resonant frequencies in the system, the size of the range of frequencies for

which the isolators were effective remained practically unaffected by these additional peaks.

The eccentric weight of the system seemed to significantly affect frequencies at which various resonant vibration modes occurred in the system, especially for cases where the eccentricity was large. For all cases, the eccentricity caused the first peak in the transmissibility plot to shift toward a higher frequency than the first peak for the symmetric case. This effect may be undesirable if the isolators are intended to isolate low-frequency vibrations. The other peaks in the transmissibility plots also shifted due to the various eccentricities, and it was found that larger eccentricities actually increased the range of frequencies for which the isolators were effective.

From the free vibration analysis, it was found that the plate could have rotational vibration modes which did not show up in the forced vibration analysis because of symmetries that existed in the system. Like the rotational modes of vibration obtained in the forced vibration analysis, these modes occurred at frequencies near the first resonant frequency of the system. When considering a system similar to the one analyzed in this research, it is important to consider all vibration modes, including those which are not expected to occur under forced vibrations, because there may be some imperfection in the system which could cause the system to vibrate in one of these modes (e.g., there may be a disturbance other than the expected forcing).

5.2 Recommendations for Future Research

Experimental testing of the proposed isolation device is certainly necessary before the device could be used in any realistic applications. While it would be extremely difficult to physically model the three dimensional movements of the supported mass that were investigated in this research, experimental tests could be developed to analyze the isolation device possibly in a single-degree-of-freedom system. Such experiments could explore the effects of different filler materials and various geometric configurations on the isolator's efficiency. The results from such experiments could be used to validate the

analytical models used in this research or, perhaps, to develop more accurate analytical models.

Another possibility for extending this research is to consider various types of excitations including multi-frequency vibrations, random vibrations, and shock excitations. Because many types of vibrations are not simple harmonic excitations, investigating the effects of various excitations would be essential to broadening the application of this isolation device. Such analyses could provide ideas for improving the vibration isolator or possibly offer insight into the fundamental behavior of this vibration isolator.

In this research, the plate was restricted against lateral movement and against rotation about the vertical direction. Realistically, these types of motion may occur in such a system, and so it would be interesting to see what effects these types of motion have on the behavior of the vibration isolator. To do this, a significantly more complex model for the vibration isolator would need to be developed to account for the complex behavior that would occur under such loading.

5.3 Concluding Remarks

This research has focused on analyzing a new type of vibration isolator which has the potential for effectively isolating harmonic vibrations in a vertical system. This analysis considered the effects of various movements of the supported mass, and it was found that the vibration isolator maintained a sufficient degree of effectiveness for various eccentricities in the system. This research only considered simple harmonic vibrations and did not take into consideration rotations about the vertical direction of lateral movements of the supported mass. Despite limitations in this research, the results from this analysis show that there is much potential for future investigations of the proposed vibration isolator.

References

Bonello, P., Brennan, M.J., and Elliott, S.J. (2005) "Vibration control using an adaptive tuned vibration absorber with a variable curvature stiffness element," *Smart Materials and Structures*, 14, 1055-1065.

Chin, E.J., Lee, K.T., Winterflood, J., Ju, L., and Blair, D.G. (2005). "Low frequency vertical geometric anti-spring vibration isolators," *Physics Letters A*, 336, 97-105.

Chopra, A.K. (2001). *Dynamics of Structures*, 2nd ed., Prentice Hall, Inc., Upper Saddle River, New Jersey.

Crede, C.E., and Ruzicka, J.E. (1976). "Theory of Vibration Isolation," *Shock and Vibration Handbook*, 2nd ed., C.M. Harris, ed., McGraw-Hill, Inc., New York, 30.22-30.25.

Dumas, J.C., Lee, K.T., Winterflood, J., Ju, L., Blair, D.G., and Jacob, J. (2004). "Testing of a multi-stage low-frequency isolator using Euler spring and self-damped pendulums," *Classical and Quantum Gravity*, 21, S965-S971.

Favor, H.M. (2004). "Two-dimensional Analysis of Vibration Isolation of Rigid Bar Supported by Buckled Struts or Pre-bent Struts," M.S. Thesis, Virginia Tech.

Ibrahim, Y.E. (2005). "A New Visco-Plastic Device for Seismic Protection of Structures," Ph.D. Dissertation, Virginia Tech.

Karnopp, D. (1995). "Active and Semi-Active Vibration Isolation," *Journal of Vibration and Acoustics*, 117, 177-185.

Mathematica, Version 5.1.0.0 (2004). Wolfram Research, Inc., Champaign, Illinois.

Meirovitch, L. (1970). *Methods of Analytical Dynamics*, McGraw-Hill, Inc., New York.

Meriam, J.L., and Kraige, L.G. (1997). *Engineering Mechanics: Statics*, 4th Ed., John Wiley and Sons, Inc., New York.

Nelson, F.C. (1994). "Vibration Isolation: A Review, I. Sinusoidal and Random Excitation," *Shock and Vibration*, 1, 485-493.

Plaut, R.H. (1996). "Rocking instability of a pulled suitcase with two wheels," *Acta Mechanica*, 117, 165-179.

Plaut, R.H., Alloway, L.A., and Virgin, L.N. (2005). "Nonlinear Oscillations of a Buckled Mechanism Used as a Vibration Isolator," *IUTAM Symposium on Chaotic*

Dynamics and Control of Systems and Processes in Mechanics, G. Rega and F. Vestroni, eds., Springer, Dordecht, The Netherlands, 241-250.

Racca, R.H., and Harris, C.M. (2002). "Shock and Vibration Isolators and Isolation Systems," *Shock and Vibration Handbook*, 5th ed., C.M. Harris, ed., McGraw-Hill, Inc., New York, 32.1-32.23.

Sciulli, D. (1997). "Dynamics and Control for Vibration Isolation Design," Ph.D. Dissertation, Virginia Tech.

Sidbury, J.E. (2003). "Analysis of Buckled and Pre-bent Columns Used as Vibration Isolators," M.S. Thesis, Virginia Tech.

Tang, Y.G., Ding, Q., and Chen, Y.S. (2003). "Vibration Control of the Platform System With Hydraulic Supports," *Journal of Vibration and Control*, 9, 1093-1100.

Virgin, L.N., and Davis, R.B. (2003). "Vibration isolation using buckled struts," *Journal of Sound and Vibration*, 260, 965-973.

Virgin, L.N., and Plaut, R.H. (2002). "A Novel Type of Vibration Isolator Utilizing Buckled Structures," Proposal to National Science Foundation, Project Summary and Description.

Winterflood, J., Barber, T., and Blair, D.G. (2002a). "Using Euler buckling springs for vibration isolation," *Classical and Quantum Gravity*, 19, 1639-1645.

Winterflood, J., Blair, D.G., and Slagmolen, B. (2002b). "High performance vibration isolation using springs in Euler column buckling mode," *Physics Letters A*, 300, 122-130.

Winterflood, J., Barber, T.A., and Blair, D.G. (2002c). "Mathematical analysis of an Euler spring vibration isolator," *Physics Letters A*, 300, 131-139.

Appendix A: Equilibrium Program

```
(*Static Equilibrium of Rigid Plate supported at 4 corners by PreBent Struts
with Bonded Filler; Plate is symmetric or unsymmetric; Variables are defined as
follows: yi1=x, yi2=y, yi3=theta, yi4=m, yi5=q (where i=1,2,3,4 for the number
of the strut), yo=initial shape of unloaded strut, p=vertical component of
force, q=horizontal component of force, m=moment; Stiffnesses are modified with
βi factors so that plate is horizontal under static loads*)

Clear[w,ao,k,a1,a2,b1,b2,β1,β2,β3,β4,p1,p2,p3,p4,q1,q2,q3,q4,m1,m2,m3,m4,gp1,
gp2,gp3,gp4,gm1,gm2,gm3,gm4,gq1,gq2,gq3,gq4];

Off[General::spell1];
Off[General::spell];

po=40;
w=8*po;
ao=0.1;
k=0.1;
a1=0.35;
a2=1-a1;
α=1;
b1=α*0.45;
b2=α-b1;
β1=1.728;
β2=0.848;
β3=1.319;
β4=0.786;

For[i=1,i<8,i++,
    gp1=58.947;
    gp2=29.053;
    gp3=45.053;
    gp4=26.947;
    gm1=5.47531;
    gm2=5.47531;
    gm3=5.47531;
    gm4=5.47531;
    gq1=0.396565;
    gq2=0.396565;
    gq3=0.396565;
    gq4=0.396565;

endpt[p1_?NumericQ,p2_?NumericQ,p3_?NumericQ,p4_?NumericQ,m1_?NumericQ,m2_?Nume
ricQ,m3_?NumericQ,m4_?NumericQ,q1_?NumericQ,q2_?NumericQ,q3_?NumericQ,q4_?Numer
icQ]:=
      First[NDSolve[{y11'[t]==Cos[y13[t]],
            y12'[t]==Sin[y13[t]],
            y13'[t]==y14[t]/β1+2*π*ao*Cos[2*π*t],
            y14'[t]==y15[t]*Cos[y13[t]]-p1*Sin[y13[t]],
            y15'[t]==-k*(y12[t]-yo[t])/(yo[t]+0.0000001),
            yo'[t]==Sin[ao*Sin[2*π*t]],

            y21'[t]==Cos[y23[t]],
            y22'[t]==Sin[y23[t]],
            y23'[t]==y24[t]/β2+2*π*ao*Cos[2*π*t],
            y24'[t]==y25[t]*Cos[y23[t]]-p2*Sin[y23[t]],
            y25'[t]==-k*(y22[t]-yo[t])/(yo[t]+0.0000001),
```

```
            y31'[t]==Cos[y33[t]],
            y32'[t]==Sin[y33[t]],
            y33'[t]==y34[t]/β3+2*π*ao*Cos[2*π*t],
            y34'[t]==y35[t]*Cos[y33[t]]-p3*Sin[y33[t]],
            y35'[t]==-k*(y32[t]-yo[t])/(yo[t]+0.0000001),

            y41'[t]==Cos[y43[t]],
            y42'[t]==Sin[y43[t]],
            y43'[t]==y44[t]/β4+2*π*ao*Cos[2*π*t],
            y44'[t]==y45[t]*Cos[y43[t]]-p4*Sin[y43[t]],
            y45'[t]==-k*(y42[t]-yo[t])/(yo[t]+0.0000001),

            y11[0]==0,y12[0]==0,y13[0]==0,y14[0]==m1,y15[0]==q1,yo[0]==0,
            y21[0]==0,y22[0]==0,y23[0]==0,y24[0]==m2,y25[0]==q2,
            y31[0]==0,y32[0]==0,y33[0]==0,y34[0]==m3,y35[0]==q3,
            y41[0]==0,y42[0]==0,y43[0]==0,y44[0]==m4,y45[0]==q4},

{y11,y12,y13,y14,y15,yo,y21,y22,y23,y24,y25,y31,y32,y33,y34,y35,y41,y42,y43,
y44,y45},{t,0,1}]];

endpt[gp1,gp2,gp3,gp4,gm1,gm2,gm3,gm4,gq1,gq2,gq3,gq4];


f11[p1_?NumericQ,p2_?NumericQ,p3_?NumericQ,p4_?NumericQ,m1_?NumericQ,m2_?Numeri
cQ,m3_?NumericQ,m4_?NumericQ,q1_?NumericQ,q2_?NumericQ,q3_?NumericQ,q4_?Numeric
Q]:=y11[1]/.endpt[p1,p2,p3,p4,m1,m2,m3,m4,q1,q2,q3,q4];

f12[p1_?NumericQ,p2_?NumericQ,p3_?NumericQ,p4_?NumericQ,m1_?NumericQ,m2_?Numeri
cQ,m3_?NumericQ,m4_?NumericQ,q1_?NumericQ,q2_?NumericQ,q3_?NumericQ,q4_?Numeric
Q]:=y12[1]/.endpt[p1,p2,p3,p4,m1,m2,m3,m4,q1,q2,q3,q4];

f13[p1_?NumericQ,p2_?NumericQ,p3_?NumericQ,p4_?NumericQ,m1_?NumericQ,m2_?Numeri
cQ,m3_?NumericQ,m4_?NumericQ,q1_?NumericQ,q2_?NumericQ,q3_?NumericQ,q4_?Numeric
Q]:=y13[1]/.endpt[p1,p2,p3,p4,m1,m2,m3,m4,q1,q2,q3,q4];

f21[p1_?NumericQ,p2_?NumericQ,p3_?NumericQ,p4_?NumericQ,m1_?NumericQ,m2_?Numeri
cQ,m3_?NumericQ,m4_?NumericQ,q1_?NumericQ,q2_?NumericQ,q3_?NumericQ,q4_?Numeric
Q]:=y21[1]/.endpt[p1,p2,p3,p4,m1,m2,m3,m4,q1,q2,q3,q4];

f22[p1_?NumericQ,p2_?NumericQ,p3_?NumericQ,p4_?NumericQ,m1_?NumericQ,m2_?Numeri
cQ,m3_?NumericQ,m4_?NumericQ,q1_?NumericQ,q2_?NumericQ,q3_?NumericQ,q4_?Numeric
Q]:=y22[1]/.endpt[p1,p2,p3,p4,m1,m2,m3,m4,q1,q2,q3,q4];

f23[p1_?NumericQ,p2_?NumericQ,p3_?NumericQ,p4_?NumericQ,m1_?NumericQ,m2_?Numeri
cQ,m3_?NumericQ,m4_?NumericQ,q1_?NumericQ,q2_?NumericQ,q3_?NumericQ,q4_?Numeric
Q]:=y23[1]/.endpt[p1,p2,p3,p4,m1,m2,m3,m4,q1,q2,q3,q4];

f31[p1_?NumericQ,p2_?NumericQ,p3_?NumericQ,p4_?NumericQ,m1_?NumericQ,m2_?Numeri
cQ,m3_?NumericQ,m4_?NumericQ,q1_?NumericQ,q2_?NumericQ,q3_?NumericQ,q4_?Numeric
Q]:=y31[1]/.endpt[p1,p2,p3,p4,m1,m2,m3,m4,q1,q2,q3,q4];

f32[p1_?NumericQ,p2_?NumericQ,p3_?NumericQ,p4_?NumericQ,m1_?NumericQ,m2_?Numeri
cQ,m3_?NumericQ,m4_?NumericQ,q1_?NumericQ,q2_?NumericQ,q3_?NumericQ,q4_?Numeric
Q]:=y32[1]/.endpt[p1,p2,p3,p4,m1,m2,m3,m4,q1,q2,q3,q4];

f33[p1_?NumericQ,p2_?NumericQ,p3_?NumericQ,p4_?NumericQ,m1_?NumericQ,m2_?Numeri
cQ,m3_?NumericQ,m4_?NumericQ,q1_?NumericQ,q2_?NumericQ,q3_?NumericQ,q4_?Numeric
Q]:=y33[1]/.endpt[p1,p2,p3,p4,m1,m2,m3,m4,q1,q2,q3,q4];

f41[p1_?NumericQ,p2_?NumericQ,p3_?NumericQ,p4_?NumericQ,m1_?NumericQ,m2_?Numeri
cQ,m3_?NumericQ,m4_?NumericQ,q1_?NumericQ,q2_?NumericQ,q3_?NumericQ,q4_?Numeric
Q]:=y41[1]/.endpt[p1,p2,p3,p4,m1,m2,m3,m4,q1,q2,q3,q4];
```

```
f42[p1_?NumericQ,p2_?NumericQ,p3_?NumericQ,p4_?NumericQ,m1_?NumericQ,m2_?Numeri
cQ,m3_?NumericQ,m4_?NumericQ,q1_?NumericQ,q2_?NumericQ,q3_?NumericQ,q4_?Numeric
Q]:=y42[1]/.endpt[p1,p2,p3,p4,m1,m2,m3,m4,q1,q2,q3,q4];

f43[p1_?NumericQ,p2_?NumericQ,p3_?NumericQ,p4_?NumericQ,m1_?NumericQ,m2_?Numeri
cQ,m3_?NumericQ,m4_?NumericQ,q1_?NumericQ,q2_?NumericQ,q3_?NumericQ,q4_?Numeric
Q]:=y43[1]/.endpt[p1,p2,p3,p4,m1,m2,m3,m4,q1,q2,q3,q4];


{p1,p2,p3,p4,m1,m2,m3,m4,q1,q2,q3,q4}={p1,p2,p3,p4,m1,m2,m3,m4,q1,q2,q3,q4}/.
FindRoot[{
   f12[p1,p2,p3,p4,m1,m2,m3,m4,q1,q2,q3,q4]==0,
   f13[p1,p2,p3,p4,m1,m2,m3,m4,q1,q2,q3,q4]==0,
   f22[p1,p2,p3,p4,m1,m2,m3,m4,q1,q2,q3,q4]==0,
   f23[p1,p2,p3,p4,m1,m2,m3,m4,q1,q2,q3,q4]==0,
   f32[p1,p2,p3,p4,m1,m2,m3,m4,q1,q2,q3,q4]==0,
   f33[p1,p2,p3,p4,m1,m2,m3,m4,q1,q2,q3,q4]==0,
   f42[p1,p2,p3,p4,m1,m2,m3,m4,q1,q2,q3,q4]==0,
   f43[p1,p2,p3,p4,m1,m2,m3,m4,q1,q2,q3,q4]==0,
   p1+p2+p3+p4==w/2,
   (p1+p2)*b1-(p3+p4)*b2==0,
   (p1+p3)*a1-(p2+p4)*a2==0,
   f11[p1,p2,p3,p4,m1,m2,m3,m4,q1,q2,q3,q4]-
     f21[p1,p2,p3,p4,m1,m2,m3,m4,q1,q2,q3,q4]-
     f31[p1,p2,p3,p4,m1,m2,m3,m4,q1,q2,q3,q4]+
     f41[p1,p2,p3,p4,m1,m2,m3,m4,q1,q2,q3,q4]==0},
{p1,gp1},{p2,gp2},{p3,gp3},{p4,gp4},{m1,gm1},{m2,gm2},{m3,gm3},{m4,gm4},
{q1,gq1},{q2,gq2},{q3,gq3},{q4,gq4},AccuracyGoal→4];


{yy11[t_],yy12[t_],yy13[t_],yy14[t_],yy15[t_],yyo[t_],yy21[t_],yy22[t_],yy23[t_
],yy24[t_],yy25[t_],yy31[t_],yy32[t_],yy33[t_],yy34[t_],yy35[t_],yy41[t_],yy42[
t_],yy43[t_],yy44[t_],yy45[t_]}={y11[t],y12[t],y13[t],y14[t],y15[t],yo[t],y21[t
],y22[t],y23[t],y24[t],y25[t],y31[t],y32[t],y33[t],y34[t],y35[t],y41[t],y42[t],
y43[t],y44[t],y45[t]}/.endpt[p1,p2,p3,p4,m1,m2,m3,m4,q1,q2,q3,q4];

    avgx=(yy11[1]+yy21[1]+yy31[1]+yy41[1])/4;
    newβ1=β1*avgx/yy11[1];
    newβ2=β2*avgx/yy21[1];
    newβ3=β3*avgx/yy31[1];
    newβ4=β4*avgx/yy41[1];
    β1=newβ1;β2=newβ2;β3=newβ3;β4=newβ4];

{β1,β2,β3,β4}
{avgx,yy11[1],yy21[1],yy31[1],yy41[1]}
{p1,p2,p3,p4,m1,m2,m3,m4,q1,q2,q3,q4}
```

Appendix B: Calculation of the Mass Moments of Inertia for the Plate

For the purpose of calculating the mass moment of inertia, the eccentricity of the plate will be modeled as a block set on top of the plate, where the block is positioned arbitrarily on top of the plate, as shown in Figure B.1. This model is representative of a piece of equipment set on top of the rigid plate. The plate has a thickness H_1 and the block has a height H_2 and width and depth D. The center of mass for the combination of the plate and block is given by the dimensions A_1, A_2, B_1, B_2, and C, where A_1 and A_2 give the position of the center of mass along the $\overline{X}$ -axis, B_1 and B_2 give the position of the center of mass along the $\overline{Y}$ -axis, C gives the position of the center of mass in the $\overline{Z}$ direction measured from the bottom of the plate, as shown in Figure 3.1.

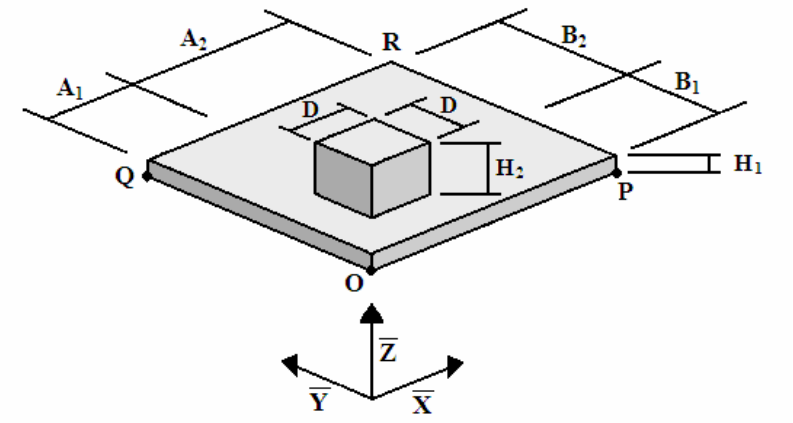

Figure B.1: Dimensions of Block on Top of Plate

The values for A_1, A_2, B_1, and B_2 are known and are specified directly. However, C must be calculated in terms of the dimensions of the block and the plate using the following equation:

$$C = \frac{\frac{(A_1 + A_2)H_1^{\,2}}{2} + DH_2\left(H_1 + \frac{H_2}{2}\right)}{(A_1 + A_2)H_1 + DH_2} \tag{B.1}$$

Assuming that the plate has mass M_1 and the block has mass M_2, the mass moments of inertia about the $\overline{X}$ and $\overline{Y}$ axes at the center of mass can be calculated as follows:

$$I_X = M_1\left\{\frac{1}{12}\left[(B_1+B_2)^2+{H_1}^2\right]+\left[\left(\frac{B_1+B_2}{2}-B_1\right)^2+\left(\frac{H_1}{2}-C\right)^2\right]\right\}+$$

$$M_2\left\{\frac{1}{12}\left({H_2}^2+D^2\right)+\left[\left(\frac{B_1(B_1+B_2)H_1-\frac{(B_1+B_2)^2H_1}{2}}{DH_2}\right)^2+\left(H_1+\frac{H_2}{2}-C\right)^2\right]\right\} \quad \text{(B.2)}$$

$$I_Y = M_1\left\{\frac{1}{12}\left[(A_1+A_2)^2+{H_1}^2\right]+\left[\left(\frac{A_1+A_2}{2}-A_1\right)^2+\left(\frac{H_1}{2}-C\right)^2\right]\right\}+$$

$$M_2\left\{\frac{1}{12}\left({H_2}^2+D^2\right)+\left[\left(\frac{A_1(A_1+A_2)H_1-\frac{(A_1+A_2)^2H_1}{2}}{DH_2}\right)^2+\left(H_1+\frac{H_2}{2}-C\right)^2\right]\right\} \quad \text{(B.3)}$$

B.1 Nondimensionalization

The nondimensional variables for A_1, A_2, B_1, and B_2 are given in Equations (2.16) – (2.19). The plate and block dimensions are nondimensionalized as follows:

$$h_1 = \frac{H_1}{A_1+A_2} \qquad h_2 = \frac{H_2}{A_1+A_2} \quad \text{(B.4, B.5)}$$

$$d = \frac{D}{A_1+A_2} \quad \text{(B.6)}$$

Substituting the relationships in Equations (2.16) – (2.19) and Equations (B.4) – (B.6) into Equation (B.1) and recognizing that $a_1 + a_2 = 1$ gives

$$c = \frac{\frac{{h_1}^2}{2}+dh_2\left(h_1+\frac{h_2}{2}\right)}{h_1+dh_2} \quad \text{(B.7)}$$

Using the stiffness parameter r defined in Equation (3.128), the total mass m of the block and plate is defined in terms of the total nondimensional weight w as

$$m = rw \quad \text{(B.8)}$$

The plate and block have volumes V_1 and V_2, respectively, given by the following equations:

$$V_1 = H_1(A_1 + A_2)(B_1 + B_2) \tag{B.9}$$

$$V_2 = H_2 D^2 \tag{B.10}$$

Putting Equations (B.9) and (B.10) in nondimensional form, and using the relationships $a_1 + a_2 = 1$ and $b_1 + b_2 = \alpha$, gives

$$v_1 = \alpha h_1 \tag{B.11}$$

$$v_2 = h_2 d^2 \tag{B.12}$$

Assuming that the block and the plate have the same density, the nondimensional masses m_1 and m_2 for the plate and block are defined as

$$m_1 = \frac{m v_1}{v_1 + v_2} \tag{B.13}$$

$$m_2 = \frac{m v_2}{v_1 + v_2} \tag{B.14}$$

where the total mass m is defined in Equation (B.8). Using the relationships in Equations (2.16) – (2.19) and Equations (B.4) – (B.7), the nondimensional mass moments of inertia about the $\overline{X}$ and $\overline{Y}$ axes are as follows:

$$i_x = m_1\left\{\frac{1}{12}\left(\alpha^2 + {h_1}^2\right) + \left[\left(\frac{\alpha}{2} - b_1\right)^2 + \left(\frac{h_1}{2} - c\right)^2\right]\right\} +$$

$$m_2\left\{\frac{1}{12}\left({h_2}^2 + d^2\right) + \left[\left(\frac{\alpha b_1 h_1 - \frac{\alpha^2 h_1}{2}}{d h_2}\right)^2 + \left(h_1 + \frac{h_2}{2} - c\right)^2\right]\right\} \tag{B.15}$$

$$i_y = m_1\left\{\frac{1}{12}\left(1 + {h_1}^2\right) + \left[\left(\frac{1}{2} - a_1\right)^2 + \left(\frac{h_1}{2} - c\right)^2\right]\right\} +$$

$$m_2\left\{\frac{1}{12}\left({h_2}^2 + d^2\right) + \left[\left(\frac{a_1 h_1 - \frac{h_1}{2}}{d h_2}\right)^2 + \left(h_1 + \frac{h_2}{2} - c\right)^2\right]\right\} \tag{B.16}$$

Appendix C: Dynamic Program

```
(*Dynamic Analysis of Rigid Plate supported at 4 corners by PreBent Struts with
Bonded Filler; Plate is symmetric or unsymmetric; Variables are defined as
follows: yi1=x_e, yi2=y_e, yi3=theta_e, yi4=m_e, yi5=q_e, yi6=x_d,
yi7=y_d,yi8=theta_d, yi9=m_d, yi10=p_d, yi11=q_d, (where i=1,2,3,4 for the
number of the strut, "e" is for equilibrium and "d" is for dynamic), yo=initial
shape of unloaded strut, p=vertical component of force, q=horizontal component
of force, m=moment; Stiffnesses are modified with βi factors so that plate is
horizontal under static loads*)

Off[General::spell1];
Off[General::spell];

r=1;
mass=r*w;
cf=1;
uo=0.01;

k1=.1;
k2=.1;
k3=.1;
k4=.1;
k5=.1;
k6=.1;
k7=.1;
k8=.1;

h1=0.05;
h2=0.3;
d=0.3;

v1=α*h1;
v2=(d^2)*h2;
mass1=mass*v1/(v1+v2);
mass2=mass*v2/(v1+v2);
c=(h1^2/2+d*h2*(h1+h2/2))/(h1+d*h2);
ix=mass1*((α^2+h1^2)/12+(α/2-b1)^2+(h1/2-c)^2)+
  mass2*((h2^2+d^2)/12+((b1*α*h1+b1*d*h2-h1*α^2/2)/(d*h2)-b1)^2+(h1+h2/2-c)^2);
iy=mass1*((1^2+h1^2)/12+(1/2-a1)^2+(h1/2-c)^2)+
  mass2*((h2^2+d^2)/12+((a1*h1+a1*d*h2-h1/2)/(d*h2)-a1)^2+(h1+h2/2-c)^2);

gp1d=-0.0082-( 1.6537×10^-10)i;
gp2d=-0.0082-( 1.6537×10^-10)i;
gp3d=-0.0082-( 1.6537×10^-10)i;
gp4d=-0.0082-( 1.6537×10^-10)i;
gm1d=1.9765-0.0007 i;
gm2d=2.8761-0.0033 i;
gm3d=1.9765-0.0007 i;
gm4d=2.8761-0.0033 i;
gq1d=-21.3180+0.0103 i;
gq2d=-32.4360+0.0373 i;
gq3d=-21.3180+0.0103 i;
gq4d=-32.4360+0.0373 i;
gxod=0.0001+0.0000001i;
gxpd=0.0001+0.0000001i;
gyod=0.0001+0.0000001i;
gyqd=0.0001+0.0000001i;
```

```
Do[{{ω=m;

endpt[p1d_?NumericQ,p2d_?NumericQ,p3d_?NumericQ,p4d_?NumericQ,m1d_?NumericQ,m2d
_?NumericQ,m3d_?NumericQ,m4d_?NumericQ,q1d_?NumericQ,q2d_?NumericQ,q3d_?Numeric
Q,q4d_?NumericQ]:=
  First[NDSolve[{y11'[t]==Cos[y13[t]],
   y12'[t]==Sin[y13[t]],
   y13'[t]==y14[t]/β1+2*π*ao*Cos[2*π*t],
   y14'[t]==y15[t]*Cos[y13[t]]-p1*Sin[y13[t]],
   y15'[t]==-k*(y12[t]-yo[t])/(yo[t]+0.0000001),
   yo'[t]==Sin[ao*Sin[2*π*t]],
   y16'[t]==-y18[t]*Sin[y13[t]],
   y17'[t]==y18[t]*Cos[y13[t]],
   y18'[t]==y19[t]/β1,
   y19'[t]==(y111[t]-p1*y18[t])*Cos[y13[t]]-(y110[t]+y15[t]*y18[t])*Sin[y13[t]],
   y110'[t]==β1*(ω^2)*y16[t],
   y111'[t]==(β1*(ω^2)-i*ω*cf*yo[t]-k/(yo[t]+0.0000001))*y17[t],

   y21'[t]==Cos[y23[t]],
   y22'[t]==Sin[y23[t]],
   y23'[t]==y24[t]/β2+2*π*ao*Cos[2*π*t],
   y24'[t]==y25[t]*Cos[y23[t]]-p2*Sin[y23[t]],
   y25'[t]==-k*(y22[t]-yo[t])/(yo[t]+0.0000001),
   y26'[t]==-y28[t]*Sin[y23[t]],
   y27'[t]==y28[t]*Cos[y23[t]],
   y28'[t]==y29[t]/β2,
   y29'[t]==(y211[t]-p2*y28[t])*Cos[y23[t]]-(y210[t]+y25[t]*y28[t])*Sin[y23[t]],
   y210'[t]==β2*(ω^2)*y26[t],
   y211'[t]==(β2*(ω^2)-i*ω*cf*yo[t]-k/(yo[t]+0.0000001))*y27[t],

   y31'[t]==Cos[y33[t]],
   y32'[t]==Sin[y33[t]],
   y33'[t]==y34[t]/β3+2*π*ao*Cos[2*π*t],
   y34'[t]==y35[t]*Cos[y33[t]]-p3*Sin[y33[t]],
   y35'[t]==-k*(y32[t]-yo[t])/(yo[t]+0.0000001),
   y36'[t]==-y38[t]*Sin[y33[t]],
   y37'[t]==y38[t]*Cos[y33[t]],
   y38'[t]==y39[t]/β3,
   y39'[t]==(y311[t]-p3*y38[t])*Cos[y33[t]]-(y310[t]+y35[t]*y38[t])*Sin[y33[t]],
   y310'[t]==β3*(ω^2)*y36[t],
   y311'[t]==(β3*(ω^2)-i*ω*cf*yo[t]-k/(yo[t]+0.0000001))*y37[t],

   y41'[t]==Cos[y43[t]],
   y42'[t]==Sin[y43[t]],
   y43'[t]==y44[t]/β4+2*π*ao*Cos[2*π*t],
   y44'[t]==y45[t]*Cos[y43[t]]-p4*Sin[y43[t]],
   y45'[t]==-k*(y42[t]-yo[t])/(yo[t]+0.0000001),
   y46'[t]==-y48[t]*Sin[y43[t]],
   y47'[t]==y48[t]*Cos[y43[t]],
   y48'[t]==y49[t]/β4,
   y49'[t]==(y411[t]-p4*y48[t])*Cos[y43[t]]-(y410[t]+y45[t]*y48[t])*Sin[y43[t]],
   y410'[t]==β4*(ω^2)*y46[t],
   y411'[t]==(β4*(ω^2)-i*ω*cf*yo[t]-k/(yo[t]+0.0000001))*y47[t],


   y11[0]==0,y12[0]==0,y13[0]==0,y14[0]==m1,y15[0]==q1,yo[0]==0,
   y21[0]==0,y22[0]==0,y23[0]==0,y24[0]==m2,y25[0]==q2,
   y31[0]==0,y32[0]==0,y33[0]==0,y34[0]==m3,y35[0]==q3,
   y41[0]==0,y42[0]==0,y43[0]==0,y44[0]==m4,y45[0]==q4,
   y16[0]==uo,y17[0]==0,y18[0]==0,y19[0]==m1d,y110[0]==p1d,y111[0]==q1d,
   y26[0]==uo,y27[0]==0,y28[0]==0,y29[0]==m2d,y210[0]==p2d,y211[0]==q2d,
   y36[0]==uo,y37[0]==0,y38[0]==0,y39[0]==m3d,y310[0]==p3d,y311[0]==q3d,
```

```
   y46[0]==uo,y47[0]==0,y48[0]==0,y49[0]==m4d,y410[0]==p4d,y411[0]==q4d},
{y11,y12,y13,y14,y15,yo,y21,y22,y23,y24,y25,y31,y32,y33,y34,y35,y41,y42,y43,
y44,y45,y16,y17,y18,y19,y110,y111,y26,y27,y28,y29,y210,y211,y36,y37,y38,y39,
y310,y311,y46,y47,y48,y49,y410,y411},{t,0,1}]];

endpt[gp1d,gp2d,gp3d,gp4d,gm1d,gm2d,gm3d,gm4d,gq1d,gq2d,gq3d,gq4d];

f16[p1d_?NumericQ,p2d_?NumericQ,p3d_?NumericQ,p4d_?NumericQ,m1d_?NumericQ,m2d_?
  NumericQ,m3d_?NumericQ,m4d_?NumericQ,q1d_?NumericQ,q2d_?NumericQ,q3d_?NumericQ
  ,q4d_?NumericQ]:=y16[1]/.endpt[p1d,p2d,p3d,p4d,m1d,m2d,m3d,m4d,q1d,q2d,q3d,q4d
  ];
f17[p1d_?NumericQ,p2d_?NumericQ,p3d_?NumericQ,p4d_?NumericQ,m1d_?NumericQ,m2d_?
  NumericQ,m3d_?NumericQ,m4d_?NumericQ,q1d_?NumericQ,q2d_?NumericQ,q3d_?NumericQ
  ,q4d_?NumericQ]:=y17[1]/.endpt[p1d,p2d,p3d,p4d,m1d,m2d,m3d,m4d,q1d,q2d,q3d,q4d
  ];
f18[p1d_?NumericQ,p2d_?NumericQ,p3d_?NumericQ,p4d_?NumericQ,m1d_?NumericQ,m2d_?
  NumericQ,m3d_?NumericQ,m4d_?NumericQ,q1d_?NumericQ,q2d_?NumericQ,q3d_?NumericQ
  ,q4d_?NumericQ]:=y18[1]/.endpt[p1d,p2d,p3d,p4d,m1d,m2d,m3d,m4d,q1d,q2d,q3d,q4d
  ];
f26[p1d_?NumericQ,p2d_?NumericQ,p3d_?NumericQ,p4d_?NumericQ,m1d_?NumericQ,m2d_?
  NumericQ,m3d_?NumericQ,m4d_?NumericQ,q1d_?NumericQ,q2d_?NumericQ,q3d_?NumericQ
  ,q4d_?NumericQ]:=y26[1]/.endpt[p1d,p2d,p3d,p4d,m1d,m2d,m3d,m4d,q1d,q2d,q3d,q4d
  ];
f27[p1d_?NumericQ,p2d_?NumericQ,p3d_?NumericQ,p4d_?NumericQ,m1d_?NumericQ,m2d_?
  NumericQ,m3d_?NumericQ,m4d_?NumericQ,q1d_?NumericQ,q2d_?NumericQ,q3d_?NumericQ
  ,q4d_?NumericQ]:=y27[1]/.endpt[p1d,p2d,p3d,p4d,m1d,m2d,m3d,m4d,q1d,q2d,q3d,q4d
  ];
f28[p1d_?NumericQ,p2d_?NumericQ,p3d_?NumericQ,p4d_?NumericQ,m1d_?NumericQ,m2d_?
  NumericQ,m3d_?NumericQ,m4d_?NumericQ,q1d_?NumericQ,q2d_?NumericQ,q3d_?NumericQ
  ,q4d_?NumericQ]:=y28[1]/.endpt[p1d,p2d,p3d,p4d,m1d,m2d,m3d,m4d,q1d,q2d,q3d,q4d
  ];
f36[p1d_?NumericQ,p2d_?NumericQ,p3d_?NumericQ,p4d_?NumericQ,m1d_?NumericQ,m2d_?
  NumericQ,m3d_?NumericQ,m4d_?NumericQ,q1d_?NumericQ,q2d_?NumericQ,q3d_?NumericQ
  ,q4d_?NumericQ]:=y36[1]/.endpt[p1d,p2d,p3d,p4d,m1d,m2d,m3d,m4d,q1d,q2d,q3d,q4d
  ];
f37[p1d_?NumericQ,p2d_?NumericQ,p3d_?NumericQ,p4d_?NumericQ,m1d_?NumericQ,m2d_?
  NumericQ,m3d_?NumericQ,m4d_?NumericQ,q1d_?NumericQ,q2d_?NumericQ,q3d_?NumericQ
  ,q4d_?NumericQ]:=y37[1]/.endpt[p1d,p2d,p3d,p4d,m1d,m2d,m3d,m4d,q1d,q2d,q3d,q4d
  ];
f38[p1d_?NumericQ,p2d_?NumericQ,p3d_?NumericQ,p4d_?NumericQ,m1d_?NumericQ,m2d_?
  NumericQ,m3d_?NumericQ,m4d_?NumericQ,q1d_?NumericQ,q2d_?NumericQ,q3d_?NumericQ
  ,q4d_?NumericQ]:=y38[1]/.endpt[p1d,p2d,p3d,p4d,m1d,m2d,m3d,m4d,q1d,q2d,q3d,q4d
  ];
f46[p1d_?NumericQ,p2d_?NumericQ,p3d_?NumericQ,p4d_?NumericQ,m1d_?NumericQ,m2d_?
  NumericQ,m3d_?NumericQ,m4d_?NumericQ,q1d_?NumericQ,q2d_?NumericQ,q3d_?NumericQ
  ,q4d_?NumericQ]:=y46[1]/.endpt[p1d,p2d,p3d,p4d,m1d,m2d,m3d,m4d,q1d,q2d,q3d,q4d
  ];
f47[p1d_?NumericQ,p2d_?NumericQ,p3d_?NumericQ,p4d_?NumericQ,m1d_?NumericQ,m2d_?
  NumericQ,m3d_?NumericQ,m4d_?NumericQ,q1d_?NumericQ,q2d_?NumericQ,q3d_?NumericQ
  ,q4d_?NumericQ]:=y47[1]/.endpt[p1d,p2d,p3d,p4d,m1d,m2d,m3d,m4d,q1d,q2d,q3d,q4d
  ];
f48[p1d_?NumericQ,p2d_?NumericQ,p3d_?NumericQ,p4d_?NumericQ,m1d_?NumericQ,m2d_?
  NumericQ,m3d_?NumericQ,m4d_?NumericQ,q1d_?NumericQ,q2d_?NumericQ,q3d_?NumericQ
  ,q4d_?NumericQ]:=y48[1]/.endpt[p1d,p2d,p3d,p4d,m1d,m2d,m3d,m4d,q1d,q2d,q3d,q4d
  ];

{p1d,p2d,p3d,p4d,m1d,m2d,m3d,m4d,q1d,q2d,q3d,q4d,xod,xpd,yod,yqd}=
  {p1d,p2d,p3d,p4d,m1d,m2d,m3d,m4d,q1d,q2d,q3d,q4d,xod,xpd,yod,yqd}
  /.FindRoot[{f17[p1d,p2d,p3d,p4d,m1d,m2d,m3d,m4d,q1d,q2d,q3d,q4d]==0,
    f18[p1d,p2d,p3d,p4d,m1d,m2d,m3d,m4d,q1d,q2d,q3d,q4d]==0,
    f27[p1d,p2d,p3d,p4d,m1d,m2d,m3d,m4d,q1d,q2d,q3d,q4d]==0,
    f28[p1d,p2d,p3d,p4d,m1d,m2d,m3d,m4d,q1d,q2d,q3d,q4d]==0,
    f37[p1d,p2d,p3d,p4d,m1d,m2d,m3d,m4d,q1d,q2d,q3d,q4d]==0,
```

```
    f38[p1d,p2d,p3d,p4d,m1d,m2d,m3d,m4d,q1d,q2d,q3d,q4d]==0,
    f47[p1d,p2d,p3d,p4d,m1d,m2d,m3d,m4d,q1d,q2d,q3d,q4d]==0,
    f48[p1d,p2d,p3d,p4d,m1d,m2d,m3d,m4d,q1d,q2d,q3d,q4d]==0,

     0==(yod-yqd),
     0==(xod-xpd),
     f16[p1d,p2d,p3d,p4d,m1d,m2d,m3d,m4d,q1d,q2d,q3d,q4d]-
      f26[p1d,p2d,p3d,p4d,m1d,m2d,m3d,m4d,q1d,q2d,q3d,q4d]-
      f36[p1d,p2d,p3d,p4d,m1d,m2d,m3d,m4d,q1d,q2d,q3d,q4d]+
      f46[p1d,p2d,p3d,p4d,m1d,m2d,m3d,m4d,q1d,q2d,q3d,q4d]==0,

    -r*w*(ω^2)*(a1*xpd+a2*xod-
       c*f26[p1d,p2d,p3d,p4d,m1d,m2d,m3d,m4d,q1d,q2d,q3d,q4d]+
       c*f16[p1d,p2d,p3d,p4d,m1d,m2d,m3d,m4d,q1d,q2d,q3d,q4d])+
       (k3+k4)*xpd+(k7+k8)*xod==0,
    -r*w*(ω^2)/α*(b1*yqd+b2*yod-
       c*f36[p1d,p2d,p3d,p4d,m1d,m2d,m3d,m4d,q1d,q2d,q3d,q4d]+
       c*f16[p1d,p2d,p3d,p4d,m1d,m2d,m3d,m4d,q1d,q2d,q3d,q4d])+
       (k1+k2)*yod+(k5+k6)*yqd==0,
    -r*w*(ω^2)*(a1*f26[p1d,p2d,p3d,p4d,m1d,m2d,m3d,m4d,q1d,q2d,q3d,q4d]+
       a2*f16[p1d,p2d,p3d,p4d,m1d,m2d,m3d,m4d,q1d,q2d,q3d,q4d]+c*xpd-c*xod)-
      r*w*(ω^2)/α*(b1*f36[p1d,p2d,p3d,p4d,m1d,m2d,m3d,m4d,q1d,q2d,q3d,q4d]-
       b1*f16[p1d,p2d,p3d,p4d,m1d,m2d,m3d,m4d,q1d,q2d,q3d,q4d]+c*yqd-c*yod)==
       2*(p1d+p2d+p3d+p4d),
    -ix*(ω^2)/α*(f36[p1d,p2d,p3d,p4d,m1d,m2d,m3d,m4d,q1d,q2d,q3d,q4d]-
       f16[p1d,p2d,p3d,p4d,m1d,m2d,m3d,m4d,q1d,q2d,q3d,q4d])==
       -2*(p1d+p2d)*b1+2*(p3d+p4d)*b2,
    -iy*(ω^2)*(f26[p1d,p2d,p3d,p4d,m1d,m2d,m3d,m4d,q1d,q2d,q3d,q4d]-
       f16[p1d,p2d,p3d,p4d,m1d,m2d,m3d,m4d,q1d,q2d,q3d,q4d])==
       -2*(p1d+p3d)*a1+2*(p2d+p4d)*a2},

{p1d,gp1d},{p2d,gp2d},{p3d,gp3d},{p4d,gp4d},{m1d,gm1d},{m2d,gm2d},{m3d,gm3d},
{m4d,gm4d},{q1d,gq1d},{q2d,gq2d},{q3d,gq3d},{q4d,gq4d},{xod,gxod},{xpd,gxpd},
{yod,gyod},{yqd,gyqd},AccuracyGoal→3,MaxIterations→10000];

TR1=((((Re[f16[p1d,p2d,p3d,p4d,m1d,m2d,m3d,m4d,q1d,q2d,q3d,q4d]])^2+
   (Im[f16[p1d,p2d,p3d,p4d,m1d,m2d,m3d,m4d,q1d,q2d,q3d,q4d]])^2))^0.5)/uo;
TR2=((((Re[f26[p1d,p2d,p3d,p4d,m1d,m2d,m3d,m4d,q1d,q2d,q3d,q4d]])^2+
   (Im[f26[p1d,p2d,p3d,p4d,m1d,m2d,m3d,m4d,q1d,q2d,q3d,q4d]])^2))^0.5)/uo;
TR3=((((Re[f36[p1d,p2d,p3d,p4d,m1d,m2d,m3d,m4d,q1d,q2d,q3d,q4d]])^2+
   (Im[f36[p1d,p2d,p3d,p4d,m1d,m2d,m3d,m4d,q1d,q2d,q3d,q4d]])^2))^0.5)/uo;
TR4=((((Re[f46[p1d,p2d,p3d,p4d,m1d,m2d,m3d,m4d,q1d,q2d,q3d,q4d]])^2+
   (Im[f46[p1d,p2d,p3d,p4d,m1d,m2d,m3d,m4d,q1d,q2d,q3d,q4d]])^2))^0.5)/uo;
TR=(TR1+TR2+TR3+TR4)/4;
        gp1d=p1d;
        gm1d=m1d;
        gq1d=q1d;
        gp2d=p2d;
        gm2d=m2d;
        gq2d=q2d;
        gp3d=p3d;
        gm3d=m3d;
        gq3d=q3d;
        gp4d=p4d;
        gm4d=m4d;
        gq4d=q4d;
        gxod=xod;
        gxpd=xpd;
        gyod=yod;
        gyqd=yqd;}}

Print[PaddedForm[TableForm[{{ω,TR,p1d,p2d,p3d,p4d,xod,yod}}],{5,4}]],{m,46.1,46
.9,.1}];
```

Appendix D: Nodal Lines for the Fully Symmetric Case

From the free vibration analysis (discussed in Section 4.2), it was found that the fully symmetric case had rotational modes of vibration about all lines passing through the center of the plate and that these rotational modes occurred at the same frequency. The following example is used to demonstrate that any line that passes through the center of the plate (e.g., lines $A - A'$, $B - B'$, $C - C'$, and $D - D'$ in Figure 4.23(a)) for the fully symmetric case should be a nodal line, and that rotations about any of these nodal lines will have the same frequency of vibration.

Consider a thin uniform square plate with mass m. The plate is initially horizontal, and the sides of the plate have lengths l. Each corner of the plate is supported by a massless spring with stiffness coefficient k, as shown in Figure D.1.

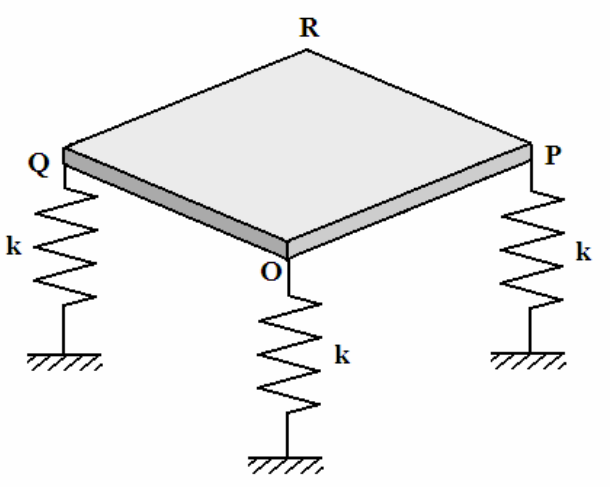

Figure D.1: Square Plate Supported by Massless Springs

Suppose the plate rotates at an angle θ about an arbitrary line, shown in Figure D.2, which passes through the center of the plate. If damping is neglected, the equation of motion for the rotation of the plate about this nodal line can be written as

$$I\ddot{\theta} + M_s = 0 \qquad \text{(D.1)}$$

where I is the mass moment of inertia about the axis of rotation and M_s is the resultant moment caused by the forces in the springs. For a uniform square plate, the mass moment of inertia about any line passing through the center of the plate is the same, regardless of the orientation of the line (Meriam and Kraige, 1997). If it can be shown that the resultant moment M_s of the spring forces about any line passing through the center of the plate remains the same, then any line passing through the center of the plate can be considered a nodal line, and a rotation about any of these nodal lines will have the same frequency of vibration.

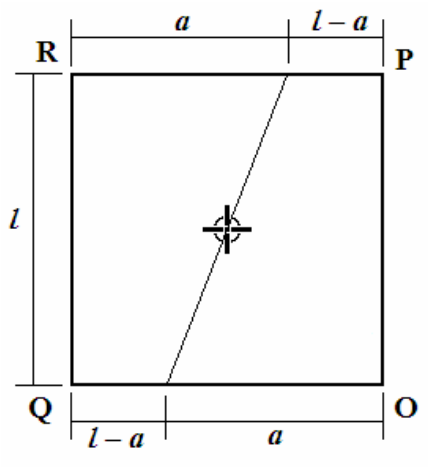

Figure D.2: Position of an Arbitrary Nodal Line Passing Through the Center of the Plate

The perpendicular distances R_O, R_P, R_Q, and R_R from the nodal line to corners O, P, Q, and R can be computed as

$$R_O = \frac{a}{\sqrt{\left(\frac{2a-l}{l}\right)^2 + 1}} \qquad R_P = \frac{l-a}{\sqrt{\left(\frac{2a-l}{l}\right)^2 + 1}} \tag{D.2, D.3}$$

$$R_Q = \frac{l-a}{\sqrt{\left(\frac{2a-l}{l}\right)^2 + 1}} \qquad R_R = \frac{a}{\sqrt{\left(\frac{2a-l}{l}\right)^2 + 1}} \tag{D.4, D.5}$$

Using small-angle approximations (i.e., $\sin\theta \approx \theta$), the restoring moment caused by the springs attached to the plate due to a rotation about the nodal line shown in Figure D.2 can be calculated as

$$M_s = (kR_O\theta)R_O + (kR_P\theta)R_P - (-kR_Q\theta)R_Q - (-kR_R\theta)R_R \tag{D.6}$$

Substituting Equations (D.2) – (D.5) into Equation (D.6) gives the resultant moment as

$$M_s = \frac{k\theta\left[2a^2 + 2(l-a)^2\right]}{\left(\frac{2a-l}{l}\right)^2 + 1} = k\theta l^2 \tag{D.7}$$

Equation (D.7) shows that the resultant moment due to the spring forces is independent of the orientation of the nodal line passing through the center of the plate. Therefore, it can be concluded that the plate has an infinite number of nodal lines which pass through the center of the plate, and rotations about any of these nodal lines will have the same frequency of vibration.